Insights into the role and regulation of the mitochondrial unfolded protein response during pathogen infection

by

MOHAMMED ADNAN MOHAMMED HANIF QURESHI

DISSERTATION

Submitted in partial fulfillment of the requirements

for the degree of

DOCTOR OF PHILOSOPHY

THE UNIVERSITY OF TEXAS AT ARLINGTON

DEC 2021

Supervising Committee

Dr. Mark W. Pellegrino, Supervising Professor

Dr. Esther Betran

Dr. Laura Mydlarz

Dr. Subhrangsu S. Mandal

Dr. Matthew Fujita

COPYRIGHT

ACKNOWLEDGEMENT

This is certainly not easy to complete in a page or two, but I will give it a try. This thesis is a culmination of efforts, love, sacrifice, determination, selflessness, and kindness of a lot of people. I begin by acknowledging my compassionate and courageous Meem who has and keeps making immense sacrifices only for me to get educated and be a successful person. The determination and effort of my visionary and kind Dad is the sole reason I am where I am. Words can never describe the love, care, motivation and guidance that my Meem and Dad have given me. I can never thank them enough. My sister, Nida Qureshi who has had so much faith in me and always guiding me to be a better person by being an excellent example. My brother, Kamran Qureshi has been a constant support and humor in my life. Being here in the States I have missed no one more than my nephew Ahmed, the pure joy of my life. My brother-in-law Faisal Qureshi who's caring attitude has helped me focus on my dissertation while he has owned immense responsibilities. Special mention to my uncle Kashif Sayyed, chachu Rais Qureshi, chacha Salamat Qureshi, mama Ashraf Qureshi and other family members for always believing in me. I hope my work brings pride to the Nadir Hussain Qureshi and Shabbir Qureshi families.

I am grateful to Dr. Mark Pellegrino for providing me the opportunity to be a part of his lab and being a great mentor. My supervising committee Dr. Ester Betran, Dr. Laura Mydlarz, Dr. Subhrangsu S. Mandal and Dr. Matthew Fujita who have shaped and guided my research. I want to thank Dr. Clark without whom I wouldn't have the opportunity to be a part of UTA and the Biology department.

I have had the fortune of working with some of the most compassionate and intelligent people. The two pillars of Pellegrino lab, Siraje Mahmud and Madhab Sapkota. They have constantly been there during the tough times to help me and mould me as a researcher. Their knowledge and experience are unparallel and this thesis is more of their work than mine. I also have had the pleasure of working with Raisa Amin who is the little sister I never had, constantly bickering while being a caring companion during my time in the Pellegrino lab. When I was low and needed a friend to talk to and share my feelings I always had Douja Chamseddine. One of the most hardworking and selfless person. I will miss our coffee breaks! My lab members, Josh, Dominic and Yiting have been the best people I could have worked with. And special mention to all my undergrads (Yves, Charlton, Fred, Johnathan, Eric, Roomeeka) I had the privilege of working with and they have helped me greatly in my experiments. The members of the quad (Pellegrino, Boutte, Boll and Ghose lab) have always been there to share and exchange ideas and are just awesome people to work with. I have had great friends here at UTA who have been there through fun and difficult times. I thank Suman Shrestha, Swatantra Neupane, Farah Shamma, Fatema Ruma, Sarabjeet Niraula and others. I cannot thank my brother Balan Ramesh as the word cannot convey my gratitude towards him for all that he has done.

The special friends who shaped me as person, Darshini Shah, Kanisha Shah, Akshay Murty, Ronald Nath, Shivendra Chauhan, Shakti Sagar and Abhash Bhattacharya. I have spent the most wonderful years of my life in the company of my VIT friends.

Lastly, this has been as much of my journey through grad school as of my beautiful, caring, supportive and loving wife, Nazmeen Qureshi. She is the one who has made it possible for me to be sane enough to carry out my research and complete this work.

DEDICATION

I would like to dedicate this dissertation to my lovely and wonderful Meem Rubeena Qureshi and my thoughtful and wise father Mohammed Hanif Qureshi. Their unconditional love and sacrifice has made it possible for me to achieve all that I have.

ABSTRACT

Mitochondria are essential cellular organelles known for their role in energy production, apoptosis, aging, calcium signaling and others. Due to their essential nature, mitochondria are often under attack by numerous pathogens as a means to promote their infection. Consequently, mitochondrial function is often perturbed during infection, a phenomenon that must be mitigated in order for the host to survive. Cells employ various tactics to repair damaged mitochondria during stresses such as pathogenic infection. One way of countering mitochondrial stress is through the recovery mechanism known as the mitochondrial unfolded protein response (UPR^{mt}). The UPR^{mt} supports mitochondrial recovery by promoting mitochondrial proteostasis via chaperones and quality control proteases, as well as regulating the detoxification of free radicals, and supporting metabolic adaptations. In addition, the UPR^{mt} is also coupled to the regulation of innate immunity, to defend the host against pathogenic infections. However, pathogens have also evolved means to subvert this stress response pathway in an effort to out-maneuver the host. The following dissertation explores the relationship between the UPR^{mt} and bacterial infection by first characterizing an output of the UPR^{mt} that has direct antimicrobial activity. Second, the mechanism by which an opportunistic pathogen, *Pseudomonas aeruginosa*, represses the UPR^{mt} protective pathway is explored both at the level of pathogen and the host.

TABLE OF CONTENTS

COPYRIGHT i
ACKNOWLEDGEMENT ii
DEDICATION iv
ABSTRACT v
TABLE OF CONTENTS vi
LIST OF TABLES viii
LIST OF FIGURES ix
1. On the offense and defense: mitochondrial recovery programs amidst targeted pathogenic assault 1
ABSTRACT 1
INTRODUCTION 2
MITOCHONDRIAL SURVEILLANCE MECHANISMS 4
MITOCHONDRIA AS A TARGET OF BACTERIAL PATHOGENS 14
MITOCHONDRIAL RECOVERY MECHANISMS DURING INFECTION 24
CONCLUSION 29
REFERENCES 31
FIGURES 58
2. A nematode-derived, mitochondrial stress signaling-regulated peptide exhibits broad antibacterial activity 64
ABSTRACT 64
INTRODUCTION 65
RESULTS 67
DISCUSSION 73
MATERIALS AND METHODS 76
REFERENCES 82
FIGURES 87
3. A pathogen branched-chain amino acid catabolic pathway subverts host survival by impairing energy metabolism and the mitochondrial UPR 95
ABSTRACT 95
INTRODUCTION 96
RESULTS 98

DISCUSSION 109
MATERIAL AND METHODS 113
REFERENCES 126
FIGURES 135
4. Elucidating valine's pro-survival role during infection via the mitochondrial UPR 163
ABSTRACT 163
INTRODUCTION 165
RESULTS 167
DISCUSSION 172
MATERIALS AND METHODS 175
REFERENCES 178
FIGURES 181

LIST OF TABLES

Table 2.1 MBCs of various bacterial strains following CNC-4 treatment. 94
Table 2.2 The effects of salts and pH on MBCs of CNC-4 against *E. coli* W3110..... 94
Table 4.1 Survival statistics 190

LIST OF FIGURES

Figure 1.1 Mitochondrial recovery pathways. 58
Figure 1.2 Bacterial pathogens and their target: the mitochondrion..... 61
Figure 1.3 Engagement and subversion of mitochondrial recovery pathways during bacterial pathogen infection..... 63
Figure 2.1 The expression of *cnc-4* is upregulated during mitochondrial stress signaling..... 87
Figure 2.2 CNC-4 demonstrates antibacterial activity..... 88
Figure 2.3 The GGYG motif is necessary for CNC-4 antibacterial activity 90
Figure 2.4 CNC-4 exposure results in increased bacterial membrane permeability..... 91
Figure 2.5 CNC-4 localizes intracellularly and directly binds DNA..... 92
Figure 2.6 CNC-4 does not exhibit toxicity to mammalian epithelial cells..... 93
Figure 3.1 *P. aeruginosa* FadE2 mediates the repression of the UPRmt 136
Figure 3.2 *P. aeruginosa* impairs host mitochondrial activity via FadE2 138
Figure 3.3 *P. aeruginosa* FadE2 is an acyl-CoA dehydrogenase involved in valine and leucine catabolism 140
Figure 3.4 Host metabolic gene expression is repressed with *P. aeruginosa* in a FadE2 dependent manner..... 142
Figure 3.5 *P. aeruginosa* FadE2 mediates the suppression of host energy pathways during infection 144
Figure 3.6 Valine or leucine supplementation is sufficient to restore the UPR^{mt} and protect the host during infection 146
Figure 3.7 Model..... 148
Figure 4.1 Valine supplementation results in changes to gene expression in wild-type animals during chronic *P. aeruginosa* infection. 181
Figure 4.2 The transcription factor MLS-2 is a positive mediator of valine-induced UPR^{mt} activity during chronic *P. aeruginosa* infection. 183
Figure 4.3 *P. aeruginosa* infection downregulates *mls-2* gene expression due to a lack of valine availability..... 185
Figure 4.4 Valine promotes host survival during infection via MLS-2. 186
Figure 4.5 MLS-2 acts cell non-autonomously in the regulation of the UPR^{mt} 187
Figure 4.6 Forward genetic screen for suppressors of *mls-2(tm252gf)* activation of the UPR^{mt}.189

1. On the offense and defense: mitochondrial recovery programs amidst targeted pathogenic assault

Siraje A. Mahmud, Mohammed A. Qureshi, and Mark W. Pellegrino*

Department of Biology, University of Texas Arlington, Arlington, Texas, USA

*corresponding author: mark.pellegrino@uta.edu

ABSTRACT

Bacterial pathogens employ a variety of tactics to persist in their host and promote infection. Pathogens often target host organelles in order to benefit their survival, either through manipulation or subversion of their function. Mitochondria are regularly targeted by bacterial pathogens owing to their diverse cellular roles, including energy production and regulation of programmed cell death. However, disruption of normal mitochondrial function during infection can be detrimental to cell viability because of their essential nature. In response, cells use multiple quality control programs to mitigate mitochondrial dysfunction and promote recovery. In this review, we will provide an overview of mitochondrial recovery programs including mitochondrial dynamics, the mitochondrial unfolded protein response (UPR^{mt}), and mitophagy. We will then discuss the various approaches used by bacterial pathogens to target mitochondria which result in mitochondrial dysfunction. Lastly, we will discuss how cells leverage mitochondrial recovery programs beyond their role in organelle repair, to promote host defense against pathogen infection.

INTRODUCTION

Bacterial pathogens leverage an array of effector molecules to undermine their host by modulating host cell function, metabolism, and survival. In doing so, these effector proteins can benefit the pathogen by liberating essential nutrients, providing a more favorable growth environment, and/or eluding host antimicrobial defense systems. To manipulate host cell function, bacterial pathogens often target and alter cellular organelles and structures to their advantage. For example, various pathogens target the ER and endolysosomal network of the host cell [1, 2]. This targeting strategy is often used by intracellular pathogens that must survive and replicate within host cells through the creation of specialized vacuoles that provide a protective niche. The nucleus is also targeted by bacterial pathogens in order to promote their infection. Here, pathogens can modulate host gene expression through the use of specialized effectors known as nucleomodulins that have multiple targets such as transcription factors, histones, and splicing factors [3]. In addition, bacterial pathogens often target the host cell cytoskeleton to promote their infection. For example, the intracellular pathogen *Listeria monocytogenes* hijacks the host actin network via the virulence factor ActA to promote its migration throughout the cell [4]. Also, the pathogen *Salmonella enterica* subverts the host actin network in order to internalize itself into non-phagocytic cells [5]. Finally, mitochondria, the "powerhouse of the cell", are repeatedly targeted by bacteria owing to their central role in mediating various essential cell functions. The interplay between bacterial pathogen and mitochondria will be the main focus of this review.

These pathogen-associated effector molecules, however, require access to the host cell interior to execute these diverse cell manipulations, that is achieved using elaborate secretion systems. There are currently seven known multimeric secretion complexes (Types I-VII) [6-8], each secreting specific classes of bacterial effectors. Once inside the host cell interior, the effector must be

directed to their intended compartment, often via specific targeting sequences embedded in their protein sequence. In response to these pathogen attacks, host cells must engage immunity programs and possibly alter their metabolism as a means of defense. Equally as important, host cells must at times promote repair of these targeted organelles to ensure proper function.

Mitochondria mediate a diverse set of principal functions in eukaryotic cells. In addition to serving as the main locale of ATP production, mitochondria also play important roles in ion homeostasis, fatty acid metabolism, iron-sulfur cluster biogenesis, calcium storage, and importantly, programmed cell death (also known as apoptosis). Mitochondria mediate energy production through the actions of multimeric electron transport chain complexes that drive OXPHOS. Therefore, it is not surprising that mitochondria are frequently targeted by microbial pathogens due to their critical importance, but also because these organelles are rich in heme and iron-sulfur proteins [9], which are scarce resources crucial for pathogen survival [10, 11]. Moreover, manipulating cell-death pathways allow bacterial pathogens to eradicate cells that hinder their survival (e.g. immune cells such as macrophages) or, in the case of intracellular pathogens, to prevent cell death allowing their propagation [12]. Mitochondria also play an influential role in regulating the immune response [13] that can be compromised during infection by certain pathogens.

Considering their importance, mitochondria are often targeted by bacterial pathogens in an effort to support their survival and/or transmission. Considerable effort has been devoted to understanding the molecular basis of mitochondrial targeting by bacterial pathogen effectors and how these effector molecules subvert host physiology. In addition, how the host responds to these pathogenic insults is of equal interest. This review will first summarize the mechanisms used by host cells to recover damaged mitochondria. This will be followed by a survey of known bacterial

effectors that target mitochondria. We will then discuss mitochondrial-associated defense programs that are leveraged to promote host protection during infection.

MITOCHONDRIAL SURVEILLANCE MECHANISMS

Impaired mitochondrial function can have dramatic effects on cell viability. Consistently, a number of human pathologies are associated with mitochondrial dysfunction including cancer, neurodegenerative disease, and diabetes, as well as being part of the normal aging process [14]. Disorder to mitochondrial function is also observed during infection by either bacterial or viral pathogens [15]. As a countermeasure to this dysfunction, cells employ various mitochondrial recovery pathways that promote homeostasis and survival. The following section will provide an overview of three such recovery mechanisms: mitochondrial dynamics, the mitochondrial unfolded protein response, and mitophagy (Figure 1.1).

Mitochondrial Dynamics

Mitochondria are not static organelles. Rather, mitochondria are constantly in a state of flux with regards to size and form. Referred to as mitochondrial dynamics, mitochondria undergo two general phases. First, mitochondria can undergo fusion whereby distinct mitochondria merge and blend each organelle's materials to promote recovery from damage. Second, mitochondria undergo fission involving the scission of mitochondria, which can be coupled with the removal of damaged areas by mitophagy (see section "Mitophagy") [16].

Mitochondrial fusion

Mitochondrial fusion involves the merging of the outer and inner mitochondrial membranes, with each sub compartment having their own set of regulators. Two large evolutionary conserved GTPases constitute the core machinery involved in the fusion of mitochondrial outer membranes: Mfn-1 and Mfn-2. Mitofusins insert themselves in the outer membrane via their transmembrane domains, with their GTPase domain exposed to the cytosol. They also possess coiled-coil HR domains, HR1 and HR2, [17, 18], which are thought to be exposed to the cytosolic face and intermembrane space, respectively [19]. The GTPase and/or HR domains of each mitochondrion interact with one another and GTP hydrolysis stimulates the actual fusion of the outer membranes [18, 20, 21]. Based on the topology that places the HR2 domain in the intermembrane space, it has been suggested that redox signaling may promote mitochondrial fusion via cysteine residues in the HR2 domain that are oxidized [19]. According to this model, the oxidation of cysteine residues promotes disulfide bond formation and the oligomerization of Mitofusins that is necessary for mitochondrial outer membrane fusion.

Mitochondrial inner membrane fusion proceeds after the fusion of the outer membranes and is regulated by a distinct GTPase, OPA1 [22]. OPA1 is inserted in the inner membrane via its amino-terminal targeting sequence and transmembrane domain [23]. Interestingly, while the OPA1 GTPase domain displays *bona fid*e GTP hydrolysis activity, its role during the fusion process is unclear. Also, OPA1 is subject to proteolytic cleavage, generating multiple isoforms designated as either L-OPA1 or S-OPA1 [24-27]. Multiple enzymes have been implicated in the processing of mammalian OPA1, including YMEL1, OMA1, and PARL [22, 24, 25, 28]. Whether PARL plays a direct role in OPA1 processing is somewhat controversial. Also, PARL is not required to generate the S-OPA1 isoform *per se* but rather is involved in mediating subsequent processing steps leading

to a fully functional S-OPA1 protein. There are also conflicting reports on the role these isoforms play during mitochondrial inner membrane fusion. While some studies have suggested that both L- and S-OPA1 isoforms are necessary for fusion [27], others have shown that the L-OPA1 isoform alone is sufficient [29]. Lastly, it is believed that coordination exists between the fusion machinery of the mitochondrial outer and inner membranes. Indeed, OPA1-mediated mitochondrial inner membrane fusion relies on the fusion GTPase MFN1 [30].

Mitochondrial fission

Mitochondrial fission is regulated by the GTPase DRP1 and mitochondrial FIS1. DRP1 is a cytosolic protein that localizes to future sites of mitochondrial fission but lacks any noticeable mitochondrial targeting sequence. Instead, DRP1 is recruited to these sites due to the actions of FIS1 and, in yeast, with the assistance of adaptor proteins Mdv1p and Caf4p [31]. The mechanism is somewhat different in mammals since no clear homologs of Mdv1p and Caf4p appear to exist. Alternatively, recruitment of DRP1 is accomplished by anchoring proteins MFF and MiD49 and MiD51 [32, 33]. DRP1 oligomerizes in a ring-like pattern around mitochondria causing a modest constriction [34]. Further constriction occurs following DRP1 GTP hydrolysis, which precedes division [35, 36]. While DRP1-mediated constriction marks sites of future scission, it is not sufficient for division by itself [37]. It is believed that DRP1 requires extra factors to mediate the scission of mitochondria. Indeed, it has been suggested that the GTPase DNM2 assists DRP1 in executing mitochondrial fission [38]. However, a more recent investigation provides evidence opposing this model [39]. In this study, fibroblast cells devoid of all three mammalian dynamins (DNM1, DNM2, DNM3) were found to have negligible effects on mitochondrial morphology in multiple cell lines tested. Individual knockout of DNM2 yielded a similar result. Furthermore,

DNM2 was generally cytoplasmic but not present at mitochondria or in its vicinity, whereas DRP1 showed clear localization to sites of mitochondrial fission. Thus, it may be possible that DNM2 possesses cryptic roles in mitochondrial fission that may only be revealed under specific contexts or cell types.

Interestingly, while DRP1-mediated constriction marks sites of mitochondrial fission, the initial step of division involves marking of the site by ER tubules. In a seminal study using high-resolution microscopy, Friedman et al. (2011) discovered that sites of mitochondrial constriction and scission co-localized with ER tubules in yeast and mammalian cells [40]. Further, ER tubule-mitochondrial contact sites co-localized with DRP1/DNM1 to mediate mitochondrial fission. Temporally, ER tubules mark the sites of constriction prior to the recruitment of DRP1 [40]. ER tubules not only mark the sites of mitochondrial division but also that of mitochondrial fusion. Here, mitofusins were shown to accumulate at ER-mitochondrial contact sites to drive fusion [41]. Since ER tubules mark both the sites of mitochondrial fusion and fission, there must be signals that dictate one outcome over the other. Indeed, while depolarization of mitochondria was shown to drive ER-mitochondrial contact site mediated mitochondrial fusion [41], it should be noted that it is also associated with mitochondrial fission suggesting other regulators that need to be identified.

Mitochondrial Unfolded Protein Response (UPR^{mt})

The mitochondrial proteome relies heavily on quality control systems to maintain efficient folding and assembly of proteins by molecular chaperones, while simultaneously promoting the turnover of unfolded/misfolded proteins via mitochondrial proteases [42]. The capacity of mitochondrial

protein quality control systems can be challenged due to stresses such as damaging ROS and toxins. Thus, there is a critical need to induce these systems during times of stress, including the activation of retrograde signaling pathways. Retrograde signaling refers to the production of a signal that is sent to the nucleus, resulting in changes to gene expression as a response to altered organelle function. This type of signaling is relevant with respect to mitochondrial protein quality control since the machinery related to mitochondrial proteostasis is encoded by the nuclear genome. The UPR^{mt} is a prominent retrograde signaling pathway involved in mitigating stress to mitochondria and promoting protein quality control. In addition, the UPR^{mt} mediates other cell functions important for recovery including detoxification of damaging ROS, regulation of mitochondrial dynamics, and metabolic adaptation [43]. Another notable retrograde signaling pathway is the yeast retrograde response. This pathway mediates metabolic adaptations to stress via the transcription factors Rtg1 and Rtg3 [44, 45]. Rtg3 is subject to phosphorylation when mitochondria are healthy causing it to be retained in the cytoplasm in complex with Rtg1. During stress, Rtg3 is partially dephosphorylated, resulting in transit of the Rtg1/3 complex to the nucleus. The phosphorylation status of Rtg3 is under the control of positive (Rtg2, Grr1) and negative regulators (Mks1, Bmh1/2). Rtg2, a cytoplasmic protein possessing an N-terminal ATP-binding domain [46], promotes the dephosphorylation of Rtg3 by inhibiting the phosphoprotein Mks1 [47]. Mks1 inhibits Rtg3 dephosphorylation when in a complex with the 14-3-3 proteins Bmh1/2p [48, 49]. Bmh1/2p prevents the ubiquitination and subsequent degradation of Mks1 by Grr1, a F-box component of the SCF E3 ubiquitin ligase [47, 50].

The UPR^{mt} was first discovered in mammalian cell culture when conditions of mitochondrial stress were found to induce the transcriptional upregulation of mitochondrial proteostasis genes such as the mitochondrial chaperone *Hsp60* and protease *ClpP*, while genes related to ER protein

homeostasis were unaffected [51]. The transcription factor CHOP appears to directly regulate the expression of these genes [52]. Additionally, the kinase JNK2 also has a role in regulating the UPR^{mt} since it is phosphorylated during stress and also induces mitochondrial proteostasis gene expression, likely via regulation of CHOP [53].

Undoubtably, the study of the UPR^{mt} made significant advancements using the nematode model organism *Caenorhabditis elegans*. Among its many advantages is its transparency that allows for easy use of fluorescent reporters, and the power of its genetics to understand complex cellular pathways. The generation of transcriptional GFP reporters in *C. elegans* as a proxy for UPR^{mt} activity fundamentally advanced our understanding of the UPR^{mt} [54]. Leveraging these advantages, Haynes et al. (2007) conducted a genome-wide RNAi screen to identify regulators of the UPR^{mt} [55]. Three notable regulators were discovered: the mitochondrial matrix protease CLPP-1, the homeodomain-containing transcription factor DVE-1, and UBL-5. The nuclear localization of DVE-1 is enriched during mitochondrial stress, and UBL-5 is suggested to form a complex with this transcription factor. The function of the CLPP-1 was further clarified with a follow-up study that identified the mitochondrial ATP-binding cassette protein HAF-1 as a positive regulator of the UPR^{mt} [56]. HAF-1 is thought to mediate the efflux of peptides that are likely generated by CLPP-1 protease. HAF-1 appears to be a modest modulator of this stress response since it only appears to be required during times of specific stress conditions [57, 58]. A critical finding from the HAF-1 study was the identification of the bZIP transcription factor ATFS-1 that acts downstream of HAF-1 peptide efflux in the regulation of the UPR^{mt} [56]. A pivotal follow-up study resolved the mechanism of ATFS-1 regulation involving mitochondrial import efficiency [58, 59]. In addition to a nuclear localization signal, ATFS-1 contains a mitochondrial targeting sequence at its amino-terminus that directs its localization to healthy mitochondria where

it is degraded by LonP protease. However, transit into mitochondria is reduced during stress due to impaired mitochondrial protein import efficiency [58]. In addition, the mitochondrial targeting sequence of ATFS-1 is relatively weak, likely conferring an ability for this transcription factor to efficiently respond to stress conditions that impair mitochondrial import [60]. Nuclear ATFS-1 transcriptionally regulates a suite of mitochondrial protective genes that support recovery and organismal fitness during stress. As part of the UPR^{mt} recovery program, ATFS-1 was also found to directly repress OXPHOS gene expression from both the nuclear and mitochondrial genomes to support organelle recovery, while simultaneously promoting the expression of glycolytic genes as an alternative energy supply [61].

Other modes of UPR^{mt} regulation have since been unveiled. Notably, the regulation of the UPR^{mt} is reliant on remodeling of chromatin. Specifically, the histone methyltransferase MET-2 and the nuclear co-factor LIN-65 were found to mediate the di-methylation of histone H3K9 [62]. Remodeling by MET-2/LIN-65 was found to silence global chromatin while simultaneously opening up regions for the binding of DVE-1 to induce the UPR^{mt}. In addition to MET-2/LIN-65, the histone demethylases JMJD-1.2 and JMJD-3.1 were also discovered as positive regulators of the UPR^{mt}, as well as the histone acetylase HDA-1 [63, 64]. Outside of chromatin remodeling, biosynthesis of the lipid ceramide was also found to regulate the UPR^{mt}, in addition to the mevalonate pathway [65]. Interestingly, ATFS-1 was found to regulate components of the mevalonate pathway [66], supporting its importance for this stress response.

Remarkably, the UPR^{mt} can be activated in tissues that are not experiencing any apparent stress. Indeed, neurons act as central hubs that transmit stress signals (also known as mitokines) to distal tissues, resulting in cell non-autonomous activation of the UPR^{mt} [67]. Multiple mitokines have

since been revealed that mediate cell non-autonomous activation of the UPR^{mt} including the neurotransmitter serotonin, the neuropeptide FLP-2, and lastly Wnt [68-70].

Finally, the identity of the mammalian homolog of ATFS-1 gained much interest following its discovery in *C. elegans*. Based on protein homology, the bZIP transcription factor ATF5 was identified as a likely homolog of ATFS-1 that regulates the mammalian UPR^{mt} [71]. Similar to ATFS-1, ATF5 possesses a mitochondrial targeting sequence and is regulated by mitochondrial protein import efficiency. ATF5 is also associated with the regulation of mitochondrial proteostasis genes [71-74]. Mammalian ATF5, but not the closely related ATF4, was able to functionally rescue a *C. elegans atfs-1* mutant, indicating that it is the true homolog of ATFS-1 [71]. However, other studies have suggested that ATF4 is the mediator of a UPR^{mt} or alternative stress signaling pathway [75, 76]. Interestingly, ATF5, ATF4 and CHOP function together in other biological contexts such as the ISR [77, 78]. Briefly, the ISR copes with cellular stress by downregulating protein synthesis through the activities of four separate kinases: PERK, GCN2, PKR, and HRI (reviewed in [79]). Global translation rates are attenuated via the phosphorylation of eIF2a, which results in the preferential synthesis of other targets including ATF4, ATF5, and CHOP via the translation of upstream open reading frames that exist in each mRNA. ATF5 can be transcribed by both CHOP and ATF4 [77, 78]. Recently, it was found that during mitochondrial stress CHOP fine-tunes the stimulation of ATF4 via interaction with C/EBPb so as to prevent exacerbated activation that could lead to cell death [80]. The role of ATF5 during this mitochondrial adaptive response is still not fully resolved.

Mitophagy

While stress responses such as the UPR^{mt} attempt to repair dysfunctional mitochondria, those that are irreparably damaged may pose significant risks to the cell due to build-up of damaging ROS and the possibility of inducing mitochondrial-associated programmed cell death. Thus, severely impaired mitochondria need to be eliminated for the benefit of the cell as a whole. Autophagy refers to lysosomal-mediated degradation of intracellular contents that is provoked either by nutritional stress or as a response to cellular damage [81]. Autophagy involves the encapsulation of cellular contents by a double-membrane structure forming the autophagosome, which then fuses with the lysosome for degradation [82]. A key player of autophagy is the soluble protein LC3. When conjugated to phosphatidylethanolamine, LC3 binds to autophagosomal membranes to recruit substrates to be turned over [83]. An important outcome of autophagy is the recovery of fatty acids and amino acids that can be used for energy production when cells are experiencing nutrient stress. Mitophagy is a specialized form of autophagy that is activated by a variety of stresses including oxidative stress, disruptions to proteostasis, hypoxia, and loss of mitochondrial potential [84]. The execution of mitophagy is achieved through the use of specialized regulators that can be divided into two general groups: receptor-mediated and ubiquitin-mediated. The following will briefly review the key elements of each mechanism.

Receptor-mediated mitophagy

This form of mitophagy employs receptors at the mitochondrial outer membrane that bind protein subfamily members of the mammalian Atg8 family in the formation of the autophagosome: LC3 (including LC3A-C), and GABARAP (including GABARAP-L1 and GABARA-L2). While the

yeast model system has uncovered important insights into the regulation of receptor-mediated mitophagy, some differences exist with the mammalian system that are worth noting. For instance, in yeast the mitophagy receptor Atg32 is presented at the mitochondrial outer membrane which promotes the fusion with the autophagosome following binding to the receptors Atg8 and Atg11 [85]. Mammalian receptor-mediated mitophagy is regulated by various receptors, including FUNDC1. Mechanistically, phosphorylation by ULK1 and PGAM5 mediates the binding of FUNDC1 to LC3 [86]. Other members involved in receptor-mediated mitophagy include NIX [87], Bcl2L13 [88], and BNIP3 [89]. In addition, the receptor FKBP8 has also been implicated in receptor-mediated mitophagy [90]. Overexpression of FKBP8 induces mitochondrial fission, similar to the receptors BNIP3 and NIX. However, each of these receptor proteins bind specific members of the Atg8 protein family: FUNDC1 and BNIP3 bind LC3B [91, 92], NIX binds GABARAP-L1 [87], and finally FKBP8 can directly recruit LC3A [90].

Ubiquitination-mediated mitophagy

The main players in the ubiquitination-mediated pathway are PINK1 and the E3 ubiquitin ligase Parkin. Briefly, ubiquitination-mediated mitophagy involves the presentation of PINK1 at the mitochondrial outer membrane during stress which recruits and phosphorylates Parkin, thus activating its E3 ubiquitin ligase activity [93]. Intriguingly, the regulation of PINK1 closely mirrors that of the UPR^{mt} regulators ATFS-1/ATF5, whereby each are controlled by mitochondrial protein import efficiency. Much like ATFS-1/ATF5, PINK1 contains a mitochondrial targeting sequence that directs its localization to healthy mitochondria, whereupon it is degraded by the protease PARL [94, 95]. However, mitochondrial import efficiency of PINK1 is reduced during stresses that cause reductions in mitochondrial membrane potential, resulting in its accumulation

at the outer membrane and the recruitment/phosphorylation of Parkin [96, 97]. A variety of stress conditions have been implicated with PINK1/Parkin activation including mitochondrial uncouplers, disruption to OXPHOS, ROS, and mitochondrial proteotoxicity [98-101]. Parkin mediates the ubiquitination of multiple outer membrane substrates that mark the damaged mitochondrion for mitophagy [102]. Adaptor proteins then mediate the interaction of the ubiquitinated proteins with LC3, allowing for engulfment by the autophagosome and fusion with the lysosome [103].

MITOCHONDRIA AS A TARGET OF BACTERIAL PATHOGENS

Bacterial pathogens alter mitochondrial function using various approaches, notably through the production of virulence factors that are directed to the organelle using precise targeting sequences [1]. During both intracellular and extracellular bacterial infection, various bacterial effector proteins are secreted into the host cell by a variety of complex secretory machines [15, 104]. Once released into the host cell cytosol, bacterial effector proteins must then be targeted to the correct cellular location. Typically, effector proteins are fully equipped with this targeting information, and exploit the host cell's protein transit pathways through molecular mimicry of eukaryotic transit signals. The consequences of effectors that are targeted to mitochondria are variable, but manipulation of apoptosis is typically observed [105]. The outcome of whether apoptosis is induced or prevented is likely dependent on the bacterial pathogen's infection strategy. For instance, it is often beneficial to the pathogen to induce apoptosis in host cells that mediate an anti-bacterial response such as immune cells, whereas it would be beneficial to prevent cell death for those pathogens that persist intracellularly. Mitochondria promote apoptosis through a mechanistically complex process involving the release of cytochrome c from the intermembrane

space to the cytosol through pores formed by Bax and Bak. Cytosolic cytochrome c then binds to Apaf-1, stimulating the formation of the apoptosome and the induction of cell death [106].

Eukaryotic proteins that are targeted to mitochondria use a highly regulated system of protein sorting. Mitochondria possess their own genome that transcribes and translates a subset of proteins that constitute the mitochondrial proteome. However, the majority of the mitochondrial proteome is encoded by the nucleus [107-109]. Nuclear-encoded mitochondrial proteins are synthesized on cytosolic ribosomes and transit to specific mitochondrial sub-compartments based on precise signal sequences embedded in their protein sequence (Figure 1.2) [110]. Mitochondria possess multiple sub-compartments including an outer membrane, intermembrane space, inner membrane, and matrix, each employing specific protein import pathways. The machinery involved with mitochondrial protein sorting is complex and involves the following critical components: (1) The TOM complex represents the initial entry point for incoming mitochondrial proteins. The TOM complex mediates the translocation of mitochondrial proteins across most sub-compartments; (2) the SAM complex inserts β-barrel proteins into the outer membrane; (3) the MIA machinery mediates the localization of proteins destined for the intermembrane space; (4) The TIM complex facilitates the transfer of proteins to the inner membrane or matrix with the assistance of the PAM complex. Proteins entering the TIM complex contain specific amino-terminal mitochondrial targeting sequences that are cleaved by the MPP, (5) the chaperone complex (TIM9-TIM10) assists with the transport of hydrophobic precursor proteins through the intermembrane space for delivery to either the TIM22 complex for insertion into the inner membrane or to the SAM complex for insertion into the outer membrane. Bacterial pathogens can manipulate the mitochondrial import pathway through molecular mimicry. For example, bacterial effector proteins often contain a

similar mitochondrial targeting sequence domain that directs their localization to mitochondria, as outlined below.

Despite mitochondria and bacteria having similar structures, bacterial pathogens are likely unaffected by toxins containing a mitochondrial targeting sequence since they lack the necessary mitochondrial import machinery. With regards to other mitochondrial-directed small molecule toxins, bacterial pathogens are also impervious to their effects despite having similar structures. For example, hydrogen cyanide is produced by some bacterial pathogens which targets the mitochondrial electron transport chain and impairs cellular respiration. Even though mitochondria and bacteria share some similarities in their respiratory system, many bacteria are unaffected by this toxin since they express appropriate detoxification systems and have respiratory components that are resistant to its inhibitory effects [111, 112].

BACTERIAL EFFECTORS THAT TARGET MITOCHONDRIA

Bacterial pathogens can possess one or more effector proteins or compounds that target mitochondria. Once they reach mitochondria, they carry out their prescribed function and modulate organelle activity. Herein, we briefly discuss a collection of clinically relevant intra- and extracellular pathogens and the effector molecules they produce that target mitochondria (Figure 1.2).

Extracellular pathogens

Vibrio cholerae

V. cholerae is an extracellular pathogen that causes acute symptoms of diarrhea via the cholera toxin that increases the production of cyclic AMP through modulation of adenylate cyclase [113]. In addition, *V. cholerae* promotes its virulence by targeting mitochondria. Recently, *V. cholerae* was shown to target mitochondria via VopE, a virulence factor that gains access to the cell interior via the T3SS [114]. VopE contains a mitochondrial targeting sequence at its amino-terminus that allows precise targeting to mitochondria by hijacking the mitochondrial import machinery [115]. Interestingly, VopE interacts with the GTPase Miro at the mitochondrial outer membrane. This interaction was found to perturb mitochondrial perinuclear clustering which is needed to activate MAVS-mediated NF-kB signaling, an important contributor to the host inflammatory response (see "Mitochondrial dynamics and MAVS signaling") [115]. In addition, *V. cholerae* disrupts mitochondrial function by elevating ROS production through the production of Chx and GbpA, two virulence factors that promote intestinal colonization by suppressing the immune response and increasing mucus production, respectively [116, 117]. *V. cholerae* also produces cytolysin (VCC), a pore-forming toxin that leads to permeabilization of target cell membranes [118]. The anion channel activity of cytolysin was later found to stimulate mitochondrial-associated apoptosis of enteric cells, leading to the severe diarrheal symptoms that is characteristic of this infection [119]. Lastly, OmpU, a major porin in *V. cholerae,* promotes apoptosis of innate immune cells through modulation of the mitochondrial permeability transition pore, an inner mitochondrial membrane protein complex that regulates small molecule flux and cell death in response to physiological cues [120].

Pseudomonas aeruginosa

P. aeruginosa, a Gram-negative facultative pathogen, causes severe infections in immunocompromised individuals, those with cystic fibrosis, and burn victims. *P. aeruginosa* can

cause significant morbidity following colonization of the respiratory tract. The respiratory tract employs certain barriers to prevent the presence of *P. aeruginosa* including the production of mucus and the actions of immune cells. However, *P. aeruginosa* produces various virulence factors that disrupt these structural barriers, predominantly through the induction of apoptosis. For example, *P. aeruginosa* secretes an effector, ExoT, through its T3SS, which promotes mitochondrial-associated apoptosis by reducing mitochondrial membrane potential and increasing levels of proapoptotic proteins Bax, Bid, and Bim, ultimately causing the release of cytochrome c [121]. Its quorum-sensing molecule, 3-oxo-C12-HSL, also disrupts mitochondrial structure, promotes ROS generation, and induces apoptosis within bronchial epithelial cells by reducing the expression of PGC-1α [122]. *P. aeruginosa* also produces phenazine derivatives such as pyocyanin and 1-hydroxyphenazine that inhibit mitochondrial respiration [123]. In addition, *P. aeruginosa* impairs mitochondrial OXPHOS through production of toxins such as cyanide and siderophores (that compete for host iron) resulting in dysfunction [124, 125].

Enteropathogenic *Escherichia coli*

EPEC is a human intestinal pathogen which causes severe diarrhea symptoms, likely due to its ability to promote apoptotic death of epithelial cells during infection [126]. The pathology of EPEC infections is thought to be linked to two virulence factors, Map and EspF, both of which target mitochondria. Much like *V. cholerae* VopE, each of these effector proteins contain a mitochondrial targeting sequence allowing their entry via mitochondrial import pathways. Map has modest effects on mitochondrial morphology and membrane potential [127]. It has been hypothesized that mitochondrial targeting of Map may serve a protective role to reduce cytosolic levels of this effector protein in order to prevent it from reorganizing the actin cytoskeleton network [128]. Indeed, the effect of Map on the actin network was found to be independent of its localization to

mitochondria [128]. EspF, on the other hand, is reported to stimulate cell death by triggering the release of cytochrome c from mitochondria [128, 129]. EPEC produces another mitochondrial-associated virulence factor, EspZ, but in contrast to EspF, EspZ delays apoptosis during infection [130, 131]. This effector protein delays apoptosis in part through its ability to associate with the inner mitochondrial membrane where it prevents fluctuations in mitochondrial membrane potential [130]. The contrasting effects of EspZ and EspF with regard to the regulation of apoptosis is intriguing. The timing of EspF and EspZ delivery is likely the determining factor that decides the fate of the host cell: EspZ is delivered into the host cell prior to EspF, thus promoting cell survival until optimal levels of bacterial colonization is achieved and apoptosis can be induced [129, 130, 132].

Neisseria gonorrhoeae

N. gonorrhoeae is responsible for the development of the sexually transmitted disease gonorrhea, and its pathophysiology is intimately related to its ability to evoke apoptosis in both epithelial and immune cells [133]. *N. gonorrhoeae* can execute cell death by transmitting its effector molecules to the host by way of outer membrane vesicles. One of these effector proteins, PorB, targets mitochondria, triggering cytochrome c release and the onset of apoptosis [134, 135]. Interestingly, PorB bears some structural similarity with VDAC [104], a complex that regulates transit of metabolites across the mitochondrial outer membrane. Perhaps owing to their shared structural features, both PorB and VDAC share similar import pathways [136].

Helicobacter pylori

H. pylori is associated with gastric unrest and the development of gastric cancer. An important contributor to the pathogenesis of *H. pylori* infections is VacA, a secreted toxin that targets

mitochondria and induces apoptosis [137]. Increased apoptosis of the gastric epithelium disrupts the monolayer of the gastric epithelium, which may increase gastric cancer risk by facilitating malignant cell expansion or increasing susceptibility to carcinogenic molecules [138]. Intriguingly, while VacA has a confirmed presence in mitochondria, it lacks characteristic features of a classical mitochondrial targeting sequence [139]. VacA translocation to mitochondria results in dysfunction through the formation of anion-selective channels in mitochondrial membranes [140]. This results in loss of mitochondrial membrane potential, release of cytochrome c, and ultimately death of the cell by apoptosis [141, 142].

Intracellular pathogens

Mycobacterium tuberculosis

M. tuberculosis is a facultative intracellular pathogen and the causative agent of tuberculosis. *M. tuberculosis* replicates in a unique phagosome compartment within human macrophages [143]. Successful infection by this pathogen centers on its ability to induce or inhibit apoptosis of host cells. *M. tuberculosis* prevents cell death in order so that it can survive within the host macrophage. Alternatively, *M. tuberculosis* promotes macrophage cell death in order for the pathogen to be released and infect other host cells. This type of cell death shares features of both necrosis and apoptosis [144, 145]. It is likely that *M. tuberculosis* controls the production of pro- and anti-apoptotic effectors so as to allow sufficient growth until it is ready to be released to infect neighboring cells. Various effectors of *M. tuberculosis* that manipulate host cell death are targeted to mitochondria. One representative *M. tuberculosis* protein that targets host mitochondria is Cpn60.2, a cytosolic chaperone protein that prevents apoptosis of the host cell. Mechanistically,

Cpn60.2 crosses the phagolysosome membrane after being released from the bacterial surface. Cpn60.2 is then targeted to mitochondria where it associates with mortalin (also known as GRP75), a mitochondrial protein of the Hsp70 family involved in the prevention of apoptosis. One mechanism used by Mortalin/GRP75 to control apoptosis is through regulation of calcium transfer from the ER to mitochondria via IP3 receptors, whereby mitochondrial calcium levels dictate whether it will adopt an apoptotic fate [146]. Cpn60.2 blocks apoptosis through its interaction with mortalin, thus ensuring bacterial persistence inside the host [147].

In contrast to Cpn60.2, the effector protein PE_PGRS33 promotes cell death in the host macrophage. Historically, PE_PGRS33 was one of the first pathogen proteins found to co-localize with mitochondria [148, 149]. The pro-apoptotic function of PE_PGRS33 is thought to be linked with its highly conserved "linker" region that presumably interacts with TLR2 [148]. The interaction between PE_PGRS33 and TLR2 is believed to stimulate signaling events that culminate with the secretion of TNF-α and, consequently, apoptosis.

Finally, *M. tuberculosis* effector protein LprG (RV1411c/p27) results in changes in mitochondrial dynamics. While *M. tuberculosis* LprG induces mitochondrial fission, it is not the cause of cell death [150]. It is believed that LprG assumes alternative roles outside of controlling cell death, perhaps by modulating host energy status. Indeed, LprG alters mitochondrial calcium uptake and reduces overall respiratory rates through an as-of-yet undescribed mechanism [150].

Legionella pneumophila

This intracellular parasite is the causative agent of legionellosis in humans, a disease with pneumonia-like symptoms. *L. pneumophila* uses the T4SS to inject effector proteins into host cells [151]. One such effector protein is LncP which, curiously, is grouped with members of the

Mitochondrial Carrier Family [152], membranous proteins that mediate the transport of metabolites across the inner membrane of mitochondria. Following its internalization into macrophages, LncP assembles at the mitochondrial inner membrane where it is involved in the transport of ATP [152]. In addition to LncP, *L. pneumophila* also secretes the Ran GTPase activator MitF via the T4SS. MitF induces mitochondrial division and dramatically reduces respiratory efficiency while increasing glycolysis capacity [153]. The rewiring in metabolism from respiration to glycolysis is thought to benefit *L. pneumophila* replication and survival [154]. *L. pneumophila* does not use glucose for respiration but rather other metabolites such as amino acids including serine and alanine [155]. It is believed that *L. pneumophila* induces the glycolytic shift in the infected macrophage to indirectly increase the supply of serine which is produced from the glycolytic intermediate 3-phosphoglycerate [153].

S. enterica

S. enterica is the causative agent of salmonellosis, characterized by symptoms of gastrointestinal distress. Interestingly, *Salmonella* relies on the host inflammatory response to persist. Specifically, *Salmonella* must leverage the inflammatory response in order to damage tissues and liberate important metabolites required for its replication [156, 157]. *S. enterica* produces a T3SS-associated toxin, SopA, to stimulate inflammation. Intriguingly, SopA is targeted to mitochondria during infection [158]. Mechanistically, SopA possesses E3 ubiquitin ligase activity to stimulate interferon-beta activity by targeting proteins of the TRIM family of E3 ubiquitin ligases, TRIM56 and TRIM65 [159]. While the function of TRIM65 in the context of inflammation is not clear, TRIM56 is thought to stimulate RIG-1 signaling through direct ubiquitination of STING [160]. RIG-1 signaling activates MAVS protein and the stimulation of pro-inflammatory cytokine production [161].

Suppression of apoptosis is a common tactic used by invasive enteric pathogens such as *Salmonella* to increase their survival. For example, *S. enterica*-associated effector protein, fimbrial subunit A, FimA, associates with the outer mitochondrial membrane via interaction with VDAC1 resulting in repression of apoptosis [162]. Mechanistically, FimA stalls apoptosis by stabilizing the interaction of VDAC1 with the glycolytic enzyme hexokinase. Interaction between VDAC1 and hexokinase prevents cell death by blocking the release of cytochrome c [163, 164].

Lastly, *S. enterica* effector SipB during infection of macrophages distorts mitochondrial cristae morphology in macrophages that is believed to promote autophagy-mediated cell death by increasing autophagosome numbers [165]. The relationship between SipB-mediated alterations in mitochondrial morphology and the induction of autophagy-related cell death is not fully understood, although there is speculation that changes in mitochondrial dynamics arising from these altered mitochondrial structures may play some role [165].

Chlamydiae

Members of *Chlamydiae* are obligate intracellular parasites due to their lack of machinery to synthesize ATP. Consequently, they must rely on the import of host-derived ATP via an ATP/ADP translocase [166, 167]. Fascinatingly, this pathogen draws mitochondria at their periphery through an ability to form inclusion bodies upon infection [168]. The attraction of mitochondria within the vicinity of the pathogen is thought to facilitate the transfer of ATP [169], possibly through direct targeting of the mitochondrial translocation machinery, including components of the TOM complex (TOM40 and TOM22) [170, 171].

MITOCHONDRIAL RECOVERY MECHANISMS DURING INFECTION

Mitochondrial dynamics and the MAVS pathway

The MAVS pathway is generally regarded as an anti-viral response although, as mentioned previously, bacterial pathogens also engage this pathway as well (Figure 1.3A) [115]. Viral RNA activates the MAVS pathway [172-174]. The bacterial stimulus for MAVS activation is less studied, although bacterial RNA has been implicated [175-179]. The core component of the MAVS pathway are RLRs, a member of a family of receptors controlling innate immunity that include RIG-1, MDA5, and LGP2. Members of the RLR family possess conserved features [180], including a DExD/H-box helicase domain and C-terminal domain which mediates its binding to pathogen RNA and, as for RIG-1 and MDA5, two N-terminal CARDs important for signaling necessary to induce an immune response. RIG-1 becomes activated by post-translational modifications upon detection of pathogen RNA. Specifically, RIG-1 is ubiquitinated by various ubiquitin ligases including TRIM25 RING-finger E3 ubiquitin ligase [181, 182]. Ubiquitination of RIG-1 is necessary for its association with MAVS at the mitochondrial outer membrane [183]. Once complexed, RIG-1-MAVS then form functional aggregates via interactions of their CARD domains that promotes recruitment of a suite of E3 ligases and its ubiquitination [173, 184]. Ubiquitinated RIG-1-MAVS complex is then primed to activate the kinases TBK1 and IKKe that stimulate an immune response via IRF3 and NF-kB [173, 185]. Interestingly, a recent study has demonstrated a relationship between mtDSBs and the stimulation of the RIG-1-MAVS immune pathway [186]. Here, mtDSBs promote the release of mitochondrial RNA into the cytoplasm via Bax and Bak which stimulates RIG-1-MAVS immune signaling. In addition, mtDSBs were found

to synergize with immune responses provoked by nuclear DNA damage as a means to create a powerful pathogen defense mechanism.

Mitochondrial dynamics plays a key role in the regulation of RIG-1 signaling. Indeed, activation of RLR signaling following viral infection results in mitochondrial elongation [187]. As well, the promotion of mitochondrial fusion via knockdown of mitochondrial fission regulators accelerated MAVS signaling [187]. In addition, MAVS was found to promote mitochondrial fusion through direct interaction with MFN1 [187].

Viral and bacterial pathogens target mitochondrial dynamics to modulate RIG-1 innate immune signaling and promote infection. For example, Hepatitis C virus promotes DRP1-mediated mitochondrial fission to suppress MAVS signaling [188]. Consistently, genetic suppression of mitochondrial fission led to increased MAVS signaling and lower viral secretion [188]. As mentioned previously, the bacterial pathogen *V. cholerae* secretes the effector VopE which modulates mitochondrial dynamics through direct interaction with Miro GTPases, ultimately suppressing MAVS-mediated NF-kB signaling [115]. Other pathogens have been found to promote mitochondrial fission that could potentially alter MAVS-signaling. For instance, *L. monocytogenes* secretes listeriolysin O, a pore-forming toxin that results in transient mitochondrial fission and other impairments to mitochondrial function [189]. In addition, *Brucella abortus*, an intracellular pathogen causing a variety of complications in its human host [190], also induces mitochondrial fission during infection [191]. Interestingly, both *L. monocytogenes* and *B. abortus* induce mitochondrial fragmentation in a DRP1-independent manner [191]. Alternate mechanisms of promoting mitochondrial fission during infection have been proposed. For example, the ER continues to mark the sites of mitochondrial fission in *L. monocytogenes* listeriolysin O exposed cells despite a lack of DRP1 [192]. Importantly, actin was also found to mediate mitochondrial

fragmentation in the presence of this toxin [192], whereas it had no role in *B. abortus* [191]. Lastly, and in addition to *L. monocytogenes* and *B. abortus*, VacA from *H. pylori* was also found to promote mitochondrial fission through recruitment and activation of DRP1[193].

The UPR^{mt}: coupling mitochondrial repair to host resistance

Much of what is known regarding the relationship between the UPR^{mt} and pathogen infection is based on studies using the *C. elegans* model system (Figure 1.3B). *C. elegans* exists within microbe-enriched environments, particularly decaying plant matter. As such, it will feed on a diverse array of microbes that may be beneficial or detrimental to its fitness [194]. As is clear from this review, many pathogens produce toxins that target mitochondria. Thus, it seemed only plausible that some microbes would activate the UPR^{mt} in response to these damaging substances. With this in mind, Liu et al. (2014) surveyed a collection of microbes normally encountered by *C. elegans* in its natural environment and indeed, they discovered that many of these microbes activated the UPR^{mt} [65]. While this was the first indication that the UPR^{mt} could be activated during microbial exposure, it did not address whether this response conferred any protective effect that promoted host survival. A follow-up study later confirmed that infection with *P. aeruginosa* was capable of activating the UPR^{mt} to promote host survival during infection [195]. Interestingly, the activation of the UPR^{mt} was not limited to regulation of genes involved in mitochondrial recovery, but also with functions in innate immunity to directly defend against the infection [58, 195]. Innate immune genes associated with the UPR^{mt} included secreted antimicrobial peptides and lysozymes that directly kill bacterial pathogens, in addition to C-type lectins that are believed to have a role in pathogen recognition [58, 195]. Consistent with a role in protecting the host during infection, loss of ATFS-1/UPR^{mt} reduces host survival during infection [64, 124, 195-197].

Furthermore, priming the host for the UPR^{mt} prior to pathogen exposure significantly extends their survival time [195, 198, 199]. Mechanistically, the UPR^{mt} is thought to induce innate immune gene expression via activation of the conserved p38 MAP kinase pathway. Specifically, the mitochondrial chaperone HSP-60, which is directly regulated by ATFS-1 during the UPR^{mt} [196], binds to SEK-1/MAP kinase kinase 3 of the p38 MAP kinase pathway. The binding of HSP-60 to SEK-1 is thought to stabilize the kinase, thus promoting the activation of this innate immune pathway [196].

The relationship between the UPR^{mt} and infection becomes more complex knowing that some pathogens are capable of inactivating this stress response [65, 124, 197]. Indeed, while *P. aeruginosa* activates the UPR^{mt}, it is only transient [124, 197], suggesting that this pathogen antagonizes this stress response during infection. Mechanistically, *P. aeruginosa* is thought to repress the UPR^{mt} at least in part through a manipulation of nutrient availability to the host [197]. Here, the *P. aeruginosa* acyl-CoA dehydrogenase FadE2 was found to be a critical determinant of UPR^{mt} activity. FadE2 has a substrate preference for the CoA derivative produced during catabolism of the branched-chain amino acid valine. The current model suggests that FadE2 outcompetes the host for valine catabolites which reduces the activity of the UPR^{mt} through an unknown mechanism [197]. Furthermore, host factors involved in the repression of the UPR^{mt} during *P. aeruginosa* infection have been identified. Specifically, *P. aeruginosa* inhibits the UPR^{mt} through a manipulation of *C. elegans* ZIP-3, a bZIP transcription factor and negative regulator of the UPR^{mt} [124]. The relationship between *P. aeruginosa* FadE2, *C. elegans* ZIP-3 and the UPR^{mt} is still unclear. However, there is some overlap in the genes that are differentially expressed by the presence or absence of these factors [197], suggesting shared mechanisms of action.

Mitophagy and Xenophagy: Parallels between organelle and pathogen removal

A critical point in the evolution of eukaryotes was the joining of an ancestral prokaryote with an ancient archaeon cell. The ancestral prokaryote would later lose autonomy and become the mitochondrion [200, 201]. Xenophagy refers to the autophagic removal of invading pathogens that superficially resembles mitophagy. The similarities between xenophagy and mitophagy are not unexpected when one considers the endosymbiotic origin of mitochondria. Since both share common objectives of clearing undesired endogenous or foreign material, it is not surprising that xenophagy and mitophagy use common molecular players to execute this function. Consistently, loss of the E3 ubiquitin ligase Parkin increases host susceptibility to infection by intracellular pathogens [202-204]. Interestingly, Parkin was found to target intracellular pathogens such as *M. tuberculosis* for autophagic removal in macrophages (Figure 1.3C) [204]. Here, Parkin mediates K63-linked polyubiquitination of *M. tuberculosis* to promote autophagic clearance of this intracellular pathogen, that limits infection levels both *in vitro* and *in vivo*. While unlikely a target of Parkin, the surface protein Rv1468c was nonetheless found to bind ubiquitin, causing the recruitment of the autophagy receptor p62 for delivery to autophagosomes [205].

Apart from Parkin, the kinase TBK1 also plays keys roles in both xenophagic clearance of bacterial pathogens and removal of damaged mitochondria via mitophagy. TBK1 is important stimulator of Type I interferon gene expression during both viral [206] and bacterial infection [207]. During bacterial infection, TBK1 promotes vacuolar integrity to help reduce cytosolic levels of the intracellular pathogen *Salmonella* [208]. Following infection, *Salmonella* takes residence in vacuoles known as SCVs. Some *Salmonella* however, escape from the SCV and enter the cytosol where they hyper proliferate [209]. *Salmonella* is ubiquitinated and degraded by autophagic removal as a host response to its cytosolic presence [210]. TBK1 is critical for limiting *Salmonella*

since loss of this kinase results in increased cytosolic levels of this pathogen [208, 211]. Ubiquitin-labelled *Salmonella* recruits the autophagy receptor OPTN in a TBK1-dependent manner [212]. Here, TBK1 phosphorylates OPTN which enhances the binding to LC3. Consistently, loss of OPTN increases *Salmonella* proliferation in the cytosol [212]. Interestingly, during mitophagy, TBK1 also phosphorylates OPTN to drive removal of damaged mitochondria by PINK1/Parkin-mediated mitophagy [213, 214]. As such, TBK1 provides a link between seemingly similar processes. However, one might assume that during infection with intracellular pathogens such as *Salmonella*, mitophagy would be required to remove damaged mitochondria at the same time that xenophagy is needed to remove the invader. Therefore, how are both processes coordinated when both use TBK1 to execute each process? Presumably, there would be a risk for further pathogen growth and dissemination if mitophagy was prioritized during infection due to a lack of machinery to promote xenophagy. As outlined earlier, many pathogens induce mitochondrial fission which may lead to stimulation of mitophagy, suggesting that this may be a pathogen-associated tactic to promote infection. Another possibility is that host cells upregulate mitophagy/xenophagy components as a means to balance out mitochondrial quality control and pathogen clearance.

CONCLUSION

The environment of a bacterial pathogen dramatically changes once it infects its host, which can challenge its survival due to harsh physical conditions, the immune response of the host, and possibly an altered and/or limited nutrient supply. Therefore, pathogens are in a constant state of defense and adaptation in order to survive in their host and promote infection. This is not an easy task, forcing the pathogen to execute various survival strategies including the manipulation of host organelle function. Mitochondria are integral organelles that mediate important physiological

processes including aging and the regulation of immunity. As outlined in this review, multiple pathogens target mitochondrial function in an effort to thrive. A common theme across many pathogens that target mitochondria is the manipulation of mitochondrial-associated cell death and immunity pathways. Because mitochondria are under constant attack by these pathogens, cells must engage protective pathways to maintain proper function of this essential organelle.

Interestingly, these mitochondrial protective pathways function not only in promoting mitochondrial recovery but are often coupled to bacterial defense programs. Therefore, to survive, bacterial pathogens target not only the mitochondrion itself but also its associated recovery programs in an effort to alter cellular function and defend itself against antimicrobial defense pathways. The targeting of mitochondrial recovery programs by bacterial pathogens is a relatively new concept in the field of host-pathogen interactions. As illustrated here, multiple mitochondrial protective pathways are under attack during infection. This includes mitochondrial dynamics, in which various pathogens directly or indirectly drive mitochondrial fission which alters mitochondrial function and can impact associated immune pathways such as MAVS. More recently, the UPR^{mt} was shown to be repressed during *P. aeruginosa* infection. This repression involves a metabolic pathway of the pathogen that mediates valine catabolism. This raises intriguing questions: how do these nutrients dictate UPR^{mt} activity? And, is this pathogen metabolic pathway specifically activated during infection? If we can understand how these various pathogens target host mitochondrial recovery programs and their associated immune pathways, then we can possibly devise new therapeutic strategies to promote host resistance during infection. This is particularly relevant today, since bacterial infections are the cause of significant morbidity in the clinic and are increasingly becoming more resistant to routine antibiotic treatments.

REFERENCES

1. Escoll, P., Mondino, S., Rolando, M. & Buchrieser, C. (2016) Targeting of host organelles by pathogenic bacteria: a sophisticated subversion strategy, *Nat Rev Microbiol.* **14**, 5-19.

2. Weber, M. M. & Faris, R. (2018) Subversion of the Endocytic and Secretory Pathways by Bacterial Effector Proteins, *Front Cell Dev Biol.* **6**, 1.

3. Bierne, H. & Pourpre, R. (2020) Bacterial Factors Targeting the Nucleus: The Growing Family of Nucleomodulins, *Toxins (Basel).* **12**.

4. Pistor, S., Chakraborty, T., Niebuhr, K., Domann, E. & Wehland, J. (1994) The ActA protein of Listeria monocytogenes acts as a nucleator inducing reorganization of the actin cytoskeleton, *EMBO J.* **13**, 758-63.

5. Bourdet-Sicard, R. & Tran Van Nhieu, G. (1999) Actin reorganization by SipA and Salmonella invasion of epithelial cells, *Trends Microbiol.* **7**, 309-10.

6. Bleves, S., Viarre, V., Salacha, R., Michel, G. P., Filloux, A. & Voulhoux, R. (2010) Protein secretion systems in Pseudomonas aeruginosa: A wealth of pathogenic weapons, *Int J Med Microbiol.* **300**, 534-43.

7. Simeone, R., Bottai, D. & Brosch, R. (2009) ESX/type VII secretion systems and their role in host-pathogen interaction, *Curr Opin Microbiol.* **12**, 4-10.

8. Alvarez-Martinez, C. E. & Christie, P. J. (2009) Biological diversity of prokaryotic type IV secretion systems, *Microbiol Mol Biol Rev.* **73**, 775-808.

9. Prasai, K. (2017) Regulation of mitochondrial structure and function by protein import: A current review, *Pathophysiology.* **24**, 107-122.

10. Gerwien, F., Skrahina, V., Kasper, L., Hube, B. & Brunke, S. (2018) Metals in fungal virulence, *FEMS Microbiol Rev.* **42**.

11. Chandrangsu, P., Rensing, C. & Helmann, J. D. (2017) Metal homeostasis and resistance in bacteria, *Nat Rev Microbiol.* **15**, 338-350.

12. Ashida, H., Mimuro, H., Ogawa, M., Kobayashi, T., Sanada, T., Kim, M. & Sasakawa, C. (2011) Cell death and infection: a double-edged sword for host and pathogen survival, *J Cell Biol.* **195**, 931-42.

13. West, A. P., Shadel, G. S. & Ghosh, S. (2011) Mitochondria in innate immune responses, *Nat Rev Immunol.* **11**, 389-402.

14. Sun, N., Youle, R. J. & Finkel, T. (2016) The Mitochondrial Basis of Aging, *Mol Cell.* **61**, 654-666.

15. Lobet, E., Letesson, J. J. & Arnould, T. (2015) Mitochondria: a target for bacteria, *Biochem Pharmacol.* **94**, 173-85.

16. Westermann, B. (2010) Mitochondrial fusion and fission in cell life and death, *Nat Rev Mol Cell Biol.* **11**, 872-84.

17. Rojo, M., Legros, F., Chateau, D. & Lombes, A. (2002) Membrane topology and mitochondrial targeting of mitofusins, ubiquitous mammalian homologs of the transmembrane GTPase Fzo, *J Cell Sci.* **115**, 1663-74.

18. Koshiba, T., Detmer, S. A., Kaiser, J. T., Chen, H., McCaffery, J. M. & Chan, D. C. (2004) Structural basis of mitochondrial tethering by mitofusin complexes, *Science.* **305**, 858-62.

19. Mattie, S., Riemer, J., Wideman, J. G. & McBride, H. M. (2018) A new mitofusin topology places the redox-regulated C terminus in the mitochondrial intermembrane space, *J Cell Biol.* **217**, 507-515.

20. Qi, Y., Yan, L., Yu, C., Guo, X., Zhou, X., Hu, X., Huang, X., Rao, Z., Lou, Z. & Hu, J. (2016) Structures of human mitofusin 1 provide insight into mitochondrial tethering, *J Cell Biol.* **215**, 621-629.

21. Cao, Y. L., Meng, S., Chen, Y., Feng, J. X., Gu, D. D., Yu, B., Li, Y. J., Yang, J. Y., Liao, S., Chan, D. C. & Gao, S. (2017) MFN1 structures reveal nucleotide-triggered dimerization critical for mitochondrial fusion, *Nature.* **542**, 372-376.

22. Griparic, L., van der Wel, N. N., Orozco, I. J., Peters, P. J. & van der Bliek, A. M. (2004) Loss of the intermembrane space protein Mgm1/OPA1 induces swelling and localized constrictions along the lengths of mitochondria, *J Biol Chem.* **279**, 18792-8.

23. Olichon, A., Emorine, L. J., Descoins, E., Pelloquin, L., Brichese, L., Gas, N., Guillou, E., Delettre, C., Valette, A., Hamel, C. P., Ducommun, B., Lenaers, G. & Belenguer, P. (2002) The human dynamin-related protein OPA1 is anchored to the mitochondrial inner membrane facing the inter-membrane space, *FEBS Lett.* **523**, 171-6.

24. Ehses, S., Raschke, I., Mancuso, G., Bernacchia, A., Geimer, S., Tondera, D., Martinou, J. C., Westermann, B., Rugarli, E. I. & Langer, T. (2009) Regulation of OPA1 processing and mitochondrial fusion by m-AAA protease isoenzymes and OMA1, *J Cell Biol.* **187**, 1023-36.

25. Head, B., Griparic, L., Amiri, M., Gandre-Babbe, S. & van der Bliek, A. M. (2009) Inducible proteolytic inactivation of OPA1 mediated by the OMA1 protease in mammalian cells, *J Cell Biol.* **187**, 959-66.

26. Griparic, L., Kanazawa, T. & van der Bliek, A. M. (2007) Regulation of the mitochondrial dynamin-like protein Opa1 by proteolytic cleavage, *J Cell Biol.* **178**, 757-64.

27. Song, Z., Chen, H., Fiket, M., Alexander, C. & Chan, D. C. (2007) OPA1 processing controls mitochondrial fusion and is regulated by mRNA splicing, membrane potential, and Yme1L, *J Cell Biol.* **178**, 749-55.

28. Cipolat, S., Rudka, T., Hartmann, D., Costa, V., Serneels, L., Craessaerts, K., Metzger, K., Frezza, C., Annaert, W., D'Adamio, L., Derks, C., Dejaegere, T., Pellegrini, L., D'Hooge, R., Scorrano, L. & De Strooper, B. (2006) Mitochondrial rhomboid PARL regulates cytochrome c release during apoptosis via OPA1-dependent cristae remodeling, *Cell.* **126**, 163-75.

29. Anand, R., Wai, T., Baker, M. J., Kladt, N., Schauss, A. C., Rugarli, E. & Langer, T. (2014) The i-AAA protease YME1L and OMA1 cleave OPA1 to balance mitochondrial fusion and fission, *J Cell Biol.* **204**, 919-29.

30. Cipolat, S., Martins de Brito, O., Dal Zilio, B. & Scorrano, L. (2004) OPA1 requires mitofusin 1 to promote mitochondrial fusion, *Proc Natl Acad Sci U S A.* **101**, 15927-32.

31. Griffin, E. E., Graumann, J. & Chan, D. C. (2005) The WD40 protein Caf4p is a component of the mitochondrial fission machinery and recruits Dnm1p to mitochondria, *J Cell Biol.* **170**, 237-48.

32. Palmer, C. S., Osellame, L. D., Laine, D., Koutsopoulos, O. S., Frazier, A. E. & Ryan, M. T. (2011) MiD49 and MiD51, new components of the mitochondrial fission machinery, *EMBO Rep.* **12**, 565-73.

33. Loson, O. C., Song, Z., Chen, H. & Chan, D. C. (2013) Fis1, Mff, MiD49, and MiD51 mediate Drp1 recruitment in mitochondrial fission, *Mol Biol Cell.* **24**, 659-67.

34. Ingerman, E., Perkins, E. M., Marino, M., Mears, J. A., McCaffery, J. M., Hinshaw, J. E. & Nunnari, J. (2005) Dnm1 forms spirals that are structurally tailored to fit mitochondria, *J Cell Biol.* **170**, 1021-7.

35. Kraus, F. & Ryan, M. T. (2017) The constriction and scission machineries involved in mitochondrial fission, *J Cell Sci.* **130**, 2953-2960.

36. Mears, J. A., Lackner, L. L., Fang, S., Ingerman, E., Nunnari, J. & Hinshaw, J. E. (2011) Conformational changes in Dnm1 support a contractile mechanism for mitochondrial fission, *Nat Struct Mol Biol.* **18**, 20-6.

37. Yoon, Y., Pitts, K. R. & McNiven, M. A. (2001) Mammalian dynamin-like protein DLP1 tubulates membranes, *Mol Biol Cell.* **12**, 2894-905.

38. Lee, J. E., Westrate, L. M., Wu, H., Page, C. & Voeltz, G. K. (2016) Multiple dynamin family members collaborate to drive mitochondrial division, *Nature.* **540**, 139-143.

39. Fonseca, T. B., Sanchez-Guerrero, A., Milosevic, I. & Raimundo, N. (2019) Mitochondrial fission requires DRP1 but not dynamins, *Nature.* **570**, E34-E42.

40. Friedman, J. R., Lackner, L. L., West, M., DiBenedetto, J. R., Nunnari, J. & Voeltz, G. K. (2011) ER tubules mark sites of mitochondrial division, *Science.* **334**, 358-62.

41. Abrisch, R. G., Gumbin, S. C., Wisniewski, B. T., Lackner, L. L. & Voeltz, G. K. (2020) Fission and fusion machineries converge at ER contact sites to regulate mitochondrial morphology, *J Cell Biol.* **219**.

42. Bukau, B., Weissman, J. & Horwich, A. (2006) Molecular chaperones and protein quality control, *Cell.* **125**, 443-51.

43. Pellegrino, M. W., Nargund, A. M. & Haynes, C. M. (2013) Signaling the mitochondrial unfolded protein response, *Biochim Biophys Acta.* **1833**, 410-6.

44. Rothermel, B. A., Thornton, J. L. & Butow, R. A. (1997) Rtg3p, a basic helix-loop-helix/leucine zipper protein that functions in mitochondrial-induced changes in gene expression, contains independent activation domains, *J Biol Chem.* **272**, 19801-7.

45. Sekito, T., Thornton, J. & Butow, R. A. (2000) Mitochondria-to-nuclear signaling is regulated by the subcellular localization of the transcription factors Rtg1p and Rtg3p, *Mol Biol Cell.* **11**, 2103-15.

46. Koonin, E. V. (1994) Yeast protein controlling inter-organelle communication is related to bacterial phosphatases containing the Hsp 70-type ATP-binding domain, *Trends Biochem Sci.* **19**, 156-7.

47. Liu, Z., Sekito, T., Spirek, M., Thornton, J. & Butow, R. A. (2003) Retrograde signaling is regulated by the dynamic interaction between Rtg2p and Mks1p, *Mol Cell.* **12**, 401-11.

48. Dilova, I., Aronova, S., Chen, J. C. & Powers, T. (2004) Tor signaling and nutrient-based signals converge on Mks1p phosphorylation to regulate expression of Rtg1.Rtg3p-dependent target genes, *J Biol Chem.* **279**, 46527-35.

49. Sekito, T., Liu, Z., Thornton, J. & Butow, R. A. (2002) RTG-dependent mitochondria-to-nucleus signaling is regulated by MKS1 and is linked to formation of yeast prion [URE3], *Mol Biol Cell.* **13**, 795-804.

50. Liu, Z., Spirek, M., Thornton, J. & Butow, R. A. (2005) A novel degron-mediated degradation of the RTG pathway regulator, Mks1p, by SCFGrr1, *Mol Biol Cell.* **16**, 4893-904.

51. Zhao, Q., Wang, J., Levichkin, I. V., Stasinopoulos, S., Ryan, M. T. & Hoogenraad, N. J. (2002) A mitochondrial specific stress response in mammalian cells, *EMBO J.* **21**, 4411-9.

52. Aldridge, J. E., Horibe, T. & Hoogenraad, N. J. (2007) Discovery of genes activated by the mitochondrial unfolded protein response (mtUPR) and cognate promoter elements, *PLoS One.* **2**, e874.

53. Horibe, T. & Hoogenraad, N. J. (2007) The chop gene contains an element for the positive regulation of the mitochondrial unfolded protein response, *PLoS One.* **2**, e835.

54. Yoneda, T., Benedetti, C., Urano, F., Clark, S. G., Harding, H. P. & Ron, D. (2004) Compartment-specific perturbation of protein handling activates genes encoding mitochondrial chaperones, *J Cell Sci.* **117**, 4055-66.

55. Haynes, C. M., Petrova, K., Benedetti, C., Yang, Y. & Ron, D. (2007) ClpP mediates activation of a mitochondrial unfolded protein response in C. elegans, *Dev Cell.* **13**, 467-80.

56. Haynes, C. M., Yang, Y., Blais, S. P., Neubert, T. A. & Ron, D. (2010) The matrix peptide exporter HAF-1 signals a mitochondrial UPR by activating the transcription factor ZC376.7 in C. elegans, *Mol Cell.* **37**, 529-40.

57. Runkel, E. D., Liu, S., Baumeister, R. & Schulze, E. (2013) Surveillance-activated defenses block the ROS-induced mitochondrial unfolded protein response, *PLoS Genet.* **9**, e1003346.

58. Nargund, A. M., Pellegrino, M. W., Fiorese, C. J., Baker, B. M. & Haynes, C. M. (2012) Mitochondrial import efficiency of ATFS-1 regulates mitochondrial UPR activation, *Science.* **337**, 587-90.

59. Rolland, S. G., Schneid, S., Schwarz, M., Rackles, E., Fischer, C., Haeussler, S., Regmi, S. G., Yeroslaviz, A., Habermann, B., Mokranjac, D., Lambie, E. & Conradt, B. (2019) Compromised Mitochondrial Protein Import Acts as a Signal for UPR(mt), *Cell Rep.* **28**, 1659-1669 e5.

60. Shpilka, T., Du, Y., Yang, Q., Melber, A., Uma Naresh, N., Lavelle, J., Kim, S., Liu, P., Weidberg, H., Li, R., Yu, J., Zhu, L. J., Strittmatter, L. & Haynes, C. M. (2021) UPR(mt) scales mitochondrial network expansion with protein synthesis via mitochondrial import in Caenorhabditis elegans, *Nat Commun.* **12**, 479.

61. Nargund, A. M., Fiorese, C. J., Pellegrino, M. W., Deng, P. & Haynes, C. M. (2015) Mitochondrial and nuclear accumulation of the transcription factor ATFS-1 promotes OXPHOS recovery during the UPR(mt), *Mol Cell.* **58**, 123-33.

62. Tian, Y., Garcia, G., Bian, Q., Steffen, K. K., Joe, L., Wolff, S., Meyer, B. J. & Dillin, A. (2016) Mitochondrial Stress Induces Chromatin Reorganization to Promote Longevity and UPR(mt), *Cell.* **165**, 1197-1208.

63. Merkwirth, C., Jovaisaite, V., Durieux, J., Matilainen, O., Jordan, S. D., Quiros, P. M., Steffen, K. K., Williams, E. G., Mouchiroud, L., Tronnes, S. U., Murillo, V., Wolff, S. C., Shaw, R. J., Auwerx, J. & Dillin, A. (2016) Two Conserved Histone Demethylases Regulate Mitochondrial Stress-Induced Longevity, *Cell.* **165**, 1209-1223.

64. Shao, L. W., Peng, Q., Dong, M., Gao, K., Li, Y., Li, Y., Li, C. Y. & Liu, Y. (2020) Histone deacetylase HDA-1 modulates mitochondrial stress response and longevity, *Nat Commun.* **11**, 4639.

65. Liu, Y., Samuel, B. S., Breen, P. C. & Ruvkun, G. (2014) Caenorhabditis elegans pathways that surveil and defend mitochondria, *Nature.* **508**, 406-10.

66. Oks, O., Lewin, S., Goncalves, I. L. & Sapir, A. (2018) The UPR(mt) Protects Caenorhabditis elegans from Mitochondrial Dysfunction by Upregulating Specific Enzymes of the Mevalonate Pathway, *Genetics.* **209**, 457-473.

67. Durieux, J., Wolff, S. & Dillin, A. (2011) The cell-non-autonomous nature of electron transport chain-mediated longevity, *Cell.* **144**, 79-91.

68. Shao, L. W., Niu, R. & Liu, Y. (2016) Neuropeptide signals cell non-autonomous mitochondrial unfolded protein response, *Cell Res.* **26**, 1182-1196.

69. Zhang, Q., Wu, X., Chen, P., Liu, L., Xin, N., Tian, Y. & Dillin, A. (2018) The Mitochondrial Unfolded Protein Response Is Mediated Cell-Non-autonomously by Retromer-Dependent Wnt Signaling, *Cell.* **174**, 870-883 e17.

70. Berendzen, K. M., Durieux, J., Shao, L. W., Tian, Y., Kim, H. E., Wolff, S., Liu, Y. & Dillin, A. (2016) Neuroendocrine Coordination of Mitochondrial Stress Signaling and Proteostasis, *Cell.* **166**, 1553-1563 e10.

71. Fiorese, C. J., Schulz, A. M., Lin, Y. F., Rosin, N., Pellegrino, M. W. & Haynes, C. M. (2016) The Transcription Factor ATF5 Mediates a Mammalian Mitochondrial UPR, *Curr Biol.* **26**, 2037-2043.

72. Straub, I. R., Weraarpachai, W. & Shoubridge, E. A. (2021) Multi-OMICS study of a CHCHD10 variant causing ALS demonstrates metabolic rewiring and activation of endoplasmic reticulum and mitochondrial unfolded protein responses, *Hum Mol Genet*.

73. Lai, C., Zhang, J., Tan, Z., Shen, L. F., Zhou, R. R. & Zhang, Y. Y. (2021) Maf1 suppression of ATF5-dependent mitochondrial unfolded protein response contributes to rapamycin-induced radio-sensitivity in lung cancer cell line A549, *Aging (Albany NY).* **13**, 7300-7313.

74. Urushima, Y., Haraguchi, M. & Yano, M. (2020) Depletion of TMEM65 leads to oxidative stress, apoptosis, induction of mitochondrial unfolded protein response, and upregulation of mitochondrial protein import receptor TOMM22, *Biochem Biophys Rep.* **24**, 100870.

75. Jiang, D., Cui, H., Xie, N., Banerjee, S., Liu, R. M., Dai, H., Thannickal, V. J. & Liu, G. (2020) ATF4 Mediates Mitochondrial Unfolded Protein Response in Alveolar Epithelial Cells, *Am J Respir Cell Mol Biol.* **63**, 478-489.

76. Quiros, P. M., Prado, M. A., Zamboni, N., D'Amico, D., Williams, R. W., Finley, D., Gygi, S. P. & Auwerx, J. (2017) Multi-omics analysis identifies ATF4 as a key regulator of the mitochondrial stress response in mammals, *J Cell Biol.* **216**, 2027-2045.

77. Teske, B. F., Fusakio, M. E., Zhou, D., Shan, J., McClintick, J. N., Kilberg, M. S. & Wek, R. C. (2013) CHOP induces activating transcription factor 5 (ATF5) to trigger apoptosis in response to perturbations in protein homeostasis, *Mol Biol Cell.* **24**, 2477-90.

78. Zhou, D., Palam, L. R., Jiang, L., Narasimhan, J., Staschke, K. A. & Wek, R. C. (2008) Phosphorylation of eIF2 directs ATF5 translational control in response to diverse stress conditions, *J Biol Chem.* **283**, 7064-73.

79. Costa-Mattioli, M. & Walter, P. (2020) The integrated stress response: From mechanism to disease, *Science.* **368**.

80. Kaspar, S., Oertlin, C., Szczepanowska, K., Kukat, A., Senft, K., Lucas, C., Brodesser, S., Hatzoglou, M., Larsson, O., Topisirovic, I. & Trifunovic, A. (2021) Adaptation to mitochondrial stress requires CHOP-directed tuning of ISR, *Sci Adv.* **7**.

81. Klionsky, D. J. (2007) Autophagy: from phenomenology to molecular understanding in less than a decade, *Nat Rev Mol Cell Biol.* **8**, 931-7.

82. Dunn, W. A., Jr. (1994) Autophagy and related mechanisms of lysosome-mediated protein degradation, *Trends Cell Biol.* **4**, 139-43.

83. Kabeya, Y., Mizushima, N., Ueno, T., Yamamoto, A., Kirisako, T., Noda, T., Kominami, E., Ohsumi, Y. & Yoshimori, T. (2000) LC3, a mammalian homologue of yeast Apg8p, is localized in autophagosome membranes after processing, *EMBO J.* **19**, 5720-8.

84. Youle, R. J. & Narendra, D. P. (2011) Mechanisms of mitophagy, *Nat Rev Mol Cell Biol.* **12**, 9-14.

85. Okamoto, K., Kondo-Okamoto, N. & Ohsumi, Y. (2009) Mitochondria-anchored receptor Atg32 mediates degradation of mitochondria via selective autophagy, *Dev Cell.* **17**, 87-97.

86. Wu, W., Tian, W., Hu, Z., Chen, G., Huang, L., Li, W., Zhang, X., Xue, P., Zhou, C., Liu, L., Zhu, Y., Zhang, X., Li, L., Zhang, L., Sui, S., Zhao, B. & Feng, D. (2014) ULK1 translocates to mitochondria and phosphorylates FUNDC1 to regulate mitophagy, *EMBO Rep.* **15**, 566-75.

87. Novak, I., Kirkin, V., McEwan, D. G., Zhang, J., Wild, P., Rozenknop, A., Rogov, V., Lohr, F., Popovic, D., Occhipinti, A., Reichert, A. S., Terzic, J., Dotsch, V., Ney, P. A. & Dikic, I. (2010) Nix is a selective autophagy receptor for mitochondrial clearance, *EMBO Rep.* **11**, 45-51.

88. Murakawa, T., Yamaguchi, O., Hashimoto, A., Hikoso, S., Takeda, T., Oka, T., Yasui, H., Ueda, H., Akazawa, Y., Nakayama, H., Taneike, M., Misaka, T., Omiya, S., Shah, A. M., Yamamoto, A., Nishida, K., Ohsumi, Y., Okamoto, K., Sakata, Y. & Otsu, K. (2015) Bcl-2-like protein 13 is a mammalian Atg32 homologue that mediates mitophagy and mitochondrial fragmentation, *Nat Commun.* **6**, 7527.

89. Tracy, K., Dibling, B. C., Spike, B. T., Knabb, J. R., Schumacker, P. & Macleod, K. F. (2007) BNIP3 is an RB/E2F target gene required for hypoxia-induced autophagy, *Mol Cell Biol.* **27**, 6229-42.

90. Bhujabal, Z., Birgisdottir, A. B., Sjottem, E., Brenne, H. B., Overvatn, A., Habisov, S., Kirkin, V., Lamark, T. & Johansen, T. (2017) FKBP8 recruits LC3A to mediate Parkin-independent mitophagy, *EMBO Rep.* **18**, 947-961.

91. Hanna, R. A., Quinsay, M. N., Orogo, A. M., Giang, K., Rikka, S. & Gustafsson, A. B. (2012) Microtubule-associated protein 1 light chain 3 (LC3) interacts with Bnip3 protein to selectively remove endoplasmic reticulum and mitochondria via autophagy, *J Biol Chem.* **287**, 19094-104.

92. Liu, L., Feng, D., Chen, G., Chen, M., Zheng, Q., Song, P., Ma, Q., Zhu, C., Wang, R., Qi, W., Huang, L., Xue, P., Li, B., Wang, X., Jin, H., Wang, J., Yang, F., Liu, P., Zhu, Y., Sui, S. & Chen, Q. (2012) Mitochondrial outer-membrane protein FUNDC1 mediates hypoxia-induced mitophagy in mammalian cells, *Nat Cell Biol.* **14**, 177-85.

93. Palikaras, K., Lionaki, E. & Tavernarakis, N. (2018) Mechanisms of mitophagy in cellular homeostasis, physiology and pathology, *Nat Cell Biol.* **20**, 1013-1022.

94. Jin, S. M., Lazarou, M., Wang, C., Kane, L. A., Narendra, D. P. & Youle, R. J. (2010) Mitochondrial membrane potential regulates PINK1 import and proteolytic destabilization by PARL, *J Cell Biol.* **191**, 933-42.

95. Matsuda, N., Sato, S., Shiba, K., Okatsu, K., Saisho, K., Gautier, C. A., Sou, Y. S., Saiki, S., Kawajiri, S., Sato, F., Kimura, M., Komatsu, M., Hattori, N. & Tanaka, K. (2010) PINK1 stabilized by mitochondrial depolarization recruits Parkin to damaged mitochondria and activates latent Parkin for mitophagy, *J Cell Biol.* **189**, 211-21.

96. Koyano, F., Okatsu, K., Kosako, H., Tamura, Y., Go, E., Kimura, M., Kimura, Y., Tsuchiya, H., Yoshihara, H., Hirokawa, T., Endo, T., Fon, E. A., Trempe, J. F., Saeki, Y., Tanaka, K. & Matsuda, N. (2014) Ubiquitin is phosphorylated by PINK1 to activate parkin, *Nature.* **510**, 162-6.

97. Kane, L. A., Lazarou, M., Fogel, A. I., Li, Y., Yamano, K., Sarraf, S. A., Banerjee, S. & Youle, R. J. (2014) PINK1 phosphorylates ubiquitin to activate Parkin E3 ubiquitin ligase activity, *J Cell Biol.* **205**, 143-53.

98. Xiao, B., Goh, J. Y., Xiao, L., Xian, H., Lim, K. L. & Liou, Y. C. (2017) Reactive oxygen species trigger Parkin/PINK1 pathway-dependent mitophagy by inducing mitochondrial recruitment of Parkin, *J Biol Chem.* **292**, 16697-16708.

99. Vives-Bauza, C., Zhou, C., Huang, Y., Cui, M., de Vries, R. L., Kim, J., May, J., Tocilescu, M. A., Liu, W., Ko, H. S., Magrane, J., Moore, D. J., Dawson, V. L., Grailhe, R., Dawson, T. M., Li, C., Tieu, K. & Przedborski, S. (2010) PINK1-dependent recruitment of Parkin to mitochondria in mitophagy, *Proc Natl Acad Sci U S A.* **107**, 378-83.

100. Okatsu, K., Oka, T., Iguchi, M., Imamura, K., Kosako, H., Tani, N., Kimura, M., Go, E., Koyano, F., Funayama, M., Shiba-Fukushima, K., Sato, S., Shimizu, H., Fukunaga, Y., Taniguchi, H., Komatsu, M., Hattori, N., Mihara, K., Tanaka, K. & Matsuda, N. (2012) PINK1 autophosphorylation upon membrane potential dissipation is essential for Parkin recruitment to damaged mitochondria, *Nat Commun.* **3**, 1016.

101. Jin, S. M. & Youle, R. J. (2013) The accumulation of misfolded proteins in the mitochondrial matrix is sensed by PINK1 to induce PARK2/Parkin-mediated mitophagy of polarized mitochondria, *Autophagy.* **9**, 1750-7.

102. Narendra, D., Tanaka, A., Suen, D. F. & Youle, R. J. (2008) Parkin is recruited selectively to impaired mitochondria and promotes their autophagy, *J Cell Biol.* **183**, 795-803.

103. Lazarou, M., Sliter, D. A., Kane, L. A., Sarraf, S. A., Wang, C., Burman, J. L., Sideris, D. P., Fogel, A. I. & Youle, R. J. (2015) The ubiquitin kinase PINK1 recruits autophagy receptors to induce mitophagy, *Nature.* **524**, 309-314.

104. Rudel, T., Kepp, O. & Kozjak-Pavlovic, V. (2010) Interactions between bacterial pathogens and mitochondrial cell death pathways, *Nat Rev Microbiol.* **8**, 693-705.

105. Naderer, T. & Fulcher, M. C. (2018) Targeting apoptosis pathways in infections, *J Leukoc Biol.* **103**, 275-285.

106. Ow, Y. P., Green, D. R., Hao, Z. & Mak, T. W. (2008) Cytochrome c: functions beyond respiration, *Nat Rev Mol Cell Biol.* **9**, 532-42.

107. Baker, B. M. & Haynes, C. M. (2011) Mitochondrial protein quality control during biogenesis and aging, *Trends Biochem Sci.* **36**, 254-61.

108. Neupert, W. & Herrmann, J. M. (2007) Translocation of proteins into mitochondria, *Annu Rev Biochem.* **76**, 723-49.

109. Harbauer, A. B., Zahedi, R. P., Sickmann, A., Pfanner, N. & Meisinger, C. (2014) The protein import machinery of mitochondria-a regulatory hub in metabolism, stress, and disease, *Cell Metab.* **19**, 357-72.

110. Schmidt, O., Pfanner, N. & Meisinger, C. (2010) Mitochondrial protein import: from proteomics to functional mechanisms, *Nat Rev Mol Cell Biol.* **11**, 655-67.

111. Zlosnik, J. E. A., Tavankar, G. R., Bundy, J. G., Mossialos, D., O'Toole, R. & Williams, H. D. (2006) Investigation of the physiological relationship between the cyanide-insensitive oxidase and cyanide production in Pseudomonas aeruginosa, *Microbiology (Reading).* **152**, 1407-1415.

112. Cunningham, L., Pitt, M. & Williams, H. D. (1997) The cioAB genes from Pseudomonas aeruginosa code for a novel cyanide-insensitive terminal oxidase related to the cytochrome bd quinol oxidases, *Mol Microbiol.* **24**, 579-91.

113. Hewlett, E. L., Guerrant, R. L., Evans, D. J., Jr. & Greenough, W. B., 3rd (1974) Toxins of Vibrio cholerae and Escherichia coli stimulate adenyl cyclase in rat fat cells, *Nature.* **249**, 371-3.

114. Alam, A., Miller, K. A., Chaand, M., Butler, J. S. & Dziejman, M. (2011) Identification of Vibrio cholerae type III secretion system effector proteins, *Infect Immun.* **79**, 1728-40.

115. Suzuki, M., Danilchanka, O. & Mekalanos, J. J. (2014) Vibrio cholerae T3SS effector VopE modulates mitochondrial dynamics and innate immune signaling by targeting Miro GTPases, *Cell Host Microbe.* **16**, 581-91.

116. Ramamurthy, T., Nandy, R. K., Mukhopadhyay, A. K., Dutta, S., Mutreja, A., Okamoto, K., Miyoshi, S. I., Nair, G. B. & Ghosh, A. (2020) Virulence Regulation and Innate Host Response in the Pathogenicity of Vibrio cholerae, *Front Cell Infect Microbiol.* **10**, 572096.

117. Mandal, S. & Chatterjee, N. S. (2016) Vibrio cholerae GbpA elicits necrotic cell death in intestinal cells, *J Med Microbiol.* **65**, 837-847.

118. Rai, A. K. & Chattopadhyay, K. (2015) Vibrio cholerae cytolysin: structure-function mechanism of an atypical beta-barrel pore-forming toxin, *Adv Exp Med Biol.* **842**, 109-25.

119. Khilwani, B. & Chattopadhyay, K. (2015) Signaling beyond Punching Holes: Modulation of Cellular Responses by Vibrio cholerae Cytolysin, *Toxins (Basel).* **7**, 3344-58.

120. Gupta, S., Prasad, G. V. & Mukhopadhaya, A. (2015) Vibrio cholerae Porin OmpU Induces Caspase-independent Programmed Cell Death upon Translocation to the Host Cell Mitochondria, *J Biol Chem.* **290**, 31051-68.

121. Wood, S. J., Goldufsky, J. W., Bello, D., Masood, S. & Shafikhani, S. H. (2015) Pseudomonas aeruginosa ExoT Induces Mitochondrial Apoptosis in Target Host Cells in a Manner That Depends on Its GTPase-activating Protein (GAP) Domain Activity, *J Biol Chem.* **290**, 29063-73.

122. Maurice, N. M., Bedi, B., Yuan, Z., Goldberg, J. B., Koval, M., Hart, C. M. & Sadikot, R. T. (2019) Pseudomonas aeruginosa Induced Host Epithelial Cell Mitochondrial Dysfunction, *Sci Rep.* **9**, 11929.

123. McFarland, A. J., Anoopkumar-Dukie, S., Perkins, A. V., Davey, A. K. & Grant, G. D. (2012) Inhibition of autophagy by 3-methyladenine protects 1321N1 astrocytoma cells against pyocyanin- and 1-hydroxyphenazine-induced toxicity, *Arch Toxicol.* **86**, 275-84.

124. Deng, P., Uma Naresh, N., Du, Y., Lamech, L. T., Yu, J., Zhu, L. J., Pukkila-Worley, R. & Haynes, C. M. (2019) Mitochondrial UPR repression during Pseudomonas aeruginosa infection requires the bZIP protein ZIP-3, *Proc Natl Acad Sci U S A.* **116**, 6146-6151.

125. Kang, D., Kirienko, D. R., Webster, P., Fisher, A. L. & Kirienko, N. V. (2018) Pyoverdine, a siderophore from Pseudomonas aeruginosa, translocates into C. elegans, removes iron, and activates a distinct host response, *Virulence.* **9**, 804-817.

126. Crane, J. K., Majumdar, S. & Pickhardt, D. F., 3rd (1999) Host cell death due to enteropathogenic Escherichia coli has features of apoptosis, *Infect Immun.* **67**, 2575-84.

127. Papatheodorou, P., Domanska, G., Oxle, M., Mathieu, J., Selchow, O., Kenny, B. & Rassow, J. (2006) The enteropathogenic Escherichia coli (EPEC) Map effector is imported into the mitochondrial matrix by the TOM/Hsp70 system and alters organelle morphology, *Cell Microbiol.* **8**, 677-89.

128. Kenny, B. & Jepson, M. (2000) Targeting of an enteropathogenic Escherichia coli (EPEC) effector protein to host mitochondria, *Cell Microbiol.* **2**, 579-90.

129. Nougayrede, J. P. & Donnenberg, M. S. (2004) Enteropathogenic Escherichia coli EspF is targeted to mitochondria and is required to initiate the mitochondrial death pathway, *Cell Microbiol.* **6**, 1097-111.

130. Shames, S. R., Croxen, M. A., Deng, W. & Finlay, B. B. (2011) The type III system-secreted effector EspZ localizes to host mitochondria and interacts with the translocase of inner mitochondrial membrane 17b, *Infect Immun.* **79**, 4784-90.

131. Wilbur, J. S., Byrd, W., Ramamurthy, S., Ledvina, H. E., Khirfan, K., Riggs, M. W., Boedeker, E. C., Vedantam, G. & Viswanathan, V. K. (2015) The secreted effector protein EspZ is essential for virulence of rabbit enteropathogenic Escherichia coli, *Infect Immun.* **83**, 1139-49.

132. Roxas, J. L., Wilbur, J. S., Zhang, X., Martinez, G., Vedantam, G. & Viswanathan, V. K. (2012) The enteropathogenic Escherichia coli-secreted protein EspZ inhibits host cell apoptosis, *Infect Immun.* **80**, 3850-7.

133. Muller, A., Gunther, D., Dux, F., Naumann, M., Meyer, T. F. & Rudel, T. (1999) Neisserial porin (PorB) causes rapid calcium influx in target cells and induces apoptosis by the activation of cysteine proteases, *EMBO J.* **18**, 339-52.

134. Deo, P., Chow, S. H., Hay, I. D., Kleifeld, O., Costin, A., Elgass, K. D., Jiang, J. H., Ramm, G., Gabriel, K., Dougan, G., Lithgow, T., Heinz, E. & Naderer, T. (2018) Outer membrane vesicles from Neisseria gonorrhoeae target PorB to mitochondria and induce apoptosis, *PLoS Pathog.* **14**, e1006945.

135. Kozjak-Pavlovic, V., Dian-Lothrop, E. A., Meinecke, M., Kepp, O., Ross, K., Rajalingam, K., Harsman, A., Hauf, E., Brinkmann, V., Gunther, D., Herrmann, I., Hurwitz, R., Rassow, J., Wagner, R. & Rudel, T. (2009) Bacterial porin disrupts mitochondrial membrane potential and sensitizes host cells to apoptosis, *PLoS Pathog.* **5**, e1000629.

136. Muller, A., Rassow, J., Grimm, J., Machuy, N., Meyer, T. F. & Rudel, T. (2002) VDAC and the bacterial porin PorB of Neisseria gonorrhoeae share mitochondrial import pathways, *EMBO J.* **21**, 1916-29.

137. Foegeding, N. J., Caston, R. R., McClain, M. S., Ohi, M. D. & Cover, T. L. (2016) An Overview of Helicobacter pylori VacA Toxin Biology, *Toxins (Basel).* **8**.

138. McClain, M. S., Beckett, A. C. & Cover, T. L. (2017) Helicobacter pylori Vacuolating Toxin and Gastric Cancer, *Toxins (Basel).* **9**.

139. Domanska, G., Motz, C., Meinecke, M., Harsman, A., Papatheodorou, P., Reljic, B., Dian-Lothrop, E. A., Galmiche, A., Kepp, O., Becker, L., Gunnewig, K., Wagner, R. & Rassow, J.

(2010) Helicobacter pylori VacA toxin/subunit p34: targeting of an anion channel to the inner mitochondrial membrane, *PLoS Pathog.* **6**, e1000878.

140. Rassow, J. (2011) Helicobacter pylori vacuolating toxin A and apoptosis, *Cell Commun Signal.* **9**, 26.

141. Montecucco, C. & Rappuoli, R. (2001) Living dangerously: how Helicobacter pylori survives in the human stomach, *Nat Rev Mol Cell Biol.* **2**, 457-66.

142. Cover, T. L. & Blanke, S. R. (2005) Helicobacter pylori VacA, a paradigm for toxin multifunctionality, *Nat Rev Microbiol.* **3**, 320-32.

143. Schlesinger, L. S. (1996) Entry of Mycobacterium tuberculosis into mononuclear phagocytes, *Curr Top Microbiol Immunol.* **215**, 71-96.

144. Lee, J., Remold, H. G., Ieong, M. H. & Kornfeld, H. (2006) Macrophage apoptosis in response to high intracellular burden of Mycobacterium tuberculosis is mediated by a novel caspase-independent pathway, *J Immunol.* **176**, 4267-74.

145. O'Sullivan, M. P., O'Leary, S., Kelly, D. M. & Keane, J. (2007) A caspase-independent pathway mediates macrophage cell death in response to Mycobacterium tuberculosis infection, *Infect Immun.* **75**, 1984-93.

146. Decuypere, J. P., Monaco, G., Bultynck, G., Missiaen, L., De Smedt, H. & Parys, J. B. (2011) The IP(3) receptor-mitochondria connection in apoptosis and autophagy, *Biochim Biophys Acta.* **1813**, 1003-13.

147. Joseph, S., Yuen, A., Singh, V. & Hmama, Z. (2017) Mycobacterium tuberculosis Cpn60.2 (GroEL2) blocks macrophage apoptosis via interaction with mitochondrial mortalin, *Biol Open.* **6**, 481-488.

148. Basu, S., Pathak, S. K., Banerjee, A., Pathak, S., Bhattacharyya, A., Yang, Z., Talarico, S., Kundu, M. & Basu, J. (2007) Execution of macrophage apoptosis by PE_PGRS33 of Mycobacterium tuberculosis is mediated by Toll-like receptor 2-dependent release of tumor necrosis factor-alpha, *J Biol Chem.* **282**, 1039-50.

149. Cadieux, N., Parra, M., Cohen, H., Maric, D., Morris, S. L. & Brennan, M. J. (2011) Induction of cell death after localization to the host cell mitochondria by the Mycobacterium tuberculosis PE_PGRS33 protein, *Microbiology (Reading).* **157**, 793-804.

150. Aguilar-Lopez, B. A., Correa, F., Moreno-Altamirano, M. M. B., Espitia, C., Hernandez-Longoria, R., Oliva-Ramirez, J., Padierna-Olivos, J. & Sanchez-Garcia, F. J. (2019) LprG and PE_PGRS33 Mycobacterium tuberculosis virulence factors induce differential mitochondrial dynamics in macrophages, *Scand J Immunol.* **89**, e12728.

151. Segal, G., Feldman, M. & Zusman, T. (2005) The Icm/Dot type-IV secretion systems of Legionella pneumophila and Coxiella burnetii, *FEMS Microbiol Rev.* **29**, 65-81.

152. Dolezal, P., Aili, M., Tong, J., Jiang, J. H., Marobbio, C. M., Lee, S. F., Schuelein, R., Belluzzo, S., Binova, E., Mousnier, A., Frankel, G., Giannuzzi, G., Palmieri, F., Gabriel, K., Naderer, T., Hartland, E. L. & Lithgow, T. (2012) Legionella pneumophila secretes a mitochondrial carrier protein during infection, *PLoS Pathog.* **8**, e1002459.

153. Escoll, P., Song, O. R., Viana, F., Steiner, B., Lagache, T., Olivo-Marin, J. C., Impens, F., Brodin, P., Hilbi, H. & Buchrieser, C. (2017) Legionella pneumophila Modulates Mitochondrial Dynamics to Trigger Metabolic Repurposing of Infected Macrophages, *Cell Host Microbe.* **22**, 302-316 e7.

154. Ogawa, M., Yoshida, S. & Mizuguchi, Y. (1994) 2-Deoxy-D-glucose inhibits intracellular multiplication and promotes intracellular killing of Legionella pneumophila in A/J mouse macrophages, *Infect Immun.* **62**, 266-70.

155. Hauslein, I., Sahr, T., Escoll, P., Klausner, N., Eisenreich, W. & Buchrieser, C. (2017) Legionella pneumophila CsrA regulates a metabolic switch from amino acid to glycerolipid metabolism, *Open Biol.* **7**.

156. Stecher, B., Robbiani, R., Walker, A. W., Westendorf, A. M., Barthel, M., Kremer, M., Chaffron, S., Macpherson, A. J., Buer, J., Parkhill, J., Dougan, G., von Mering, C. & Hardt, W. D. (2007) Salmonella enterica serovar typhimurium exploits inflammation to compete with the intestinal microbiota, *PLoS Biol.* **5**, 2177-89.

157. Winter, S. E., Thiennimitr, P., Winter, M. G., Butler, B. P., Huseby, D. L., Crawford, R. W., Russell, J. M., Bevins, C. L., Adams, L. G., Tsolis, R. M., Roth, J. R. & Baumler, A. J. (2010) Gut inflammation provides a respiratory electron acceptor for Salmonella, *Nature.* **467**, 426-9.

158. Layton, A. N., Brown, P. J. & Galyov, E. E. (2005) The Salmonella translocated effector SopA is targeted to the mitochondria of infected cells, *J Bacteriol.* **187**, 3565-71.

159. Kamanova, J., Sun, H., Lara-Tejero, M. & Galan, J. E. (2016) The Salmonella Effector Protein SopA Modulates Innate Immune Responses by Targeting TRIM E3 Ligase Family Members, *PLoS Pathog.* **12**, e1005552.

160. Tsuchida, T., Zou, J., Saitoh, T., Kumar, H., Abe, T., Matsuura, Y., Kawai, T. & Akira, S. (2010) The ubiquitin ligase TRIM56 regulates innate immune responses to intracellular double-stranded DNA, *Immunity.* **33**, 765-76.

161. Ren, Z., Ding, T., Zuo, Z., Xu, Z., Deng, J. & Wei, Z. (2020) Regulation of MAVS Expression and Signaling Function in the Antiviral Innate Immune Response, *Front Immunol.* **11**, 1030.

162. Sukumaran, S. K., Fu, N. Y., Tin, C. B., Wan, K. F., Lee, S. S. & Yu, V. C. (2010) A soluble form of the pilus protein FimA targets the VDAC-hexokinase complex at mitochondria to suppress host cell apoptosis, *Mol Cell.* **37**, 768-83.

163. Pastorino, J. G., Hoek, J. B. & Shulga, N. (2005) Activation of glycogen synthase kinase 3beta disrupts the binding of hexokinase II to mitochondria by phosphorylating voltage-dependent anion channel and potentiates chemotherapy-induced cytotoxicity, *Cancer Res.* **65**, 10545-54.

164. Abu-Hamad, S., Zaid, H., Israelson, A., Nahon, E. & Shoshan-Barmatz, V. (2008) Hexokinase-I protection against apoptotic cell death is mediated via interaction with the voltage-dependent anion channel-1: mapping the site of binding, *J Biol Chem.* **283**, 13482-90.

165. Hernandez, L. D., Pypaert, M., Flavell, R. A. & Galan, J. E. (2003) A Salmonella protein causes macrophage cell death by inducing autophagy, *J Cell Biol.* **163**, 1123-31.

166. Wyllie, S., Ashley, R. H., Longbottom, D. & Herring, A. J. (1998) The major outer membrane protein of Chlamydia psittaci functions as a porin-like ion channel, *Infect Immun.* **66**, 5202-7.

167. Fuchs, T. M., Eisenreich, W., Heesemann, J. & Goebel, W. (2012) Metabolic adaptation of human pathogenic and related nonpathogenic bacteria to extra- and intracellular habitats, *FEMS Microbiol Rev.* **36**, 435-62.

168. Matsumoto, A., Bessho, H., Uehira, K. & Suda, T. (1991) Morphological studies of the association of mitochondria with chlamydial inclusions and the fusion of chlamydial inclusions, *J Electron Microsc (Tokyo).* **40**, 356-63.

169. Knittler, M. R. & Sachse, K. (2015) Chlamydia psittaci: update on an underestimated zoonotic agent, *Pathog Dis.* **73**, 1-15.

170. Derre, I., Pypaert, M., Dautry-Varsat, A. & Agaisse, H. (2007) RNAi screen in Drosophila cells reveals the involvement of the Tom complex in Chlamydia infection, *PLoS Pathog.* **3**, 1446-58.

171. Mirrashidi, K. M., Elwell, C. A., Verschueren, E., Johnson, J. R., Frando, A., Von Dollen, J., Rosenberg, O., Gulbahce, N., Jang, G., Johnson, T., Jager, S., Gopalakrishnan, A. M., Sherry, J., Dunn, J. D., Olive, A., Penn, B., Shales, M., Cox, J. S., Starnbach, M. N., Derre, I., Valdivia, R., Krogan, N. J. & Engel, J. (2015) Global Mapping of the Inc-Human Interactome Reveals that Retromer Restricts Chlamydia Infection, *Cell Host Microbe.* **18**, 109-21.

172. Kawai, T., Takahashi, K., Sato, S., Coban, C., Kumar, H., Kato, H., Ishii, K. J., Takeuchi, O. & Akira, S. (2005) IPS-1, an adaptor triggering RIG-I- and Mda5-mediated type I interferon induction, *Nat Immunol.* **6**, 981-8.

173. Seth, R. B., Sun, L., Ea, C. K. & Chen, Z. J. (2005) Identification and characterization of MAVS, a mitochondrial antiviral signaling protein that activates NF-kappaB and IRF 3, *Cell.* **122**, 669-82.

174. Xu, L. G., Wang, Y. Y., Han, K. J., Li, L. Y., Zhai, Z. & Shu, H. B. (2005) VISA is an adapter protein required for virus-triggered IFN-beta signaling, *Mol Cell.* **19**, 727-40.

175. Monroe, K. M., McWhirter, S. M. & Vance, R. E. (2009) Identification of host cytosolic sensors and bacterial factors regulating the type I interferon response to Legionella pneumophila, *PLoS Pathog.* **5**, e1000665.

176. Jehl, S. P., Nogueira, C. V., Zhang, X. & Starnbach, M. N. (2012) IFNgamma inhibits the cytosolic replication of Shigella flexneri via the cytoplasmic RNA sensor RIG-I, *PLoS Pathog.* **8**, e1002809.

177. Li, X. D., Chiu, Y. H., Ismail, A. S., Behrendt, C. L., Wight-Carter, M., Hooper, L. V. & Chen, Z. J. (2011) Mitochondrial antiviral signaling protein (MAVS) monitors commensal bacteria and induces an immune response that prevents experimental colitis, *Proc Natl Acad Sci U S A.* **108**, 17390-5.

178. Stetson, D. B. & Medzhitov, R. (2006) Recognition of cytosolic DNA activates an IRF3-dependent innate immune response, *Immunity.* **24**, 93-103.

179. Barber, G. N. (2011) Innate immune DNA sensing pathways: STING, AIMII and the regulation of interferon production and inflammatory responses, *Curr Opin Immunol.* **23**, 10-20.

180. Loo, Y. M. & Gale, M., Jr. (2011) Immune signaling by RIG-I-like receptors, *Immunity.* **34**, 680-92.

181. Gack, M. U., Shin, Y. C., Joo, C. H., Urano, T., Liang, C., Sun, L., Takeuchi, O., Akira, S., Chen, Z., Inoue, S. & Jung, J. U. (2007) TRIM25 RING-finger E3 ubiquitin ligase is essential for RIG-I-mediated antiviral activity, *Nature.* **446**, 916-920.

182. Okamoto, M., Kouwaki, T., Fukushima, Y. & Oshiumi, H. (2017) Regulation of RIG-I Activation by K63-Linked Polyubiquitination, *Front Immunol.* **8**, 1942.

183. Gack, M. U. (2014) Mechanisms of RIG-I-like receptor activation and manipulation by viral pathogens, *J Virol.* **88**, 5213-6.

184. Hou, F., Sun, L., Zheng, H., Skaug, B., Jiang, Q. X. & Chen, Z. J. (2011) MAVS forms functional prion-like aggregates to activate and propagate antiviral innate immune response, *Cell.* **146**, 448-61.

185. Paz, S., Vilasco, M., Werden, S. J., Arguello, M., Joseph-Pillai, D., Zhao, T., Nguyen, T. L., Sun, Q., Meurs, E. F., Lin, R. & Hiscott, J. (2011) A functional C-terminal TRAF3-binding site in MAVS participates in positive and negative regulation of the IFN antiviral response, *Cell Res.* **21**, 895-910.

186. Tigano, M., Vargas, D. C., Tremblay-Belzile, S., Fu, Y. & Sfeir, A. (2021) Nuclear sensing of breaks in mitochondrial DNA enhances immune surveillance, *Nature.* **591**, 477-481.

187. Castanier, C., Garcin, D., Vazquez, A. & Arnoult, D. (2010) Mitochondrial dynamics regulate the RIG-I-like receptor antiviral pathway, *EMBO Rep.* **11**, 133-8.

188. Kim, S. J., Syed, G. H., Khan, M., Chiu, W. W., Sohail, M. A., Gish, R. G. & Siddiqui, A. (2014) Hepatitis C virus triggers mitochondrial fission and attenuates apoptosis to promote viral persistence, *Proc Natl Acad Sci U S A.* **111**, 6413-8.

189. Stavru, F., Bouillaud, F., Sartori, A., Ricquier, D. & Cossart, P. (2011) Listeria monocytogenes transiently alters mitochondrial dynamics during infection, *Proc Natl Acad Sci U S A.* **108**, 3612-7.

190. Atluri, V. L., Xavier, M. N., de Jong, M. F., den Hartigh, A. B. & Tsolis, R. M. (2011) Interactions of the human pathogenic Brucella species with their hosts, *Annu Rev Microbiol.* **65**, 523-41.

191. Lobet, E., Willemart, K., Ninane, N., Demazy, C., Sedzicki, J., Lelubre, C., De Bolle, X., Renard, P., Raes, M., Dehio, C., Letesson, J. J. & Arnould, T. (2018) Mitochondrial fragmentation affects neither the sensitivity to TNFalpha-induced apoptosis of Brucella-infected cells nor the intracellular replication of the bacteria, *Sci Rep.* **8**, 5173.

192. Stavru, F., Palmer, A. E., Wang, C., Youle, R. J. & Cossart, P. (2013) Atypical mitochondrial fission upon bacterial infection, *Proc Natl Acad Sci U S A.* **110**, 16003-8.

193. Jain, P., Luo, Z. Q. & Blanke, S. R. (2011) Helicobacter pylori vacuolating cytotoxin A (VacA) engages the mitochondrial fission machinery to induce host cell death, *Proc Natl Acad Sci U S A.* **108**, 16032-7.

194. Schulenburg, H. & Felix, M. A. (2017) The Natural Biotic Environment of Caenorhabditis elegans, *Genetics.* **206**, 55-86.

195. Pellegrino, M. W., Nargund, A. M., Kirienko, N. V., Gillis, R., Fiorese, C. J. & Haynes, C. M. (2014) Mitochondrial UPR-regulated innate immunity provides resistance to pathogen infection, *Nature.* **516**, 414-7.

196. Jeong, D. E., Lee, D., Hwang, S. Y., Lee, Y., Lee, J. E., Seo, M., Hwang, W., Seo, K., Hwang, A. B., Artan, M., Son, H. G., Jo, J. H., Baek, H., Oh, Y. M., Ryu, Y., Kim, H. J., Ha, C. M., Yoo, J. Y. & Lee, S. V. (2017) Mitochondrial chaperone HSP-60 regulates anti-bacterial immunity via p38 MAP kinase signaling, *EMBO J.* **36**, 1046-1065.

197. Mahmud, S. A., Qureshi, M. A., Sapkota, M. & Pellegrino, M. W. (2020) A pathogen branched-chain amino acid catabolic pathway subverts host survival by impairing energy metabolism and the mitochondrial UPR, *PLoS Pathog.* **16**, e1008918.

198. Hwang, A. B., Ryu, E. A., Artan, M., Chang, H. W., Kabir, M. H., Nam, H. J., Lee, D., Yang, J. S., Kim, S., Mair, W. B., Lee, C., Lee, S. S. & Lee, S. J. (2014) Feedback regulation via AMPK and HIF-1 mediates ROS-dependent longevity in Caenorhabditis elegans, *Proc Natl Acad Sci U S A.* **111**, E4458-67.

199. Amin, M. R., Mahmud, S. A., Dowgielewicz, J. L., Sapkota, M. & Pellegrino, M. W. (2020) A novel gene-diet interaction promotes organismal lifespan and host protection during infection via the mitochondrial UPR, *PLoS Genet.* **16**, e1009234.

200. Sagan, L. (1967) On the origin of mitosing cells, *J Theor Biol.* **14**, 255-74.

201. Zachar, I. & Boza, G. (2020) Endosymbiosis before eukaryotes: mitochondrial establishment in protoeukaryotes, *Cell Mol Life Sci.* **77**, 3503-3523.

202. Mira, M. T., Alcais, A., Nguyen, V. T., Moraes, M. O., Di Flumeri, C., Vu, H. T., Mai, C. P., Nguyen, T. H., Nguyen, N. B., Pham, X. K., Sarno, E. N., Alter, A., Montpetit, A., Moraes, M. E., Moraes, J. R., Dore, C., Gallant, C. J., Lepage, P., Verner, A., Van De Vosse, E., Hudson, T. J., Abel, L. & Schurr, E. (2004) Susceptibility to leprosy is associated with PARK2 and PACRG, *Nature.* **427**, 636-40.

203. Ali, S., Vollaard, A. M., Widjaja, S., Surjadi, C., van de Vosse, E. & van Dissel, J. T. (2006) PARK2/PACRG polymorphisms and susceptibility to typhoid and paratyphoid fever, *Clin Exp Immunol.* **144**, 425-31.

204. Manzanillo, P. S., Ayres, J. S., Watson, R. O., Collins, A. C., Souza, G., Rae, C. S., Schneider, D. S., Nakamura, K., Shiloh, M. U. & Cox, J. S. (2013) The ubiquitin ligase parkin mediates resistance to intracellular pathogens, *Nature.* **501**, 512-6.

205. Chai, Q., Wang, X., Qiang, L., Zhang, Y., Ge, P., Lu, Z., Zhong, Y., Li, B., Wang, J., Zhang, L., Zhou, D., Li, W., Dong, W., Pang, Y., Gao, G. F. & Liu, C. H. (2019) A Mycobacterium tuberculosis surface protein recruits ubiquitin to trigger host xenophagy, *Nat Commun.* **10**, 1973.

206. Sharma, S., tenOever, B. R., Grandvaux, N., Zhou, G. P., Lin, R. & Hiscott, J. (2003) Triggering the interferon antiviral response through an IKK-related pathway, *Science.* **300**, 1148-51.

207. Kawai, T., Takeuchi, O., Fujita, T., Inoue, J., Muhlradt, P. F., Sato, S., Hoshino, K. & Akira, S. (2001) Lipopolysaccharide stimulates the MyD88-independent pathway and results in activation of IFN-regulatory factor 3 and the expression of a subset of lipopolysaccharide-inducible genes, *J Immunol.* **167**, 5887-94.

208. Radtke, A. L., Delbridge, L. M., Balachandran, S., Barber, G. N. & O'Riordan, M. X. (2007) TBK1 protects vacuolar integrity during intracellular bacterial infection, *PLoS Pathog.* **3**, e29.

209. Knodler, L. A., Vallance, B. A., Celli, J., Winfree, S., Hansen, B., Montero, M. & Steele-Mortimer, O. (2010) Dissemination of invasive Salmonella via bacterial-induced extrusion of mucosal epithelia, *Proc Natl Acad Sci U S A.* **107**, 17733-8.

210. Perrin, A. J., Jiang, X., Birmingham, C. L., So, N. S. & Brumell, J. H. (2004) Recognition of bacteria in the cytosol of Mammalian cells by the ubiquitin system, *Curr Biol.* **14**, 806-11.

211. Thurston, T. L., Ryzhakov, G., Bloor, S., von Muhlinen, N. & Randow, F. (2009) The TBK1 adaptor and autophagy receptor NDP52 restricts the proliferation of ubiquitin-coated bacteria, *Nat Immunol.* **10**, 1215-21.

212. Wild, P., Farhan, H., McEwan, D. G., Wagner, S., Rogov, V. V., Brady, N. R., Richter, B., Korac, J., Waidmann, O., Choudhary, C., Dotsch, V., Bumann, D. & Dikic, I. (2011) Phosphorylation of the autophagy receptor optineurin restricts Salmonella growth, *Science.* **333**, 228-33.

213. Heo, J. M., Ordureau, A., Paulo, J. A., Rinehart, J. & Harper, J. W. (2015) The PINK1-PARKIN Mitochondrial Ubiquitylation Pathway Drives a Program of OPTN/NDP52 Recruitment and TBK1 Activation to Promote Mitophagy, *Mol Cell.* **60**, 7-20.

214. Moore, A. S. & Holzbaur, E. L. (2016) Spatiotemporal dynamics of autophagy receptors in selective mitophagy, *Autophagy.* **12**, 1956-1957.

FIGURES

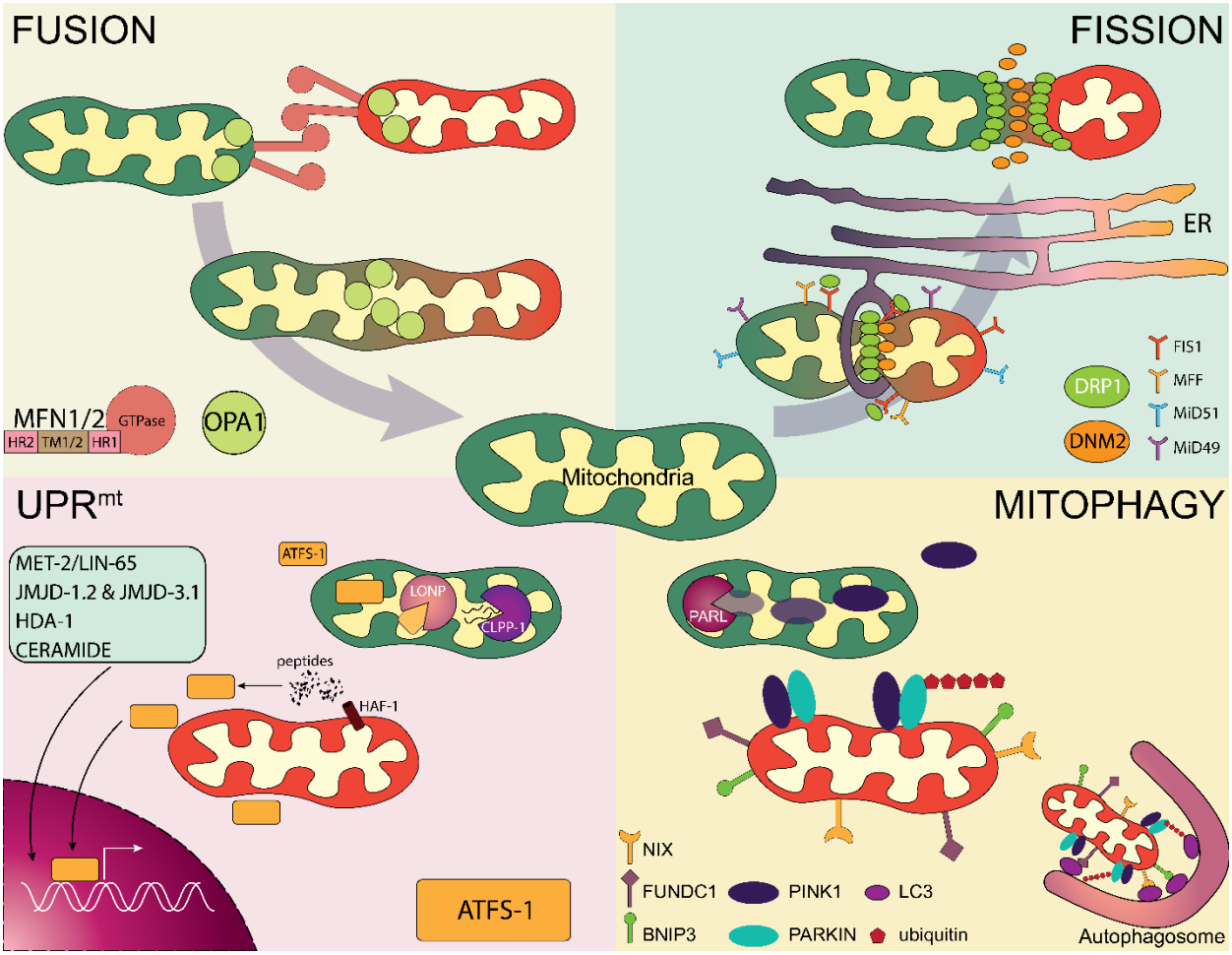

Figure 1.1 Mitochondrial recovery pathways.

Cells engage multiple pathways to restore mitochondrial function during stress. *Mitochondrial fusion* involves the merging of distinct mitochondria with the help of protein regulators at the outer and inner membrane, including the GTPases MFN1/2 and OPA1, respectively. *Mitochondrial fission* involves the division of mitochondria. ER tubules mark the future scission site and the constrictive forces of DRP1 GTPase mediate the actual division. DRP1 was proposed to function with DNM2 for mitochondrial fission, although this relationship is somewhat controversial. *UPR^{mt}* regulation is mediated by the transcription factor ATFS-1 in *C. elegans* (ATF5 in mammals) that contains a mitochondrial targeting sequence directing its localization to healthy mitochondria for

degradation by the protease LONP. Stressed mitochondria display reduced mitochondrial protein import, allowing ATFS-1 to translocate to the nucleus in order to regulate mitochondrial protective gene expression. Various regulators of the UPR^{mt} have been discovered and are shown in the boxed region. *Mitophagy* is a specialized form of autophagy that removes damaged mitochondria. Two main players in mitophagy are PINK1 and Parkin. In healthy mitochondria, PINK1 is degraded by the protease PARL. However, mitochondrial import efficiency of PINK1 is reduced in dysfunctional mitochondria, resulting in its presentation at the outer membrane. Here, PINK1 recruits the E3 ubiquitin ligase Parkin that ubiquitinates various substrates ultimately marking the damaged organelle for removal by an autophagic mechanism.

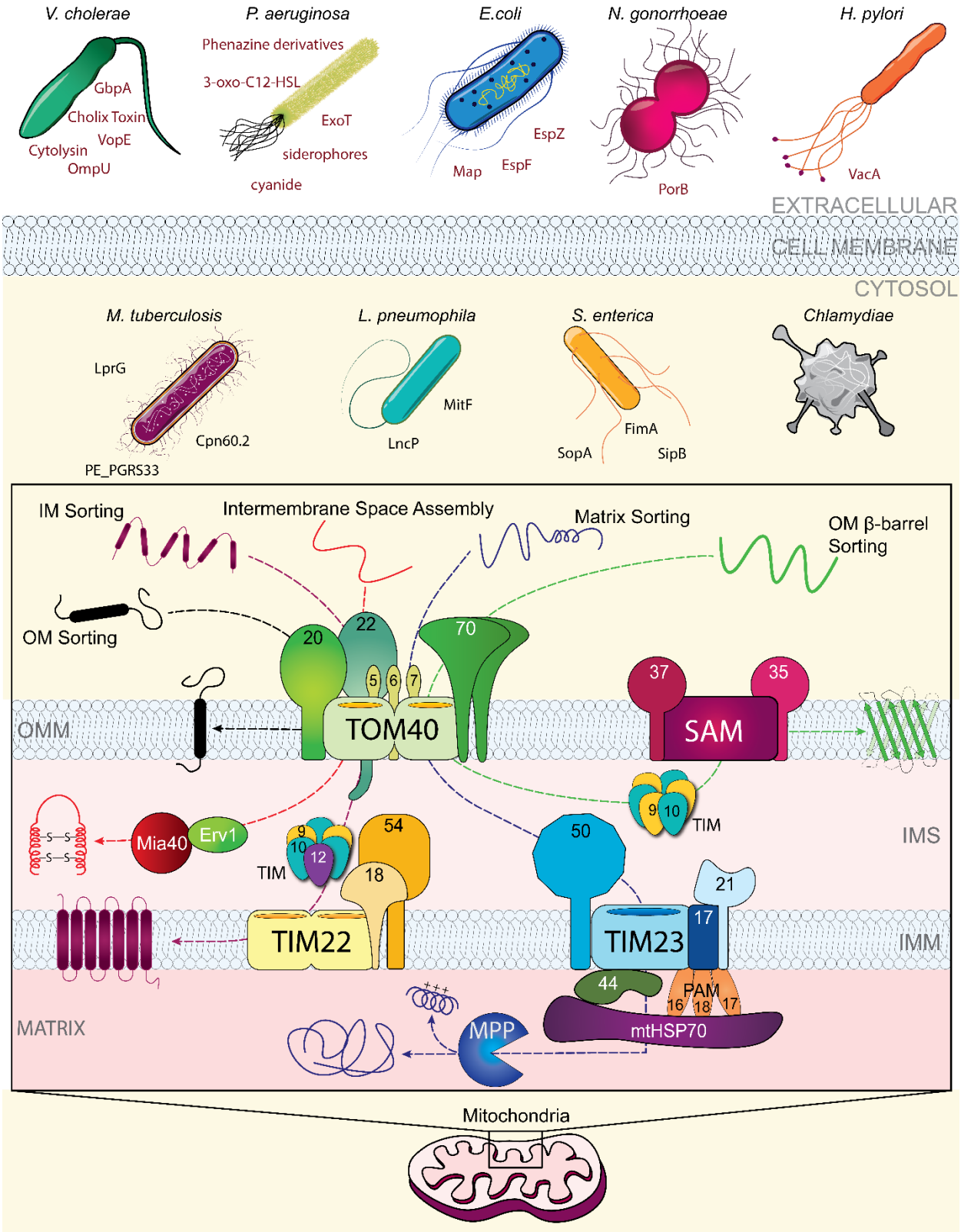
V. cholerae
GbpA
Cholix Toxin
VopE
Cytolysin
OmpU
P. aeruginosa
Phenazine derivatives
3-oxo-C12-HSL
ExoT
siderophores
cyanide
E.coli
EspZ
Map
EspF
N. gonorrhoeae
PorB
H. pylori
VacA
EXTRACELLULAR
CELL MEMBRANE
CYTOSOL
M. tuberculosis
LprG
Cpn60.2
PE_PGRS33
L. pneumophila
MitF
LncP
S. enterica
FimA
SopA
SipB
Chlamydiae
IM Sorting
Intermembrane Space Assembly
Matrix Sorting
OM β-barrel Sorting
OM Sorting
20
22
70
5
6
7
TOM40
OMM
37
35
SAM
9
10
TIM
IMS
Mia40
Erv1
S—S
S—S
9
10
12
TIM
54
18
50
21
17
TIM22
TIM23
IMM
44
PAM
16
18
17
mtHSP70
MPP
MATRIX
Mitochondria

Figure 1.2 Bacterial pathogens and their target: the mitochondrion

Mitochondria are double-membrane organelles. Complex transport systems mediate the import of mitochondrial proteins to specific sub-compartments. At the mitochondrial outer membrane, the TOM complex is first to recognize incoming mitochondrial proteins present in the cytosol and transfers these proteins to various compartments depending on their specific signal sequences. The SAM complex mediates the transfer of proteins into the outer membrane. The TIM22 and TIM23 complex regulate the transport of proteins into the mitochondrial inner membrane, while TIM23 mediates the transit of proteins into the matrix interior. The Mia40/Erv1 mediate the transport of proteins into the intermembrane space. The mitochondrial processing peptidase MPP cleaves the amino terminal signal sequence of nuclear-encoded mitochondrial proteins. Bacterial pathogens target various mitochondrial functions to promote their survival and infectivity. Shown here are extracellular and intracellular pathogens and their respective virulence factors that alter mitochondrial functions. *OM*, outer membrane; *IM*, inner membrane; *OMM*, outer mitochondrial membrane; *IMM*, inner mitochondrial membrane.

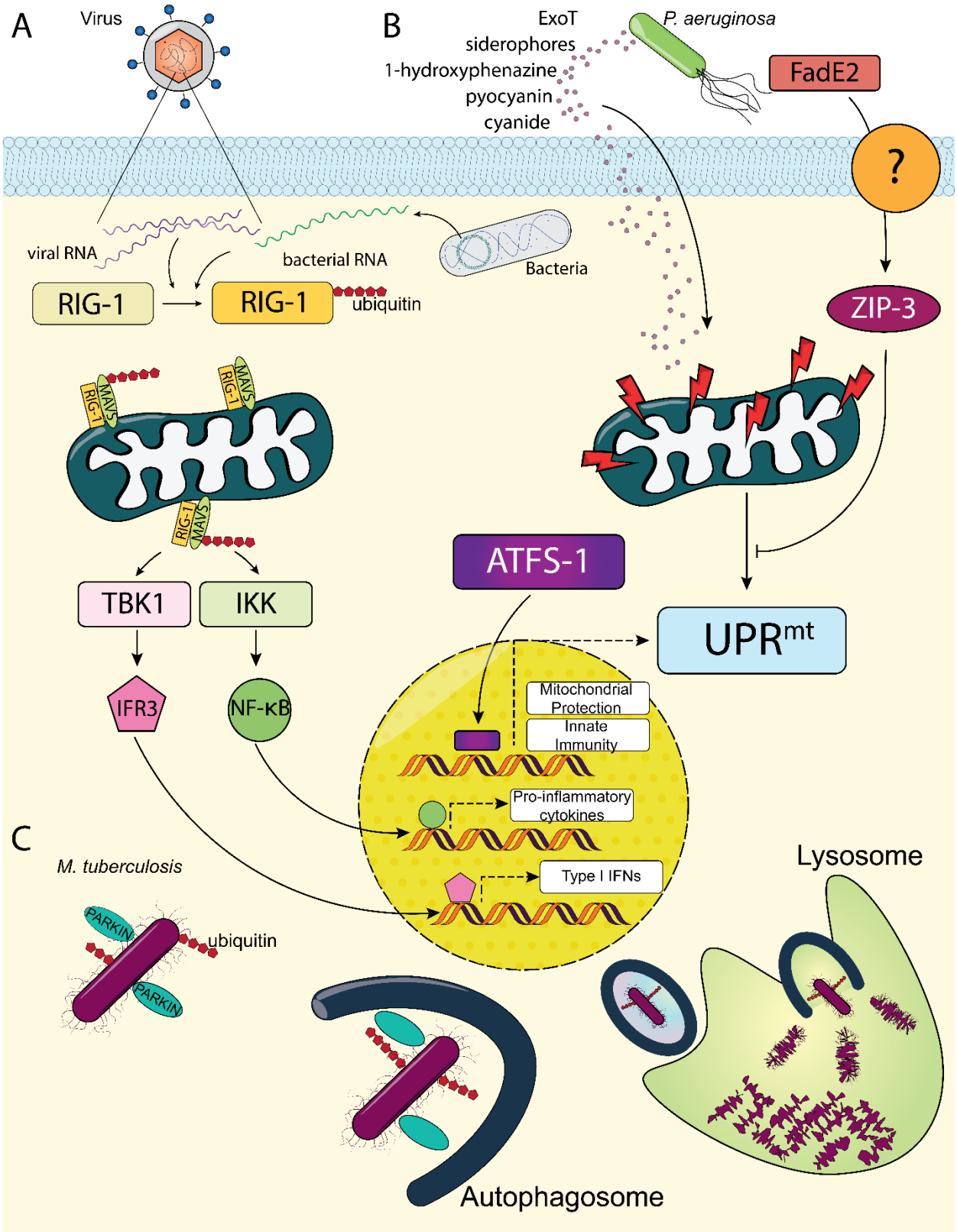
A
Virus
viral RNA
bacterial RNA
Bacteria
RIG-1
RIG-1
ubiquitin
MAVS
TBK1
IKK
IFR3
NF-κB
B
ExoT
siderophores
1-hydroxyphenazine
pyocyanin
cyanide
P. aeruginosa
FadE2
?
ZIP-3
ATFS-1
UPRmt
Mitochondrial Protection
Innate Immunity
Pro-inflammatory cytokines
Type I IFNs
C
M. tuberculosis
PARKIN
ubiquitin
Lysosome
Autophagosome

Figure 1.3 Engagement and subversion of mitochondrial recovery pathways during bacterial pathogen infection.

(A) The MAVS pathway responds to viral and bacterial RNA via the RLR RIG-1, which associate with MAVS protein at the mitochondrial outer membrane once activated. The RIG-1/MAVS complex becomes ubiquitinated, leading to the activation of the immune response regulators IFR3 and NF-kB via the kinases TBK1 and IKKe. (B) The UPR^{mt} is activated by toxins produced by *P. aeruginosa*, involving the translocation of ATFS-1 into the nucleus and the regulation of gene expression related to mitochondrial recovery and pathogen defense. *P. aeruginosa* also represses the UPR^{mt} via its metabolic enzyme FadE2 through an unresolved mechanism. In addition, *P. aeruginosa* manipulates the host transcription factor ZIP-3 to repress UPR^{mt} activity. (C) The ubiquitin ligase Parkin, involved in the clearance of damaged mitochondria by mitophagy, mediates the removal of intracellular pathogens such as *M. tuberculosis*. Parkin mediates the ubiquitination of *M. tuberculosis* which marks it for delivery to the autophagosome and eventual degradation by the lysosome.

2. A nematode-derived, mitochondrial stress signaling-regulated peptide exhibits broad antibacterial activity

Madhab Sapkota[1], Mohammed Adnan Qureshi[1], Siraje Arif Mahmud[1], Yves Balikosa[1†], Charlton Nguyen[1†], Joseph M. Boll[1], and Mark W. Pellegrino[1*]

[1]Department of Biology, University of Texas Arlington, Arlington, Texas, USA

*Author of correspondence: mark.pellegrino@uta.edu

[†]equal contribution

Key words: CNC-4, caenacins, antimicrobial peptide, mitochondria, mitochondrial UPR, stress response, innate immunity

ABSTRACT

A dramatic rise of infections with antibiotic-resistant bacterial pathogens continue to challenge the healthcare field due to the lack of effective treatment regimes. As such, there is an urgent need to develop new antimicrobial agents that can combat these multidrug-resistant superbugs. Mitochondria are central regulators of metabolism and other cellular functions, including the regulation of innate immunity pathways involved in the defense against infection. The mitochondrial unfolded protein response (UPR^{mt}) is a stress-activated pathway that mitigates mitochondrial dysfunction through the regulation of genes that promote recovery of the organelle.

In the model organism *Caenorhabditis elegans*, the UPR^{mt} also mediates an antibacterial defense program that combats pathogen infection which promotes host survival. We sought to identify and characterize antimicrobial effectors that are regulated during the UPR^{mt}. From our search, we discovered that the antimicrobial peptide CNC-4 is upregulated during this stress response. CNC-4 belongs to the caenacin family of antimicrobial peptides, which are predominantly found in nematodes and are known to have anti-fungal properties. Here, we find that CNC-4 also possesses potent antimicrobial activity against a spectrum of bacterial species and report on its characterization.

INTRODUCTION

Treatment of multidrug-resistant pathogenic infections has become a significant challenge in recent years, demonstrated by prolonged hospital stays, higher medical costs and increased mortality (Dadgostar, 2019). There is a considerable need, therefore, to discover and develop new antimicrobial therapeutics to combat these potentially difficult-to-treat infections. In addition, identification and characterization of host antimicrobial pathways may unveil new strategies in the fight against challenging pathogenic infections.

Mitochondria are essential organelles involved in multiple cellular functions including energy production via oxidative phosphorylation (OXPHOS), amino acid metabolism, and programmed cell death. In addition, mitochondria are important mediators of innate immunity, the host's first line of defense against pathogen infection. For example, mitochondrial reactive oxygen species (ROS) that are produced as a by-product of OXPHOS can activate innate immune

pathways such as NF-κB (Chandel et al., 2000), as well as acting directly as an anti-microbial agent (West et al., 2011). Mitochondria are also involved in the activation of the inflammasome via cardiolipin, a phospholipid present in mitochondrial membranes (Iyer et al., 2013), as well as mitochondrial ROS (Zhou et al., 2011). And, mitochondrial DNA itself can act as a damage-associated molecular pattern in the activation of innate immunity following Toll-like receptor recognition (Collins et al., 2004).

Considering their significant importance, dysfunction to mitochondria needs to be efficiently mitigated so as to avoid cellular and organismal decline. The mitochondrial unfolded protein response (UPR^{mt}) is one pathway that is activated during stress to mediate mitochondrial recovery (Qureshi et al., 2017). The mechanisms of UPR^{mt} regulation have largely been elucidated using the model organism *Caenorhabditis elegans* (Fig 2.1A). The UPR^{mt} in *C. elegans* is regulated by the bZIP transcription factor ATFS-1 which possesses transport sequences to both the nucleus and mitochondria (Nargund et al., 2012). ATFS-1 is imported into healthy mitochondria and turned over by a protease-mediated mechanism (Nargund et al., 2012). However, mitochondrial dysfunction reduces protein import efficiency and consequently the entry of ATFS-1 into the organelle, resulting in the import of ATFS-1 into the nucleus (Nargund et al., 2012; Rolland et al., 2019). ATFS-1 regulates the transcription of genes with multiple roles in recovering damaged mitochondria, including mitochondrial chaperones and proteases that mediate protein homeostasis, as well as regulators of free radical detoxification and mitochondrial dynamics (Nargund et al., 2015; Nargund et al., 2012). In addition to regulating genes that mitigate mitochondrial dysfunction, the UPR^{mt} also regulates innate immunity genes associated with defending the host against pathogenic agents. Notably, the UPR^{mt} is required for host survival during infection with bacterial pathogens such as *Pseudomonas aeruginosa* (Pellegrino et al.,

2014). In addition, priming the host for the UPR^{mt} increases its resistance to pathogen infection that enhances survival (Jeong et al., 2017; Pellegrino et al., 2014).

With the knowledge that the UPR^{mt} protects the host during infection, we sought to identify genes that are regulated during the UPR^{mt} that possess direct antibacterial activity. Our search identified CNC-4, an antimicrobial peptide of the caenacin family. We find that *cnc-4* is induced transcriptionally during the UPR^{mt} and exhibits antimicrobial activity against a broad range of bacterial pathogens. Here, we have characterized the antimicrobial activity of CNC-4.

RESULTS

The antimicrobial peptide cnc-4 is regulated by mitochondrial stress signaling

Activation of the UPR^{mt} protects the host during bacterial pathogen infection in an ATFS-1 dependent manner (Jeong et al., 2017; Pellegrino et al., 2014) (Fig 2.1A). We sought to identify genes that might contribute to the antimicrobial activity of the UPR^{mt} by referencing previously conducted gene expression analysis datasets (Lin et al., 2016; Nargund et al., 2012). We found that the antimicrobial peptide *cnc-4* was transcriptionally induced during the UPR^{mt} in both gene expression datasets analyzed, suggesting the peptide may be a relevant innate immune mechanism that contributes to the antimicrobial activity of this stress response. Antimicrobial peptides are secreted factors that form part of the host's machinery to defend itself during infection. Their antibacterial nature relates to an ability to form disruptive pores in bacterial membranes, although alternative mechanisms have also been identified (Le et al., 2017). In addition to the UPR^{mt}, *cnc-*

4 was also found to be transcriptionally induced during various genetic perturbations that result in mitochondrial stress including reduced function of OXPHOS components such as *cco-1*/COX5B (Tian et al., 2016), *clk-1*/COQ7 (Fischer et al., 2014) and *nuo-6*/NDUFB4 (Yee et al., 2014) as well as with knockdown of the mitochondrial chaperone *hsp-6*/mtHsp70 (Kim et al., 2016). We first confirmed that *cnc-4* transcript levels are increased during mitochondrial stress using the *clk-1(qm30)* loss-of-function mutant (Fig 2.1B). Next, we validated that *cnc-4* was induced during the UPR^{mt} using an *atfs-1* gain-of-function mutant which contains a mutation in the mitochondrial targeting sequence of ATFS-1 that prevents its import into mitochondria, resulting in constitutive nuclear accumulation and UPR^{mt} activation (Rauthan et al., 2013). Consistently, *cnc-4* was upregulated in ATFS-1 gain-of-function animals (Fig 2.1C), indicating that the gene encoding CNC-4 is transcriptionally induced during the UPR^{mt}.

CNC-4 belongs to the caenacin family of antimicrobial peptides which are phylogenetically related to the neuropeptide-like protein (NLP) family (Ewbank and Zugasti, 2011). Caenacins are largely restricted to nematodes and are known to be transcriptionally upregulated during fungal infection and exhibit anti-fungal properties (Couillault et al., 2004; Dierking et al., 2016).

A multiple sequence alignment of caenacins among different nematode species shows CNC-4 to be highly conserved amongst other members of the caenacin family and is rich in glycine and aromatic amino acids (Fig 2.1D and Table S1). A conserved and cleavable signal sequence is predicted from amino acids 1-18 of CNC-4, producing a mature peptide of 48 amino acids. After the signal sequence, a conserved motif of GGYG exists in all these peptides, followed by another highly conserved sequence RPGLLGML at the C-terminus. Interestingly, the GGYG motif is repeated throughout CNC-4 as well as in other caenacins, although the exact function of this motif is unknown. Phylogenetic analysis demonstrates that *C. elegans* CNC-4 forms a separate clade

with CNC-4 proteins from *C. remanei* and *C. briggasae*, and three other caenacins from *C. remanei*, *C. brenneri* and *C. nigoni* (Fig 2.1E). The other clade consists of CNC-2-related peptides from different nematodes including *C. elegans*.

CNC-4 possesses broad-spectrum antibacterial activity

Caenacins are known to respond to, and defend against, fungal infection in *C. elegans*. Whether they exhibit any antibacterial activity remained unknown. Therefore, we wished to assess potential antibacterial activity of CNC-4 by first using the *S*urface *L*ocalized *A*ntimicrobial displa*Y* (SLAY) approach (Kazi et al., 2020; Tucker et al., 2018). Briefly, the SLAY IPTG-inducible expression plasmid includes the Lpp signal sequence, transmembrane domains of OmpA for outer membrane localization, and a flexible tether, followed by the peptide of interest as a C-terminal fusion, thus localizing it to the bacterial surface. The flexible tether enables the target peptide to interact with structures on the cell surface, within the outer membrane, periplasm, and the inner membrane. Peptides with antimicrobial activity result in rapid cell death or growth inhibition. Antimicrobial activities of CNC-4 were assessed by SLAY using the *E. coli* K-12 strain W3110. As a negative control for our growth experiments, addition of IPTG inducer did not cause any growth defect in *E. coli* W3110 using the empty SLAY plasmid (Fig 2.2A). However, CNC-4 expressed within the SLAY system caused substantial growth defects in *E. coli* W3110 in a dose-dependent manner (Fig 2.2B).

To validate our findings, we chemically synthesized the active form of CNC-4 to measure its antibacterial activity in the absence of SLAY, as previously performed (Kazi et al., 2020;

Tucker et al., 2018). We treated a subset of both Gram-negative and Gram-positive bacterial species with the purified CNC-4 peptide and calculated the Minimum Bactericidal Concentration (MBC) as a reflection of its antibacterial activity. Purified CNC-4 exhibited potent antibacterial activity against Gram-negative bacteria including *E. coli*, *P. aeruginosa*, and *Acinetobacter baumanii* with MBCs ranging from < 2 µM to 8 µM (Table 1). In contrast, *Salmonella enterica* was relatively less susceptible to CNC-4 with a MBC of 128 µM (Table 1). Gram-positive bacteria were also impacted by CNC-4 treatment, including *Staphylococcus saprophyticus*, *Enterococcus faecalis*, and *Staphylococcus epidermidis* with MBC values ranging from 4 to 16 µM (Table 1), indicating that CNC-4 possesses broad-spectrum antibacterial activity.

We next evaluated whether bacterial growth phase impacted the antibacterial activity of CNC-4 using *E. coli* W3110 cells. We found that CNC-4 reduced the growth of log-phase *E. coli* W3110 cells in a concentration-dependent manner (Fig 2.2C). To examine the susceptibility of stationary phase cells, overnight cultures of *E. coli* W3110 were treated with varying concentrations of CNC-4. Stationary phase *E. coli* W3110 were also susceptible to CNC-4-dependent killing, exhibited by reduced cell viability in a concentration-dependent manner (Fig 2.2D). Therefore, bacterial growth phase stage does not impact CNC-4 antimicrobial action.

Next, we wondered whether physiological factors, including salt concentration and pH, affected the antibacterial activity of CNC-4. Salts can reduce the efficacy of antimicrobial peptides by reducing the electrostatic interaction of the peptide to the bacterial cell wall. Specifically, divalent cations such as Mg^{2+} bridge negatively charged functional groups of lipopolysaccharide located within the bacterial outer membrane, resulting in packing of lipids, while Na^{+} reduces antimicrobial peptide activity (Hancock, 1984; Kandasamy and Larson, 2006). We therefore measured the effects of monovalent (Na^{+}) and divalent (Mg^{2+}) cations on the activity of CNC-4

against *E. coli* W3110. We found that NaCl treatment led to decreases in the antibacterial activity of CNC-4 (Table 2). And, while low concentrations of $MgCl_2$ had little effect on the antibacterial activity of CNC-4, higher concentrations (1 mM and 10 mM) led to increases in the MBC against *E. coli* W3110 (Table 2). We also examined the effects of pH on CNC-4 activity against *E. coli* W3110 and found that neutral and alkaline conditions were permissive to CNC-4 activity, whereas lower pH conditions were antagonistic (Table 2). Therefore, while monovalent and divalent salt concentrations may need to be considered with regards to the potency of CNC-4, pH may be of lesser concern since physiological conditions tend to be slightly more alkaline.

Next, we wished to determine the minimal region of CNC-4 required for its antibacterial activity. We first created 12 amino acid truncations of CNC-4 and tested their antimicrobial activity using the SLAY system in *E. coli* W3110 cells (Fig 2.3A). While several truncations were measured, deletion of amino acids 13-36 of the mature CNC-4 peptide had no measurable effect on growth (Fig 2.3B-D). Interestingly, amino acids 1-12 of the mature CNC-4 contains the first GGYG motif, which is repeated three times and conserved amongst all caenacins (Fig 2.1D). We therefore created an additional truncation specifically removing the GGYG repeat to assess its possible antimicrobial role. We observed that greater amounts of CNC(1-8) was required to disrupt bacterial growth compared to the mature CNC-4 or CNC(1-12) (Fig. 2.3E), suggesting that loss of the GGYG repeat reduces, but does not eliminate, CNC-4 antibacterial activity. Thus, the GGYG likely plays an important functional role in the antibacterial activity of CNC-4.

CNC-4 increases bacterial membrane permeability

Next, we investigated the mechanism behind the antibacterial nature of CNC-4. We first examined the effect of CNC-4 on bacterial membrane permeability by quantifying the accumulation of intracellular ethidium bromide, as previously described (Kamischke et al., 2019; Kazi et al., 2020). Ethidium bromide is a fluorescent dye that intercalates DNA, but it is unable to enter Gram-negative bacteria due to their outer membrane that acts as a barrier. However, outer membrane perturbations, or loss of surface potential permits ethidium bromide entry, which can cross the cytoplasmic membrane and bind to its DNA target. We therefore quantified ethidium bromide accumulation in the presence or absence of CNC-4. Indeed, we found that CNC-4 increased the incorporation of ethidium bromide into Gram-negative bacteria including *E. coli* W3110, *P. aeruginosa*, and *A. baumannii* in a dose-dependent manner (Fig 2.4A-C). Gram-positive bacteria also displayed increases in membrane permeability in the presence of CNC-4, albeit to a lesser degree (Fig 2.4D-F). Therefore, CNC-4 increases membrane permeability as part of its antibacterial mechanism.

We also examined the localization of FITC-CNC-4 using fluorescence microscopy. We found that FITC-CNC-4 accumulated within the cytoplasm of both Gram-negative and Gram-positive bacteria based on co-localization with DAPI-stained DNA (Fig 2.5A). Consistently, intracellular localization of antimicrobial peptides which result in increased membrane permeabilization has been observed before (Farkas et al., 2017). While this suggests that the antimicrobial mode of action of CNC-4 may occur at least in part intracellularly, it is probable that CNC-4 resides at the membrane transiently, leading to increased bacterial membrane permeability and accumulation within the cytoplasm.

Since we observed intracellular accumulation of CNC-4, we also investigated other possible molecular targets of this peptide. Antimicrobial peptides can also promote their

antibacterial activity by directly binding bacterial DNA (Le et al., 2017). To examine whether CNC-4 exhibited DNA binding properties, we incubated plasmid DNA with increasing amounts of CNC-4 peptide and then assessed migratory shifts following electrophoresis. Interestingly, increasing amounts of CNC-4 prevented plasmid DNA migration during electrophoresis (Fig 2.5B), suggesting that CNC-4 possesses DNA binding activity.

CNC-4 does not show cytotoxicity against mammalian epithelial cells

Finally, we examined whether CNC-4 exhibited any toxicity towards mammalian cells using the mouse derived intestinal cell line MODE-K as previously performed (Kazi et al., 2020). To measure cytotoxicity, we employed the MTT (3-(4,5-dimethylthiazol-2-yl)-2,5-diphenyltetrazolium bromide) assay which measures the ability of viable cells to convert MTT to an insoluble formazan product. Our results indicated that MODE-K cells tolerate CNC-4 at concentrations up to 64 µM, (Fig 2.6), which is well above the MIC for several pathogens tested (Table 1). Therefore, CNC-4 may have the potential to be used as an antimicrobial agent with the added benefit of reduced toxicity to the host.

DISCUSSION

In conclusion, while mitochondrial stress signaling pathways such as the UPR^{mt} have documented benefits in increasing host resistance during pathogen infection, the effectors that mediate this protection have largely been unresolved. We have identified the antimicrobial peptide

CNC-4 as one such effector, demonstrating notable activity against several clinically important bacterial pathogens. We showed that CNC-4 exhibits antibacterial activity presumably through a mechanism involving increased membrane permeability and possibly DNA binding mechanisms. In addition, CNC-4 exhibits low cytotoxic activity against a mammalian cell line. Together, our data suggest that the nematode-originating CNC-4 may have potential applications therapeutically against challenging bacterial infections.

It was previously shown that the UPR^{mt} regulates innate immunity gene expression to protect the host against infection (Amin et al., 2020; Jeong et al., 2017; Mahmud et al., 2020; Pellegrino et al., 2014; Shao et al., 2020). The *cnc-4* gene is transcriptionally induced during mitochondrial stress as part of the UPR^{mt} protective pathway, however the exact mechanism for this UPR^{mt}-mediated *cnc-4* induction is currently unclear. One possibility is that the main UPR^{mt} transcription factor ATFS-1 directly regulates the expression of *cnc-4*. However, we did not detect any obvious ATFS-1 binding sites (Nargund et al., 2015) in the *cnc-4* promoter. Also, *cnc-4* was not identified as a direct target of ATFS-1 using chromatin immunoprecipitation (Nargund et al., 2015). Therefore, it is likely that ATFS-1 regulates *cnc-4* expression indirectly via an as-of-yet unknown regulator. It was previously found that the mitochondrial chaperone HSP-60, which is transcriptionally induced during the UPR^{mt}, can stimulate innate immunity through physical association with SEK-1/ MAP kinase kinase 3, a critical component of the p38 MAP kinase innate immunity pathway in *C. elegans* (Jeong et al., 2017). Thus, one possibility is that p38 MAP kinase signaling mediates the upregulation of *cnc-4* during the UPR^{mt}. However, gene expression for the related caenacin *cnc-2* was found to be induced during infection with the fungus *Drechmeria coniospora* in a p38 MAP kinase-independent manner (Zugasti and Ewbank, 2009). Instead, *cnc-2* gene induction was found to rely on non-canonical TGF-β signaling (Zugasti and Ewbank, 2009).

Therefore, it is possible that the UPR^{mt} and non-canonical TGF-β signaling converge to regulate *cnc-4* gene expression during stress.

A discernible feature of CNC-4 is the high representation of glycine residues in the mature peptide (40% of all amino acids), a characteristic feature of members of the caenacin family (Couillault et al., 2004). While the exact function of the glycine residues is not known, it is predicted to increase flexibility to the peptide's structure (Pelegrini et al., 2008). Another discernible feature of CNC-4 is the presence of a GGYG repeat that we showed to be necessary for its antimicrobial activity. We currently do not know the functional significance of this repeat sequence but interestingly, it is also found in a crustacean antimicrobial peptide that exhibits specific activity against Gram-positive bacteria (Imjongjirak et al., 2011). Other glycine-rich antimicrobial peptides have also been discovered that exhibit activities against fungi and/or bacteria (both Gram-negative and Gram-positive) (Bulet et al., 1991; de Jesus Oliveira et al., 2019; Lorenzini et al., 2003; Lu and Chen, 2010; Sousa et al., 2009; Sperstad et al., 2009; Verdon et al., 2016; Xie et al., 2020). While the caenacins were previously shown to possess anti-fungal properties, our study clearly demonstrates an antibacterial activity for CNC-4 against both Gram-negative and Gram-positive bacteria. Interestingly, another member of the *C. elegans* caenacin family, CNC-2, mediates anti-fungal defense specifically (Zehrbach et al., 2017), suggesting these peptides exhibit variable antimicrobial activities.

Our study has also elucidated the mechanism of action for the caenacin CNC-4. Here, we have shown that CNC-4 increases membrane permeability in both Gram-negative and Gram-positive bacteria. Supporting this finding, we also showed that fluorescently labelled CNC-4 accumulated intracellularly in both Gram-negative and Gram-positive bacteria. Lastly, we discovered that CNC-4 has the capability of binding DNA, suggesting that its buildup within the cell may have functional

significance. Interestingly, a glycine-rich antimicrobial peptide (YD1) was isolated from *Bacillus amyloliquefaciens* that displayed cell-penetrating capabilities and also DNA-binding properties (Rahman et al., 2017). In contrast to CNC-4, however, YD1 was able to penetrate bacterial membranes without the formation of disruptive pores (Rahman et al., 2017). Similarly, CF-14, an antimicrobial peptide isolated from catfish epidermal mucus, was able to access the inside of bacterial cells and bind DNA (Li et al., 2019). Lastly, the cell-penetrating synthetic antimicrobial peptide analog P7 was shown to bind bacterial DNA and inhibit cell division (Li et al., 2015). Whether CNC-4 displays cell penetrating abilities in addition to its capacity to form disruptive pores is not known. The functional significance of CNC-4's ability to bind DNA is also unclear. However, other antimicrobial peptides have been found to bind DNA resulting in cessation of DNA replication. One such example is indolicidin, an antimicrobial peptide that prevents DNA unwinding, resulting in repression of DNA replication and transcription (Ghosh et al., 2014; Subbalakshmi and Sitaram, 1998). Further mechanistic examination into the antimicrobial nature of CNC-4 is thus warranted.

MATERIALS AND METHODS

C. elegans strains and culturing

C. elegans were obtained from the Caenorhabditis Genetics Center and cultured as described previously using standard Nematode Growth Medium (Brenner, 1974). Worms were cultured at 20°C and fed *E. coli* OP50.

Bacterial strains, antibiotics and CNC-4 peptide

Strains and plasmids used in this study are listed in Table S2 and Table S3. The concentration of antibiotics used were: ampicillin (50 µg/mL) and tetracycline (5-10 µg/mL). Bacterial cultures were grown at 37^0C with shaking at 280 rpm. CNC-4 peptide was synthesized commercially (GenScript) and dissolved in 100 % DMSO to a concentration of 10 mg/mL and diluted to the appropriate concentration thereafter, as performed previously (Kazi et al., 2020; Tucker et al., 2018).

Quantitative PCR (qPCR) of cnc-4 expression

C. elegans total RNA was harvested by using Direct-zol™ RNA MiniPrep Plus kit as per manufacturer's recommendations. cDNA was synthesized using the Bio-Rad Superscript kit according to the manufacturer's instructions. qPCR of *cnc-4* was performed using primers ACAATGGGGCTACGGTCCATAT and ACTTTCCAATGAGCATTCCGAGGA , with amplification of the housekeeping gene *act-3* as a reference using primers ATCCGTAAGGACTTGTACGCCAAC and CGATGATCTTGATCTTCATGGTTC.

CNC-4 protein sequence analysis

The CNC-4 protein sequence was blasted against UniProt's UniProtKB reference proteomes plus Swiss-Prot database using BLASTP and the top ten non-redundant hits were identified. Protein sequences were gathered, and multiple sequence alignment of those proteins sequences was performed using the ClustalW tool in BioEdit. The alignment file was imported into JalView to construct the final alignment figure. For generation of the phylogenetic tree, the same alignment file was imported into MEGA 7.0 software and the tree generated using the Neighbor-Joining method using 1000 bootstraps. All positions containing gaps and missing data were eliminated.

SLAY expression plasmid construction

The CNC-4 cDNA was amplified using primers CGCGGTACCAGTCAAGAGCCTGC and AAAGTCGACTTACTTTCCAATGAGCATTCCGAGGAGCCCTGGGCGGTACATTCCCAT TCCGTAGCCACCGTACATTCCATATGGACGCATACCGTATCCGCCATACATTCCAGG GTATCCACCACCATACCCGCCATATGGACCGTAGCCCCATTGTCCTCCGATACCCGC AGCTG, and pMMB-cecropin (Tucker et al., 2018) was used as a template. The amplicon was digested with KpnI and SalI and cloned into the pMMB-tet plasmid yielding pMMB-tet-cnc-4. The construct was transformed into the *E. coli* W3110 strain by chemical transformation. CNC-4 truncated cDNA fragments were amplified using the forward primer

ACAGAATTCAGGAGGAAACGATGAAA and the following reverse primers: TTTGTCGACTTACATTCCCATTCCGTAGCC (CNC-4_1-36), TTTGTCGACTTAACGCATACCGTATCCGCC (CNC-4_1-24), TTTGTCGACTTAACCACCATACCCGCCATA (CNC-4_1-12), and TTTGTCGACTTAGCCATATGGACCGTAGCCCCATTG (CNC-4_1-8), using pMMB-tet-cnc-4 as a template) and cloned into EcoRI and SalI sites of pMMB67EH. Each construct was verified by DNA sequencing before transforming into *E. coli* W3110.

Bacterial growth determination using SLAY display expression system

Growth curves using SLAY were done as done previously described (Kazi et al., 2020; Tucker et al., 2018). Overnight cultures of *E. coli* W3110 were diluted to OD_{600} of ~0.05 and grown to an OD_{600} of 0.6-0.8 representative of exponentially growing cells or overnight for stationary phase cells. Bacterial cultures were diluted to an OD_{600} of 0.01 and loaded into 96 well plates with increasing concentration of IPTG. Bacterial growth was monitored using a BioTek SYNERGY neo2 multi-mode plate reader every 30 minutes for 8 hours. Growth curves were carried out at least three times in triplicate and plotted using GraphPad.

Determination of Minimum Bactericidal Concentration (MBC)

MBCs were performed as previously described (Kazi et al., 2020; Tucker et al., 2018), with slight modifications. The MBC was defined as the minimum concentration of the CNC-4 peptide which resulted in a three-log growth reduction of the initial inoculum. The MBC assays were carried out in Bovine Serum Albumin (BSA)-acetic acid media (Tris-medium assay). Briefly, cells were grown to an OD_{600nm} of 0.6-0.8, harvested with centrifugation at 3000 rpm for 5 min and washed at least two times with Tris-media comprised of 10 mM Tris-base (pH 7.4), 50 mM NaCl, 0.2% glucose. The OD_{600nm} of the cultures were adjusted to 0.004 in Tris-media. CNC-4 peptide was prepared in BSA-acetic acid media (0.2% BSA, 0.01% acetic acid) and then added to the cultures at varying concentrations. Solutions were mixed thoroughly and incubated in polypropylene 96 well plates for 18-24 hours at 37^0C. DMSO was used as a control for each concentration of CNC-4 peptide. 5 □l of each overnight culture was spotted on LB agar media and incubated overnight. The concentration of CNC-4 peptide which resulted in no visible growth was recorded as the MBC.

Membrane permeability assay

Permeability assays were performed as previously described (Kamischke et al., 2019; Kazi et al., 2020). Bacterial cells were grown to mid-log phase followed by washing with Tris-media. Bacteria were then diluted to OD_{600} of 0.3/ml. CNC-4 peptide was added to a concentration equivalent to 0.5xMBC,1xMBC and 2xMBC values for each strain. Ethidium bromide was added to a final concentration of 6 µM followed by measurement of fluorescence using a BioTek SYNERGY neo2 multi-mode plate reader at 545 nm excitation and 600 nm emission wavelengths.

Fluorescence Microscopy

The CNC-4 full length peptide was labelled with FITC (fluorescein isothiocyanate) at its N-terminus by GenScript. Bacterial strains were grown to mid-log phase, harvested and washed at least twice with Tris-media before treatments with 1 µM FITC-CNC-4. About 10^7 CFUs of cells were used for peptide treatment. Cells were treated for the specified amount of time and washed with Tris-media. Bacterial cells were then stained with DAPI (1 µg/mL) and images were acquired using a Zeiss Axioimager.Z2 fluorescence microscope.

CNC-4 DNA-binding assay

The interaction of CNC-4 with plasmid DNA was assessed using the gel retardation assay (Chen et al., 2013). 500 ng of pBlueScript SK(-) plasmid was combined with varying amounts of purified CNC-4 peptide. DMSO was used as a control for the peptide solvent. Each mixture was incubated at 37°C for 1 hr and separated using standard gel electrophoresis.

MTT assay for the assessment of cell viability

MTT assay was carried out using the MTT Cell Growth Assay kit as described by the manufacturer (EMD Millipore), as previously described (Kazi et al., 2020). Mouse MODE-K epithelial cell line (gift from Dr. Jason Kubinak; University of South Carolina) were used at sub-confluent (~10,000

cells/well) and confluent (~50,000 cells/well) cell densities in RPMI media with 10% FBS. MODE-K cells were treated with increasing concentrations of dimethyl sulfoxide (DMSO) or CNC-4 peptide for 24 hours. Cells were then treated with fresh media containing 0.45 mg/ml 3-(4,5-dimethyl-2-thiazolyl0-2,5-diphenyltetrazolium bromide (MTT) (Sigma Aldrich) and incubated at 37 ^{0}C for 4 hours. The liquid was then removed and 100 µl of DMSO added to each well. The plate was incubated at room temperature with shaking for 1 hour and the absorbance was measured at 570 nm. The DMSO vehicle control represents the volume equivalent used for 64 □M CNC-4.

REFERENCES

1. Amin, M.R., Mahmud, S.A., Dowgielewicz, J.L., Sapkota, M., and Pellegrino, M.W. (2020). A novel gene-diet interaction promotes organismal lifespan and host protection during infection via the mitochondrial UPR. PLoS Genet *16*, e1009234.
2. Brenner, S. (1974). The genetics of Caenorhabditis elegans. Genetics *77*, 71-94.
3. Bulet, P., Cociancich, S., Dimarcq, J.L., Lambert, J., Reichhart, J.M., Hoffmann, D., Hetru, C., and Hoffmann, J.A. (1991). Insect immunity. Isolation from a coleopteran insect of a novel inducible antibacterial peptide and of new members of the insect defensin family. J Biol Chem *266*, 24520-24525.
4. Chandel, N.S., Trzyna, W.C., McClintock, D.S., and Schumacker, P.T. (2000). Role of oxidants in NF-kappa B activation and TNF-alpha gene transcription induced by hypoxia and endotoxin. J Immunol *165*, 1013-1021.
5. Chen, H.L., Su, P.Y., Chang, Y.S., Wu, S.Y., Liao, Y.D., Yu, H.M., Lauderdale, T.L., Chang, K., and Shih, C. (2013). Identification of a novel antimicrobial peptide from human hepatitis B virus core protein arginine-rich domain (ARD). PLoS Pathog *9*, e1003425.
6. Collins, L.V., Hajizadeh, S., Holme, E., Jonsson, I.M., and Tarkowski, A. (2004). Endogenously oxidized mitochondrial DNA induces in vivo and in vitro inflammatory responses. J Leukoc Biol *75*, 995-1000.
7. Couillault, C., Pujol, N., Reboul, J., Sabatier, L., Guichou, J.F., Kohara, Y., and Ewbank, J.J. (2004). TLR-independent control of innate immunity in Caenorhabditis elegans by the TIR domain adaptor protein TIR-1, an ortholog of human SARM. Nat Immunol *5*, 488-494.

8. Dadgostar, P. (2019). Antimicrobial Resistance: Implications and Costs. Infect Drug Resist *12*, 3903-3910.

9. de Jesus Oliveira, T., Oliveira, U.C., and da Silva Junior, P.I. (2019). Serrulin: A Glycine-Rich Bioactive Peptide from the Hemolymph of the Yellow Tityus serrulatus Scorpion. Toxins (Basel) *11*.

10. Dierking, K., Yang, W., and Schulenburg, H. (2016). Antimicrobial effectors in the nematode Caenorhabditis elegans: an outgroup to the Arthropoda. Philos Trans R Soc Lond B Biol Sci *371*.

11. Ewbank, J.J., and Zugasti, O. (2011). C. elegans: model host and tool for antimicrobial drug discovery. Dis Model Mech *4*, 300-304.

12. Farkas, A., Maroti, G., Kereszt, A., and Kondorosi, E. (2017). Comparative Analysis of the Bacterial Membrane Disruption Effect of Two Natural Plant Antimicrobial Peptides. Front Microbiol *8*, 51.

13. Fischer, A., Niklowitz, P., Menke, T., and Doring, F. (2014). Promotion of growth by Coenzyme Q10 is linked to gene expression in C. elegans. Biochem Biophys Res Commun *452*, 920-927.

14. Ghosh, A., Kar, R.K., Jana, J., Saha, A., Jana, B., Krishnamoorthy, J., Kumar, D., Ghosh, S., Chatterjee, S., and Bhunia, A. (2014). Indolicidin targets duplex DNA: structural and mechanistic insight through a combination of spectroscopy and microscopy. ChemMedChem *9*, 2052-2058.

15. Hancock, R.E. (1984). Alterations in outer membrane permeability. Annu Rev Microbiol *38*, 237-264.

16. Imjongjirak, C., Amparyup, P., and Tassanakajon, A. (2011). Two novel antimicrobial peptides, arasin-likeSp and GRPSp, from the mud crab Scylla paramamosain, exhibit the activity against some crustacean pathogenic bacteria. Fish Shellfish Immunol *30*, 706-712.

17. Iyer, S.S., He, Q., Janczy, J.R., Elliott, E.I., Zhong, Z., Olivier, A.K., Sadler, J.J., Knepper-Adrian, V., Han, R., Qiao, L., *et al.* (2013). Mitochondrial cardiolipin is required for Nlrp3 inflammasome activation. Immunity *39*, 311-323.

18. Jeong, D.E., Lee, D., Hwang, S.Y., Lee, Y., Lee, J.E., Seo, M., Hwang, W., Seo, K., Hwang, A.B., Artan, M., *et al.* (2017). Mitochondrial chaperone HSP-60 regulates anti-bacterial immunity via p38 MAP kinase signaling. EMBO J *36*, 1046-1065.

19. Kamischke, C., Fan, J., Bergeron, J., Kulasekara, H.D., Dalebroux, Z.D., Burrell, A., Kollman, J.M., and Miller, S.I. (2019). The Acinetobacter baumannii Mla system and glycerophospholipid transport to the outer membrane. Elife *8*.

20. Kandasamy, S.K., and Larson, R.G. (2006). Effect of salt on the interactions of antimicrobial peptides with zwitterionic lipid bilayers. Biochim Biophys Acta *1758*, 1274-1284.

21. Kazi, M.I., Perry, B.W., Card, D.C., Schargel, R.D., Ali, H.B., Obuekwe, V.C., Sapkota, M., Kang, K.N., Pellegrino, M.W., Greenberg, D.E., *et al.* (2020). Discovery and

characterization of New Delhi metallo-beta-lactamase-1 inhibitor peptides that potentiate meropenem-dependent killing of carbapenemase-producing Enterobacteriaceae. J Antimicrob Chemother *75*, 2843-2851.

22. Kim, H.E., Grant, A.R., Simic, M.S., Kohnz, R.A., Nomura, D.K., Durieux, J., Riera, C.E., Sanchez, M., Kapernick, E., Wolff, S., *et al.* (2016). Lipid Biosynthesis Coordinates a Mitochondrial-to-Cytosolic Stress Response. Cell *166*, 1539-1552 e1516.

23. Le, C.F., Fang, C.M., and Sekaran, S.D. (2017). Intracellular Targeting Mechanisms by Antimicrobial Peptides. Antimicrob Agents Chemother *61*.

24. Li, L., Shi, Y., Cheng, X., Xia, S., Cheserek, M.J., and Le, G. (2015). A cell-penetrating peptide analogue, P7, exerts antimicrobial activity against Escherichia coli ATCC25922 via penetrating cell membrane and targeting intracellular DNA. Food Chem *166*, 231-239.

25. Li, T., Liu, Q., Wang, D., and Li, J. (2019). Characterization and antimicrobial mechanism of CF-14, a new antimicrobial peptide from the epidermal mucus of catfish. Fish Shellfish Immunol *92*, 881-888.

26. Lin, Y.F., Schulz, A.M., Pellegrino, M.W., Lu, Y., Shaham, S., and Haynes, C.M. (2016). Maintenance and propagation of a deleterious mitochondrial genome by the mitochondrial unfolded protein response. Nature *533*, 416-419.

27. Lorenzini, D.M., da Silva, P.I., Jr., Fogaca, A.C., Bulet, P., and Daffre, S. (2003). Acanthoscurrin: a novel glycine-rich antimicrobial peptide constitutively expressed in the hemocytes of the spider Acanthoscurria gomesiana. Dev Comp Immunol *27*, 781-791.

28. Lu, J., and Chen, Z.W. (2010). Isolation, characterization and anti-cancer activity of SK84, a novel glycine-rich antimicrobial peptide from Drosophila virilis. Peptides *31*, 44-50.

29. Mahmud, S.A., Qureshi, M.A., Sapkota, M., and Pellegrino, M.W. (2020). A pathogen branched-chain amino acid catabolic pathway subverts host survival by impairing energy metabolism and the mitochondrial UPR. PLoS Pathog *16*, e1008918.

30. Nargund, A.M., Fiorese, C.J., Pellegrino, M.W., Deng, P., and Haynes, C.M. (2015). Mitochondrial and nuclear accumulation of the transcription factor ATFS-1 promotes OXPHOS recovery during the UPR(mt). Mol Cell *58*, 123-133.

31. Nargund, A.M., Pellegrino, M.W., Fiorese, C.J., Baker, B.M., and Haynes, C.M. (2012). Mitochondrial import efficiency of ATFS-1 regulates mitochondrial UPR activation. Science *337*, 587-590.

32. Pelegrini, P.B., Murad, A.M., Silva, L.P., Dos Santos, R.C., Costa, F.T., Tagliari, P.D., Bloch, C., Jr., Noronha, E.F., Miller, R.N., and Franco, O.L. (2008). Identification of a novel storage glycine-rich peptide from guava (Psidium guajava) seeds with activity against Gram-negative bacteria. Peptides *29*, 1271-1279.

33. Pellegrino, M.W., Nargund, A.M., Kirienko, N.V., Gillis, R., Fiorese, C.J., and Haynes, C.M. (2014). Mitochondrial UPR-regulated innate immunity provides resistance to pathogen infection. Nature *516*, 414-417.

34. Qureshi, M.A., Haynes, C.M., and Pellegrino, M.W. (2017). The mitochondrial unfolded protein response: Signaling from the powerhouse. J Biol Chem *292*, 13500-13506.

35. Rahman, M.S., Choi, Y.H., Choi, Y.S., and Yoo, J.C. (2017). Glycin-rich antimicrobial peptide YD1 from B. amyloliquefaciens, induced morphological alteration in and showed affinity for plasmid DNA of E. coli. AMB Express *7*, 8.

36. Rauthan, M., Ranji, P., Aguilera Pradenas, N., Pitot, C., and Pilon, M. (2013). The mitochondrial unfolded protein response activator ATFS-1 protects cells from inhibition of the mevalonate pathway. Proc Natl Acad Sci U S A *110*, 5981-5986.

37. Rolland, S.G., Schneid, S., Schwarz, M., Rackles, E., Fischer, C., Haeussler, S., Regmi, S.G., Yeroslaviz, A., Habermann, B., Mokranjac, D., *et al.* (2019). Compromised Mitochondrial Protein Import Acts as a Signal for UPR(mt). Cell Rep *28*, 1659-1669 e1655.

38. Shao, L.W., Peng, Q., Dong, M., Gao, K., Li, Y., Li, Y., Li, C.Y., and Liu, Y. (2020). Histone deacetylase HDA-1 modulates mitochondrial stress response and longevity. Nat Commun *11*, 4639.

39. Sousa, J.C., Berto, R.F., Gois, E.A., Fontenele-Cardi, N.C., Honorio, J.E., Jr., Konno, K., Richardson, M., Rocha, M.F., Camargo, A.A., Pimenta, D.C., *et al.* (2009). Leptoglycin: a new Glycine/Leucine-rich antimicrobial peptide isolated from the skin secretion of the South American frog Leptodactylus pentadactylus (Leptodactylidae). Toxicon *54*, 23-32.

40. Sperstad, S.V., Haug, T., Vasskog, T., and Stensvag, K. (2009). Hyastatin, a glycine-rich multi-domain antimicrobial peptide isolated from the spider crab (Hyas araneus) hemocytes. Mol Immunol *46*, 2604-2612.

41. Subbalakshmi, C., and Sitaram, N. (1998). Mechanism of antimicrobial action of indolicidin. FEMS Microbiol Lett *160*, 91-96.

42. Tian, Y., Garcia, G., Bian, Q., Steffen, K.K., Joe, L., Wolff, S., Meyer, B.J., and Dillin, A. (2016). Mitochondrial Stress Induces Chromatin Reorganization to Promote Longevity and UPR(mt). Cell *165*, 1197-1208.

43. Tucker, A.T., Leonard, S.P., DuBois, C.D., Knauf, G.A., Cunningham, A.L., Wilke, C.O., Trent, M.S., and Davies, B.W. (2018). Discovery of Next-Generation Antimicrobials through Bacterial Self-Screening of Surface-Displayed Peptide Libraries. Cell *172*, 618-628 e613.

44. Verdon, J., Coutos-Thevenot, P., Rodier, M.H., Landon, C., Depayras, S., Noel, C., La Camera, S., Moumen, B., Greve, P., Bouchon, D., *et al.* (2016). Armadillidin H, a Glycine-Rich Peptide from the Terrestrial Crustacean Armadillidium vulgare, Displays an Unexpected Wide Antimicrobial Spectrum with Membranolytic Activity. Front Microbiol *7*, 1484.

45. West, A.P., Brodsky, I.E., Rahner, C., Woo, D.K., Erdjument-Bromage, H., Tempst, P., Walsh, M.C., Choi, Y., Shadel, G.S., and Ghosh, S. (2011). TLR signalling augments macrophage bactericidal activity through mitochondrial ROS. Nature *472*, 476-480.

46. Xie, Y., Wan, H., Zeng, X., Zhang, Z., and Wang, Y. (2020). Characterization and antimicrobial evaluation of a new Spgly-AMP, glycine-rich antimicrobial peptide from the mud crab Scylla paramamosain. Fish Shellfish Immunol *106*, 384-392.

47. Yee, C., Yang, W., and Hekimi, S. (2014). The intrinsic apoptosis pathway mediates the pro-longevity response to mitochondrial ROS in C. elegans. Cell *157*, 897-909.

48. Zehrbach, A.M.D., Rogers, A.R., and Tarr, D.E.K. (2017). An Investigation of the Potential Antifungal Properties of CNC-2 in Caenorhabditis elegans. J Nematol *49*, 472-476.

49. Zhou, R., Yazdi, A.S., Menu, P., and Tschopp, J. (2011). A role for mitochondria in NLRP3 inflammasome activation. Nature *469*, 221-225.

50. Zugasti, O., and Ewbank, J.J. (2009). Neuroimmune regulation of antimicrobial peptide expression by a noncanonical TGF-β signaling pathway in Caenorhabditis elegans epidermis. Nat Immunol *10*, 249-256.

FIGURES

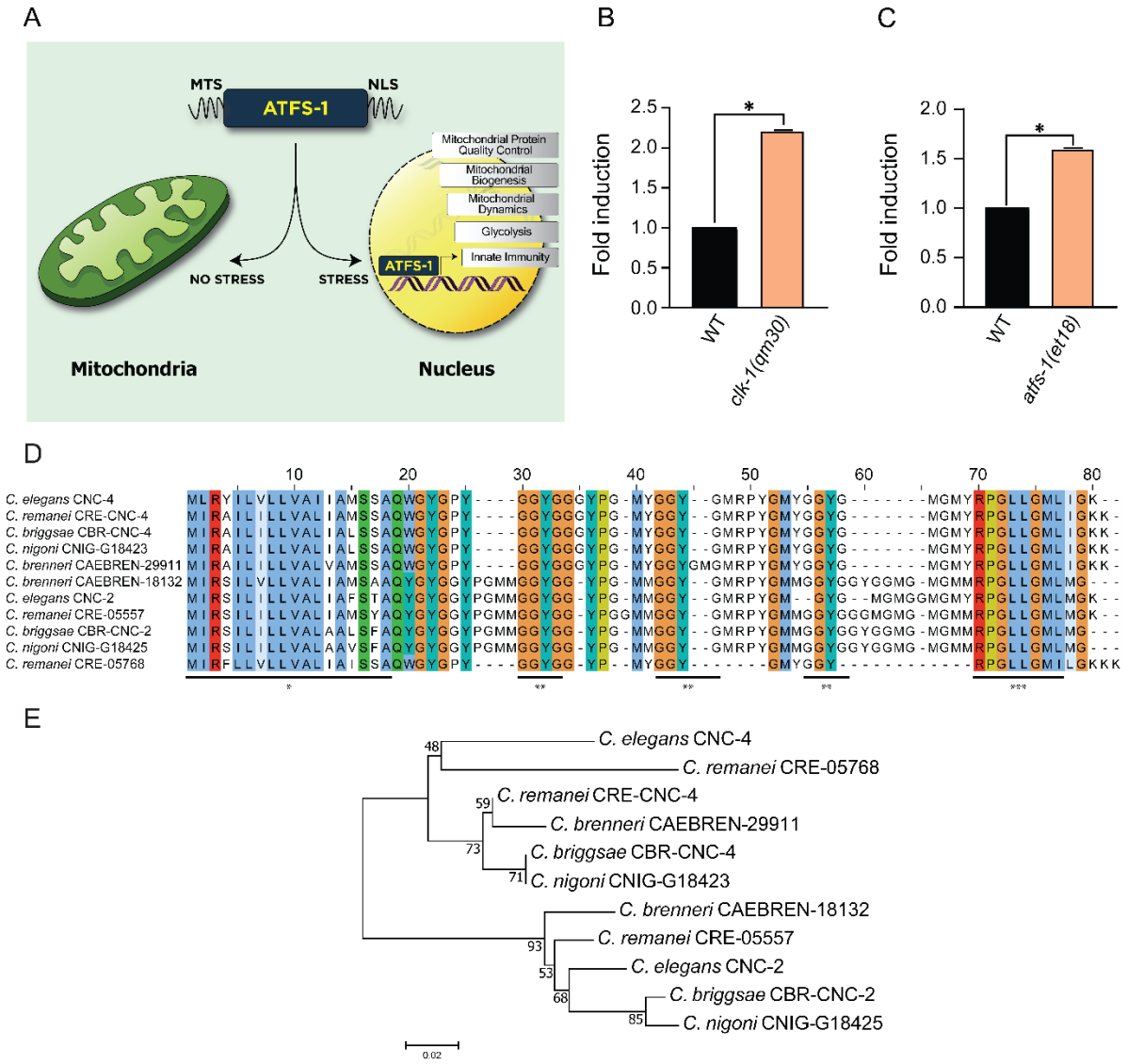

Figure 2.1 The expression of *cnc-4* is upregulated during mitochondrial stress signaling

A) Schematic of the UPR^{mt} pathway in *C. elegans*. ATFS-1 contains both a mitochondrial targeting sequence (MTS) and nuclear localization sequence (NLS). Under healthy conditions, ATFS-1 enters mitochondria and is turned over proteolytically. During stress, import of ATFS-1 into mitochondria is reduced allowing the transcription factor to localize to the nucleus to regulate genes involved in mitochondrial recovery and innate immunity.

B) Quantitative PCR of *cnc-4* transcript levels in wild-type and *clk-1(qm30)* animals (n = 3, ± SD, *p< 0.001 (Student's t-test).

C) Quantitative PCR of *cnc-4* transcript levels in wild-type and *atfs-1(et18)* animals. (n = 3, ± SD, *p< 0.001 (Student's t-test).

D) ClustalW multiple protein sequence alignment of CNC-4 with other conserved caenacin homologs. Colored regions denote conserved amino acid residues. Underlined regions: * denotes peptide signal sequence, ** denotes GGYG repeats, *** denotes conserved region of unknown function.

E) Phylogenetic analysis of CNC-4. The optimal tree with the sum of branch length= 0.428 is shown. The percentage of replicate tree in which the associated taxa clustered together in the bootstrap test are shown next to the branches. The scale bar represents 0.02 substitutions per amino acid position.

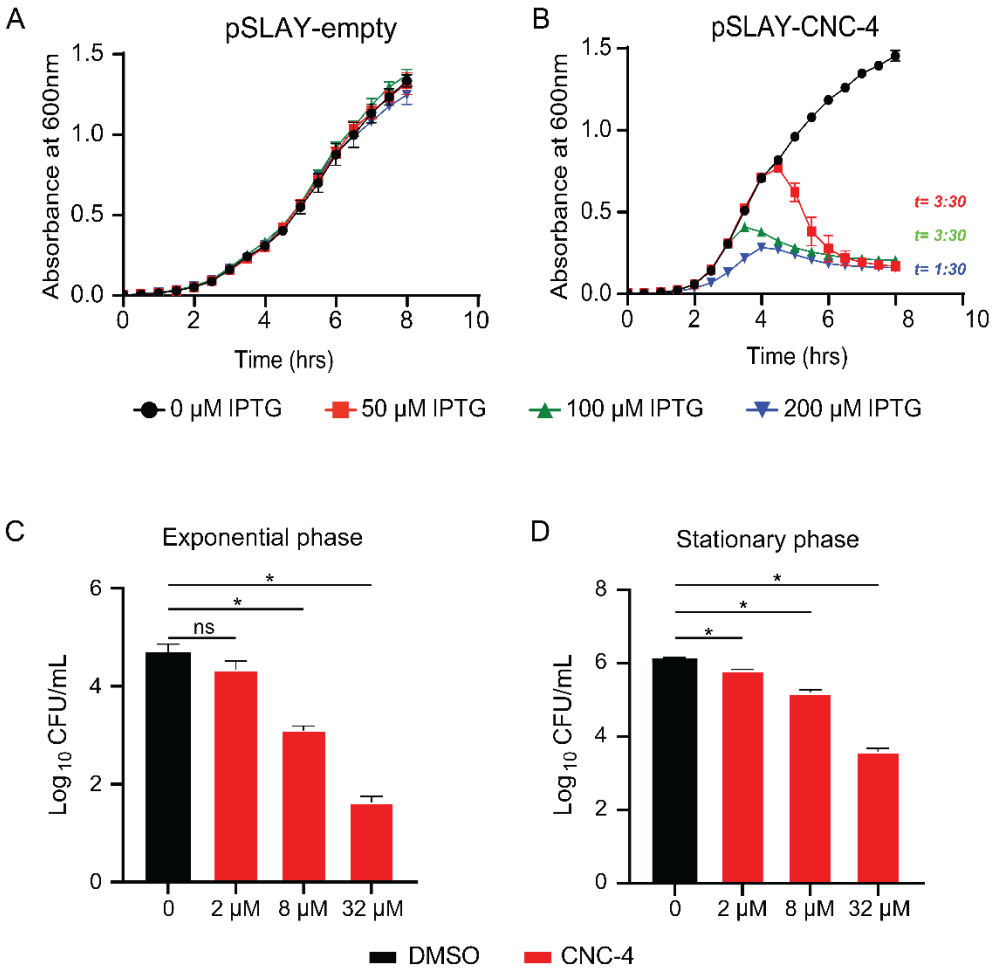

Figure 2.2 CNC-4 demonstrates antibacterial activity

(A, B) Growth of *E. coli* harboring SLAY A) without CNC-4, or B) with CNC-4. Cells were grown in increasing concentrations of IPTG and OD_{600} was measured every 0.5 h. *t*, time point after which reduction with statistical significance was achieved relative to IPTG control (n = 3, ± SD, $p < 0.05$ (Student's t-test)), (C, D) *E. coli* was treated with increasing doses of purified CNC-4 on cells isolated in C) logarithmic growth phase or D) stationary phase. DMSO was used as a control for relative comparison (n = 3, ± SD, *ns*, non-significant, $*p < 0.001$ (Student's t-test)).

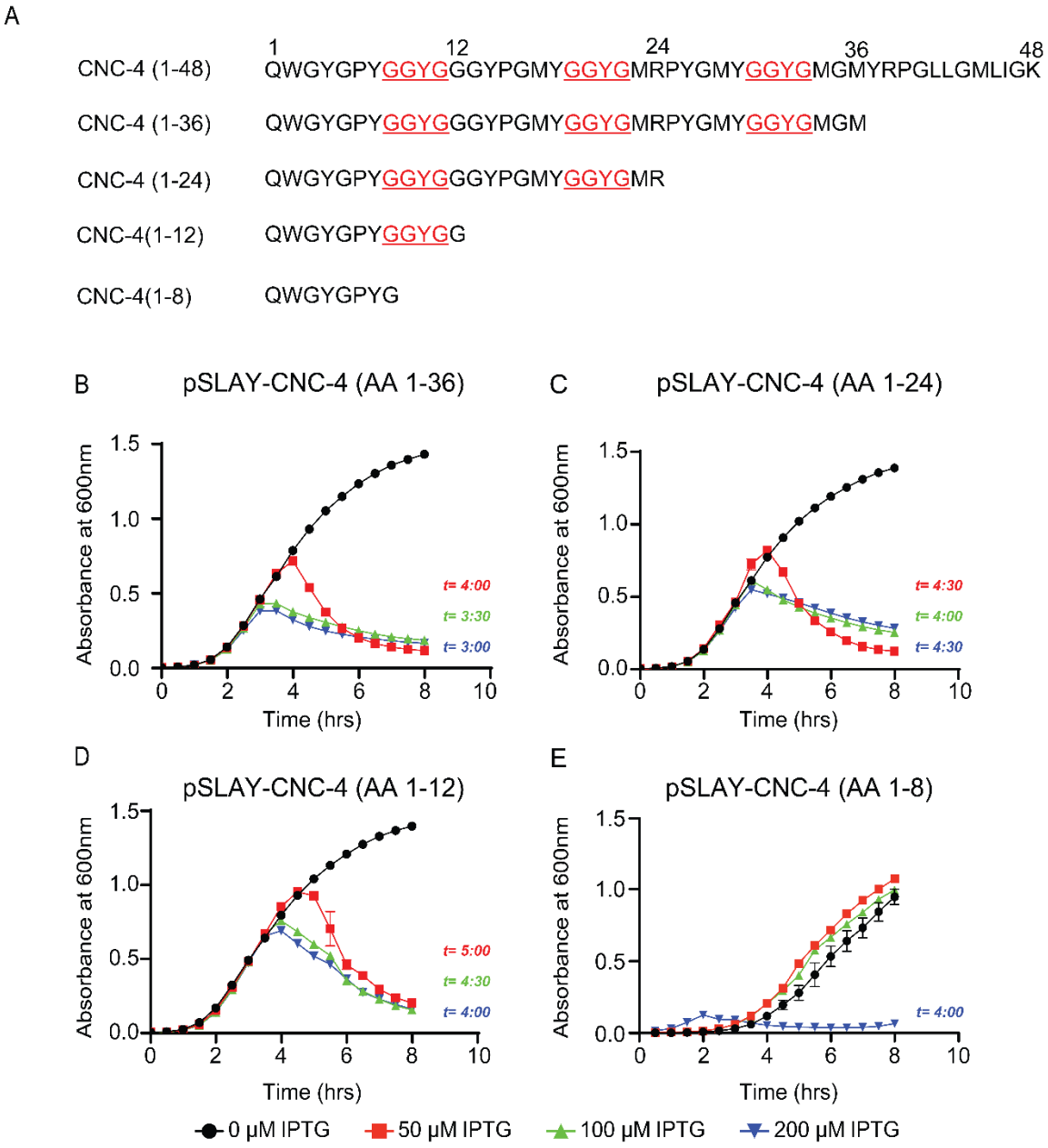

Figure 2.3 The GGYG motif is necessary for CNC-4 antibacterial activity

A) Schematic of CNC-4 and the associated truncations used to determine its minimal activity domain.

B-E) Optical density plots measured from *E. coli* carrying SLAY-CNC-4 constructs, including B) CNC-4(1-36), C) CNC-4(1-24), D) CNC-4(1-12), and E) CNC-4(1-8) grown in increasing

concentrations of IPTG. *t*, time point after which reduction with statistical significance was achieved relative to IPTG control (n = 3, ± SD, $p < 0.05$ (Student's t-test)).

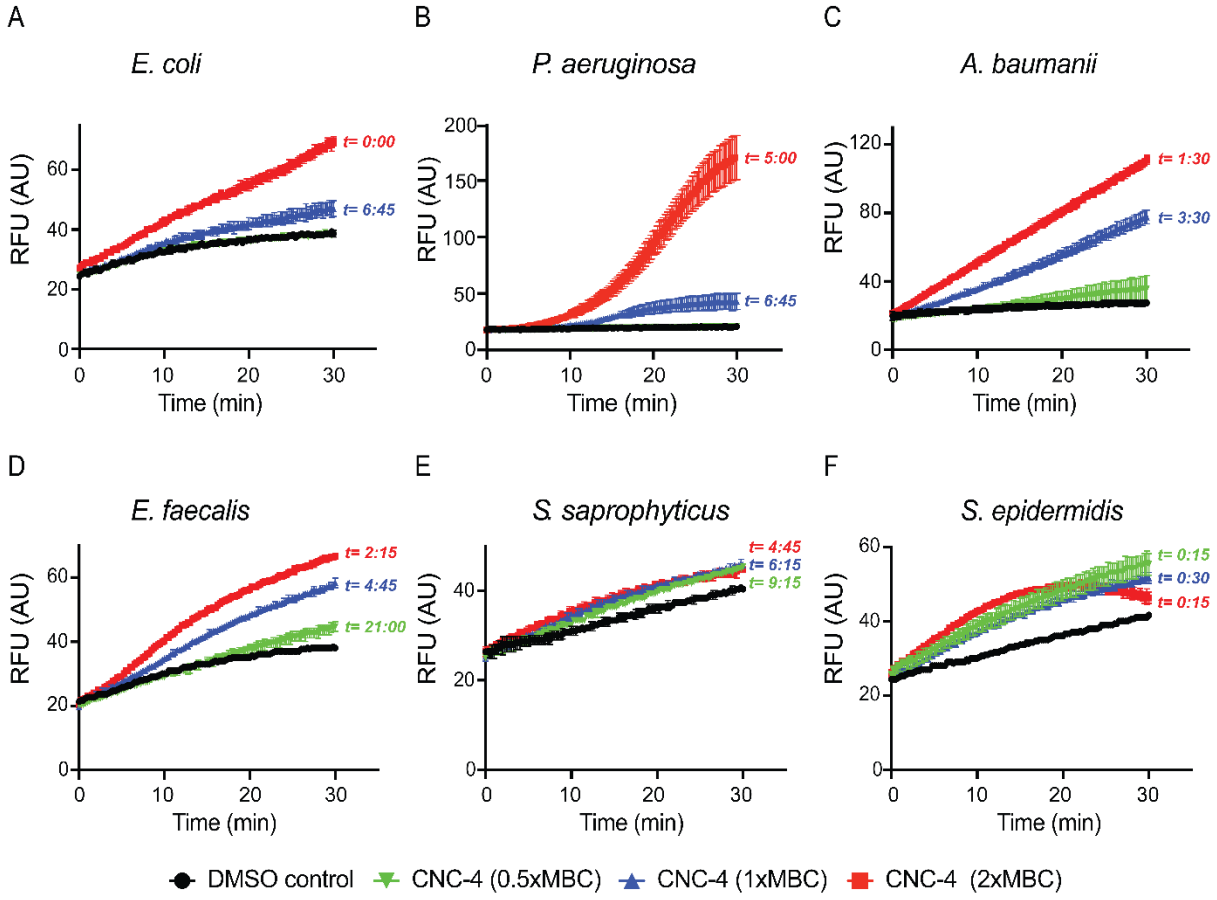

Figure 2.4 CNC-4 exposure results in increased bacterial membrane permeability

Effects of CNC-4 on outer membrane permeability in A) *E. coli* W3110, B) *P. aeruginosa*, C) *A. baumannii*, D) *E. faecalis*, E) *S. saprophyticus*, F) *S. epidermidis* using the ethidium bromide influx assay (see Materials and Methods). *t*, time point after which statistical significance was achieved relative to DMSO control (n = 3, ± SD, $p < 0.05$ (Student's t-test)).

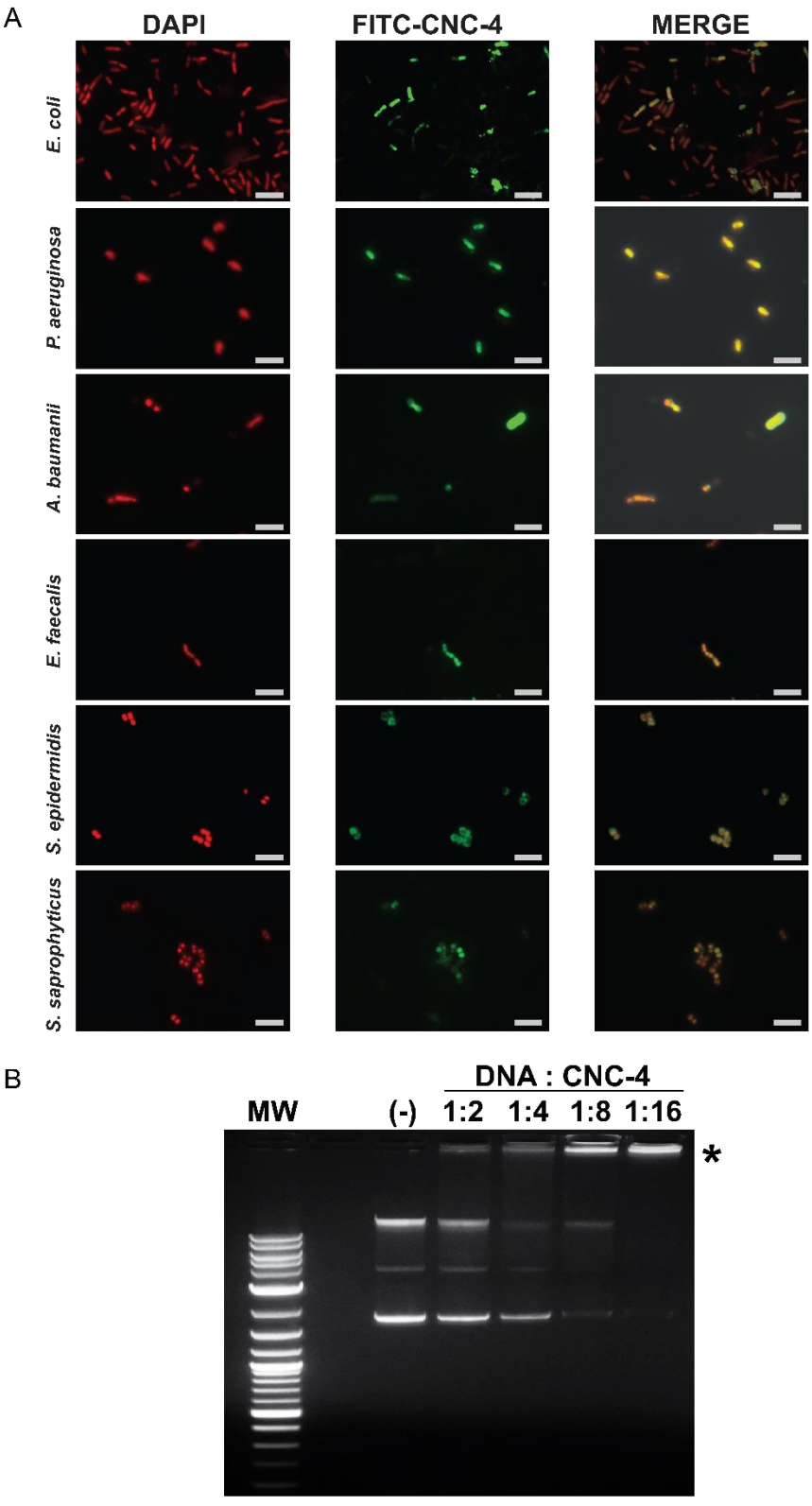

Figure 2.5 CNC-4 localizes intracellularly and directly binds DNA

A) Localization of CNC-4 using FITC-labelled CNC-4 in *E. coli* W3110, *P. aeruginosa*, and *A. baumannii, E. faecalis, S. saprophyticus, S. epidermidis*. FITC-CNC-4, DAPI, and merged images were obtained by fluorescence microscopy. Scale bar is 5 □m.

B) Image of a representative gel electrophoresis of plasmid DNA/CNC-4 combinations at the indicated mass ratios. MW; molecular weight ladder (1 kb DNA ladder; Promega), (-); plasmid DNA/DMSO negative control. Asterisk denotes region in which DNA failed to substantially migrate for DNA:CNC-4 ratios 1:4, 1:6, and 1:8.

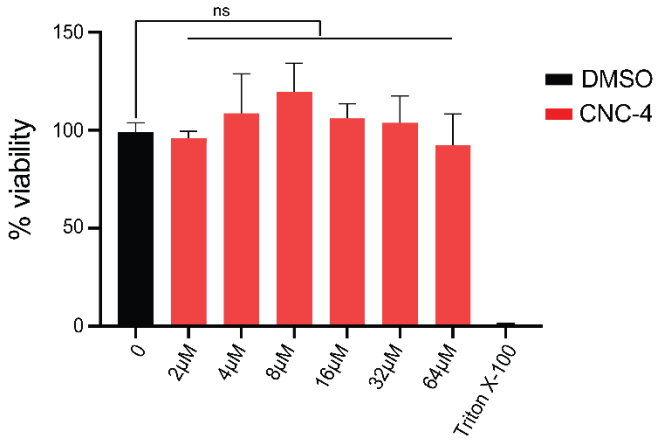

Figure 2.6 CNC-4 does not exhibit toxicity to mammalian epithelial cells

Quantification of CNC-4 toxicity to MODE-K cells using the MTT assay (see Materials and Methods). MODE-K cells at ~50,000 cells/well of density were treated with the indicated concentrations of purified CNC-4 peptide. Triton X-100 was used a positive control which leads to complete loss of cell viability. (n = 3, ± SD, *ns*, non-significant, (Student's t-test)).

Table 2.1 MBCs of various bacterial strains following CNC-4 treatment.

Pathogens	**MBCs**
P. aeruginosa PAO1	< 2μM
P. aeruginosa PA14	4μM
E. coli W3110	8μM
A. baumanii 17978	8μM
S. enterica 700720	128μM
Staphylococcus saprophyticus 15305	4μM
Enterococcus faecalis 29212	4μM
Staphylococcus epidermidis 12228	16μM

Table 2.2 The effects of salts and pH on MBCs of CNC-4 against *E. coli* W3110

NaCl	**0**	**150mM**	**300mM**
MBC	8μM	> 64μM	> 64μM

$MgCl_2$	**0**	**0.1mM**	**1mM**	**10mM**
MBC	8μM	8μM	16μM	16μM

pH	**5.5**	**6.5**	**7.4**	**8.0**
MBC	16μM	16μM	8μM	8μM

3. A pathogen branched-chain amino acid catabolic pathway subverts host survival by impairing energy metabolism and the mitochondrial UPR

Siraje A. Mahmud[1], Mohammed Adnan Qureshi[1], Madhab Sapkota, Mark W. Pellegrino[*]

Department of Biology, University of Texas Arlington, Arlington, TX, 76019

*Corresponding author. E-mail: mark.pellegrino@uta.edu

[1] Equal contribution

ABSTRACT

The mitochondrial unfolded protein response (UPR^{mt}) is a stress-activated pathway promoting mitochondrial recovery and defense against infection. In *C. elegans*, the UPR^{mt} is activated during infection with the pathogen *Pseudomonas aeruginosa* - but only transiently. As this may reflect a pathogenic strategy to target a pathway required for host survival, we conducted a *P. aeruginosa* genetic screen to uncover mechanisms associated with this temporary activation. Here, we find that loss of the *P. aeruginosa* acyl-CoA dehydrogenase FadE2 prolongs UPR^{mt} activity and extends host survival. FadE2 shows substrate preferences for the coenzyme A intermediates produced during the breakdown of the branched-chain amino acids valine and leucine. Our data suggests that during infection, FadE2 restricts the supply of these catabolites to the host hindering host energy metabolism in addition to the UPR^{mt}. Thus, a metabolic pathway in *P. aeruginosa* contributes to pathogenesis during infection through manipulation of host energy status and mitochondrial stress signaling potential.

INTRODUCTION

Mitochondria supply cellular energy in the form of ATP through the actions of the tricarboxylic acid (TCA) cycle and oxidative phosphorylation (OXPHOS). OXPHOS is performed by the electron transport chain residing in the mitochondrial inner membrane. Mitochondria face various challenges including a proteome that is encoded by two genomes requiring coordinated gene expression and assembly, as well as free radical damage that can disrupt mitochondrial proteostasis, and the accumulation of toxins.

Cells use a variety of mechanisms to mitigate mitochondrial stress including the mitochondrial unfolded protein response (UPR^{mt}) [1-3]. The UPR^{mt} is activated during stress in order to help restore mitochondrial homeostasis through the transcriptional regulation of a variety of protective genes. In *C. elegans*, the bZIP transcription factor ATFS-1 mediates the UPR^{mt} and is regulated by mitochondrial import efficiency [4, 5]. ATFS-1 contains a mitochondrial targeting sequence and is imported into healthy mitochondria where it is turned over via protease-mediated degradation. Import efficiency is reduced in dysfunctional mitochondria hindering the entry of ATFS-1 into the organelle. As a result, ATFS-1 accumulates cytoplasmically during mitochondrial stress and, because it also has a nuclear localization sequence, is imported into the nucleus to transcriptionally regulate a diverse set of genes which promote mitochondrial recovery [5].

Mitochondria mediate various defenses against pathogen infection including the regulation of innate immunity [6]. The UPR^{mt} orchestrates its own innate immune response during infection with pathogens that target mitochondrial function [7-9]. Consistent with a role in regulating innate immunity, the UPR^{mt} is both required and sufficient to protect the host during infection [7, 9, 10].

Among the bacterial pathogens that can activate the UPR^{mt} is the opportunistic pathogen *Pseudomonas aeruginosa* [7]. *P. aeruginosa* has long been used as a model in the study of host-pathogen interactions using *C. elegans* as a host [11]. *P. aeruginosa* has multiple means of subverting the health of its *C. elegans* host including deterioration of gut epithelial integrity resulting from pathogen colonization (slow killing; [12]), lethality from pathogen-derived hydrogen cyanide (fast killing; [13]), and death by hypoxia via production of iron-sequestering siderophores (liquid killing; [14]). While *P. aeruginosa* gut colonization activates the UPR^{mt} in *C. elegans*, recent evidence shows that chronic *P. aeruginosa* infection can subsequently repress this protective pathway [15]. The repression occurs at least in part through manipulation of the *C. elegans* bZIP transcription factor ZIP-3 which functions as a negative regulator of the UPR^{mt} [15]. How *P. aeruginosa* executes this repression of the UPR^{mt} is currently not known.

We conducted a genetic screen of *P. aeruginosa* mutants to uncover microbial effectors that have a role in modifying the UPR^{mt}. Using this approach, we found that a loss of function mutation in the *P. aeruginosa* gene *fadE2* leads to enhanced UPR^{mt} activity throughout infection resulting in extended host survival. FadE2 encodes an acyl-CoA dehydrogenase with a preference for isobutyryl-CoA and isovaleryl-CoA, metabolic intermediates produced during the breakdown of the branched-chain amino acids (BCAA) valine and leucine, respectively. Interestingly, host energy metabolic pathways are reduced during infection with *P. aeruginosa* due to the presence of FadE2. Consequently, loss of FadE2 restores host energy metabolism and the ability of the host to activate the UPR^{mt}. Our results suggest that *P. aeruginosa* FadE2 restricts valine and leucine catabolites during infection which antagonizes host metabolism, UPR^{mt} activity and host survival. Consistently, supplementation with valine or leucine is sufficient to counteract the repression of the UPR^{mt} and extend host survival during *P. aeruginosa* infection. Thus, we propose that by

limiting valine and leucine catabolites, *P. aeruginosa* FadE2 antagonizes host survival by altering host metabolism and the activity of the UPR^{mt}.

RESULTS

A genetic screen to identify *P. aeruginosa* effectors that repress UPR^{mt} signaling

In *C. elegans*, the activity of the UPR^{mt} can be examined using the transgenic strain SJ4100 *hsp-6$_{pr}$*::GFP [16]. The expression of the mitochondrial chaperone *hsp-6* is increased during mitochondrial stress as part of the UPR^{mt} [5]. As expected, exposure of SJ4100 animals to the wild-type PA14 strain of *P. aeruginosa* resulted in a modest activation of the *hsp-6$_{pr}$*::GFP reporter after 24 hrs, consistent with an activation of the UPR^{mt} (Fig 3.1A) [7]. However, the level of *hsp-6$_{pr}$*::GFP activation decreased with continued exposure to *P. aeruginosa* until the signal was completely absent 48 hrs post-infection (Fig 3.1B). We screened a *P. aeruginosa* transposon insertion mutant library [17] in an effort to identify *P. aeruginosa* effectors responsible for the repression of the UPR^{mt} during infection. We focused on *P. aeruginosa* mutants that were previously identified as potential virulence factors [17]. Using this screening approach, we discovered that a mutation in the *P. aeruginosa* gene PA14_31580 resulted in sustained expression of *hsp-6$_{pr}$*::GFP at 48 hrs of infection (Fig 3.1C and D). Furthermore, SJ4100 animals exposed to the *P. aeruginosa* PA14_31580 mutant displayed a higher level of *hsp-6$_{pr}$*::GFP expression following the initial 24 hrs of infection in contrast to those animals that were exposed to wild-type *P. aeruginosa* (S3.1 Fig). Other *P. aeruginosa* mutants also prolonged UPR^{mt} activity during infection, albeit at a lower penetrance than PA14_31580. These include mutations in the quorum sensing receptor *rhlR*, the flagella regulator *fleN*, and the genes encoding 2-methylisocitrate lyase and methylcitrate synthase, *prpB* and *prpC*, respectively. We focused on PA14_31580 considering

its highly penetrant effect on the activation of the UPR^{mt}. We have since named PA14_31580 as FadE2 based on protein homology and refer to the mutant as *fadE2*- henceforth.

C. elegans has an innate ability to avoid harmful bacteria as a means of protecting itself in a microbe-rich environment [18]. Potentially, the increases in UPR^{mt} activity that is observed during exposure to *fadE2*- could be due to disruptions in pathogen avoidance leading to enhanced bacterial exposure. However, we observed no difference in pathogen avoidance during infection with wild-type *P. aeruginosa* and *fadE2*- (S3.2 Fig). Therefore, the enhanced UPR^{mt} observed during infection with *fadE2*- is not likely due to differences in pathogen exposure.

Next, we examined whether the effect on the UPR^{mt} during infection with *fadE2*- was specific since other cellular stress responses are also activated during infection with this pathogen. The endoplasmic reticulum (ER) exhibits organellar stress during *P. aeruginosa* infection due to the increased production of host secreted anti-microbial agents that results in activation of the ER unfolded protein response (UPR^{ER}) [19]. Also, *P. aeruginosa* produces the exotoxin ToxA that attenuates host protein translation by ribosylating EF-2 causing activation of a surveillance program mediated by the bZIP transcription factor ZIP-2 [20-22]. We therefore monitored the activities of the UPR^{ER} and ZIP-2 translation surveillance program using transgenic animals expressing transcriptional reporters *hsp-4$_{pr}$*::GFP and *irg-1$_{pr}$*::GFP, respectively. We observed no further increase in activities of these stress responses (Fig 3.1E and 1F). Thus, loss of FadE2 function appears to specifically enhance the activity of the UPR^{mt} stress response pathway.

Mitochondrial activity is impaired during infection with *P. aeruginosa* through the actions of FadE2

Exposure to *fadE2*- led to increased UPR^{mt} activity, prompting us to explore mitochondrial function in these animals. We first examined mitochondrial OXPHOS efficiency by monitoring oxygen consumption in wild-type *C. elegans* exposed to non-pathogenic *E. coli* OP50, wild-type *P. aeruginosa* or *fadE2*-. While no differences in oxygen consumption rates (OCR) were observed during the first 12 hrs of exposure, animals infected with wild-type *P. aeruginosa* respired less than animals exposed to *E. coli* OP50 at 24 hrs of infection (Fig 3.2A). In contrast, OCR was increased in animals infected with *fadE2*- both at 24 and 48 hrs infection relative to wild-type *P. aeruginosa* and even *E. coli* OP50 (Fig 3.2A). Consistent with our OCR findings, ATP production was reduced at 48 hrs of infection with wild-type *P. aeruginosa* relative to animals exposed to *E. coli* OP50 (Fig 3.2B). And, infection with *fadE2*- led to greater ATP production relative to animals fed *E. coli* OP50 at 24 hrs of infection but returned to wild-type levels at 48 hrs infection (Fig 3.2B).

Buildup of reactive oxygen species (ROS) can occur with increased mitochondrial activity as a byproduct of oxidative phosphorylation which can alter protein integrity through carbonylation modification. We used the Oxyblot system to assess oxidative damage, an assay which detects carbonylated proteins that can result from ROS accumulation. Interestingly, an increase in oxidative damage was observed at 12 and 24 hrs during infection with *fadE2*-, followed by a sharp decline at 48 hrs post-infection (Fig 3.2C). Transient increase in ROS levels have been previously attributed to enhanced antioxidant defenses [23]. Consistently, we observed increased levels of the antioxidant glutathione and its derivatives following 48 hrs of infection with *fadE2*- using mass spectrometry (S3.3 Fig and Table S1).

We next assayed mitochondrial membrane potential as a reflection of mitochondrial health in our infected animals. As expected, mitochondrial membrane potential was decreased during infection

with wild-type *P. aeruginosa* relative to animals fed *E. coli* OP50 (Fig 3.2D). However, while mitochondrial membrane potential was also reduced in animals infected with *fadE2*- it nonetheless remained slightly higher than those animals infected with wild-type *P. aeruginosa* suggesting a modest improvement in mitochondrial function.

We wondered whether the restoration of the UPR^{mt} during infection with *P. aeruginosa fadE2*- promoted host survival in an ATFS-1-dependent manner. As expected, loss of ATFS-1 suppressed the activation of the UPR^{mt} during infection with *fadE2*- (Fig 3.2E). We next compared the survival of wild-type *C. elegans* during infection with wild-type *P. aeruginosa* or *fadE2*-. Consistent with previous findings [17], host survival was increased during infection with *fadE2*- relative to wild-type (Fig 3.2F; *p*-value <0.0001; see Table S2 for statistics pertaining to all survival analyses in this study). And, supporting a role of the UPR^{mt} in mediating this enhanced survivability, loss of ATFS-1 rendered animals hypersensitive to infection (Fig 3.2F; *p*-value 0.0004).

Importantly, we wished to exclude the possibility that the observed increase in host survival was either due to reduced bacterial viability and/or pathogen virulence. However, we found no differences in the rate of growth or final cell densities for *fadE2*- grown in standard Lysogeny Broth or NGM (S3.4A and S3.4B Fig). We then compared various properties associated with pathogen virulence between wild-type *P. aeruginosa* and *fadE2*- by first examining biofilm formation but found no significant difference (S3.4C Fig). Next, we examined two behaviors related to bacterial virulence: motility and twitching. Bacterial motility is a type of migration driven by flagella whereas bacterial twitching is mediated by pili, but neither were significantly affected with loss of FadE2 (S3.4D and S3.4E Fig). We also tested for possible differences in lipopolysaccharide levels in the absence of FadE2 but found no significant changes (S3.4F Fig).

Lastly, we observed no significant difference in the production of a subset of virulence factors including proteases, elastase, rhamnolipids, cyanide, and pyocyanin (S3.4G-S3.4K Fig). Together, our data suggest that the increase in host survival during exposure with *fadE2* is not a result of reduced production of virulence-associated factors or behaviors.

We next performed a rescue experiment by complementing *fadE2*- on a plasmid containing its own promoter to ensure that the effects of *fadE2*- on UPR^{mt} activity and host survival were not due to a secondary mutation. Transient UPR^{mt} activity was restored when animals were infected with the complemented strain (S3.5A Fig). As well, the susceptibility of *C. elegans* to the complemented strain was comparable to that observed when exposed to wild-type *P. aeruginosa* (S3.5B Fig; *p*-value 0.227). Therefore, the effects on the UPR^{mt} and host survival are directly due to the loss of *P. aeruginosa* FadE2.

Taken together, our results indicate that *P. aeruginosa* FadE2 mediates the suppression of mitochondrial activity and the UPR^{mt} that reduces host survival during infection.

P. aeruginosa FadE2 is an acyl-CoA dehydrogenase involved in valine and leucine catabolism

The *fadE2* gene encodes a predicted acyl-CoA dehydrogenase, a class of enzyme involved in the breakdown of fatty acids via β-oxidation and also amino acid catabolism (S3.6 Fig). Acyl-CoA dehydrogenases that are associated with fatty acid breakdown belong to the short-, medium-, long-, and very long-chain acyl-CoA dehydrogenases whereas those that mediate the breakdown of amino acids show preference for the BCAAs valine (isobutyryl-CoA dehydrogenase), leucine (isovaleryl-CoA dehydrogenase) and isoleucine ((S)-2-methyl-butanoyl-CoA dehydrogenase). FadE2 is conserved amongst other uncharacterized acyl-CoA dehydrogenases that are present in a

range of bacterial species (Fig 3.3A). Characteristic features of acyl-CoA dehydrogenases are present in FadE2 including a conserved aspartate active site and binding sites for the flavin adenine dinucleotide (FAD) cofactor. Interestingly, the acyl-CoA dehydrogenases that showed highest homology are present in other human pathogens including *Streptococcus pneumoniae* and *Acinetobacter baumannii* (Fig 3.3B).

To evaluate whether FadE2 was involved in β-oxidation, we first monitored growth of *fadE2*- in the presence of various fatty acids as the sole carbon source. Apart from observing a mild but significant decrease in growth rate when *fadE2*- was grown in the presence of the short chain fatty acid butyric acid (Fig 3.3D), no difference in *fadE2*- growth was detected for the remaining fatty acids tested (Fig 3.3E-3J). We next tested the ability of *fadE2*- to grow in the presence of BCAAs as their sole carbon source. Interestingly, growth of *fadE2*- was dramatically impaired when valine, and to a lesser extent leucine, was used as a sole carbon source (Fig 3.3K and 3.3L). No significant difference in growth was detected in the presence of isoleucine (Fig 3.3M). These results suggest that FadE2 shows a preference for BCAA substrate intermediates of valine and leucine catabolism.

We next recombinantly expressed FadE2 to biochemically validate its substrate specificities using various CoA esters (Fig 3.3N). Consistent with our growth assays using minimal media, FadE2 displayed a predominant specificity for isobutyryl-CoA, the metabolic intermediate of valine catabolism. Activity was also detected, although to a lesser extent, for isovaleryl-CoA which is the catabolic intermediate of leucine. Interestingly, FadE2 displayed modest activity for dodecanoyl-CoA (Fig 3.3N), despite no observed difference in *fadE2*- growth when its precursor fatty acid was used as a sole carbon source (Fig 3.3H).

P. aeruginosa FadE2 represses host energy pathways

We next explored global changes in transcription occurring in the host during infection with *P. aeruginosa* in the presence or absence of FadE2 by first comparing *C. elegans* genes that were differentially expressed at 24 hrs of exposure to non-pathogenic *E. coli* OP50, wild-type *P. aeruginosa* or *fadE2*- using RNAseq (Fig 3.4A and Table S3). As expected, the expression of genes of various functional categories were both increased and decreased after 24 hrs of *P. aeruginosa* infection compared to *E. coli* OP50 fed animals (Fig 3.4B and Table S3). Interestingly, infection with *fadE2*- increased the expression of many genes that were downregulated during wild-type *P. aeruginosa* infection (Fig 3.4C). In contrast, loss of FadE2 had comparatively less effect on the expression of genes that were upregulated during wild-type *P. aeruginosa* infection (Fig 3.4A). Remarkably, a large proportion of genes whose expression was higher during infection with *fadE2*- were associated with metabolic roles including fatty acid metabolism, amino acid metabolism and respiration (Fig 3.4C). A similar trend of higher metabolic gene expression during infection with *fadE2*- compared to wild-type *P. aeruginosa* was observed at 48 hrs, albeit with a greater number of differentially expressed genes (Fig 3.4D and Table S3). We find that multiple genes encoding energy promoting pathways such as glycolysis, amino acid metabolism, and β-oxidation were higher during infection with *fadE2*- relative to those infected with wild-type *P. aeruginosa* (Fig 3.4D and Table S3.3). Furthermore, various genes with roles in the tricarboxylic acid (TCA) cycle and mitochondrial OXPHOS were also expressed at a higher level when infected with *fadE2*-. Among the TCA cycle-related genes, we identified *cts-1* (citrate synthase), *idhg-2* (isocitrate dehydrogenase subunit) and *mdh-2* (malate dehydrogenase). Notable OXPHOS genes included *cox-6C/7C* (cytochrome oxidase assembly protein), *cox-4/5A* (cytochrome c oxidase subunit), *sdha-1* (succinate dehydrogenase complex subunit), *coq-1* (Coenzyme Q), *nuo-5* (NADH

ubiquinone oxidoreductase), and various genes encoding components of the ATP synthase complex (*atp-1, atp-2, atp-4, asb-2, asg-1, asg-2, F58F12.1*).

We wondered whether the increase in metabolic gene expression during infection with *fadE2*- was due to the UPR^{mt}. We therefore compared metabolic genes that were differentially expressed during *fadE2*- infection with known ATFS-1-dependent targets [5]. We find that only 7 out of 134 metabolic genes are known to be regulated by ATFS-1, suggesting that their expression is largely independent of the UPR^{mt}.

Our transcriptomic analysis indicated that expression of genes related to host energy pathways were repressed during infection with *P. aeruginosa* in a FadE2-dependent manner suggesting altered host metabolism. We therefore performed a metabolomic analysis of wild-type *C. elegans* that were exposed to non-pathogenic *E. coli* OP50, wild-type *P. aeruginosa* or *fadE2*- for 24 and 48 hrs using non-targeted quantitative mass spectrometry. We observed less overall metabolic difference following 24 hrs of infection (Table S1) in comparison to the dramatic changes observed following 48 hrs of infection with *fadE2*- (Table S1). Strikingly, multiple energy-producing pathways were reduced at 48 hrs of *P. aeruginosa* infection compared to those fed *E. coli* OP50. First, a decrease in abundance of all amino acids was detected during *P. aeruginosa* infection (Fig 3.5A). Interestingly, loss of FadE2 increased levels of all amino acids or even resulted in a restoration back to levels observed when fed *E. coli* OP50 at 48 hrs post-infection (Fig 3.5A). The decrease in total amino acid content during *P. aeruginosa* infection may be due to reduced amino acid transport, which is thought to involve the addition of a gamma-glutamyl group by gamma-glutamyl transferase [24]. Indeed, we observed lower levels of gamma-glutamyl amino acids during *P. aeruginosa* infection which was increased with *fadE2*- (S3.7A Fig).

Second, a decrease in metabolites involved in carbohydrate metabolism was also observed in animals infected with *P. aeruginosa*. Specifically, glucose and metabolic intermediates of glycolysis/gluconeogenesis were downregulated during infection with *P. aeruginosa* and increased with *fadE2*- (Fig 3.5B). We hypothesized that restored glycolysis might contribute to the extension in host survival observed during *fadE2*- infection. To examine whether glycolysis mediated the extended survival of animals infected with *fadE2*- we used a reduction of function mutant in *pfk-1.1* encoding the *C. elegans* homolog of the glycolysis rate-limiting enzyme phosphofructokinase-1. Interestingly, *pfk-1.1(ola72)* suppressed the extended host survival during infection with *fadE2*- (Fig 3.5C; *p*-value 0.085). Thus, increased glycolytic flux mediates the extension in host survival observed during *fadE2*- infection.

Our metabolomic analysis also suggested a decrease in fatty acid metabolism during infection with *P. aeruginosa,* specifically long chain and very long chain fatty acid abundance (Fig 3.5D). In addition, lower levels of carnitine metabolites were observed during *P. aeruginosa* infection which are necessary for the transport of long-chain fatty acids into mitochondria for their eventual oxidation (S3.7B Fig). Once again, levels of these fatty acid and carnitine metabolites were largely restored to wild-type levels in the absence of FadE2 (Fig 3.5D and S3.7B Fig). To determine whether β-oxidation was involved with the increase in host survival observed during *fadE2*- infection, we genetically and chemically disabled carnitine palmitoyl transferase using the *cpt-5(gk5128)* loss of function mutant or through treatment with the inhibitor etomoxir, respectively. Interestingly, both *cpt-5(gk5128)* or etomoxir similarly suppressed the increase in host survival that occurred with *fadE2*- exposure (Fig 3.5E; *p*-value 0.404 and S3.8 Fig; *p*-value 0.873), indicating an involvement of β-oxidation.

Our metabolomic and transcriptomic analyses suggest that *P. aeruginosa* FadE2 represses host energy metabolism pathways that culminate with the TCA cycle in mitochondria. To examine whether increased energy metabolism mediates the increase in host survival observed during *fadE2*- infection, we used a viable reduction of function allele (*osa2*) in the succinyl-CoA ligase beta subunit gene *sucg-1* that we had isolated in an independent study (Amin et al. *in review*). SUCG-1 is the *C. elegans* homolog of human SUCGL2 which mediates the conversion of succinyl-CoA to succinate during the TCA cycle. Interestingly, *sucg-1(osa2)* mutants suppressed the increase in host survival observed during *fadE2*- infection (Fig 3.5F; *p*-value 0.784). Importantly, we observed no difference in host survival when *sucg-1(osa2)* mutants were infected with wild-type *P. aeruginosa*, indicating that *sucg-1(osa2)* animals are not simply succumbing to inherent metabolic distress (Fig 3.5F; *p*-value 0.934). Therefore, our data suggest *P. aeruginosa* FadE2 impairs host survival by reducing host energy metabolism. In the absence of FadE2, host energy production is increased resulting in ROS generation and activation of the UPR^{mt}.

Valine or leucine supplementation is sufficient to sustain UPR^{mt} activity and increase host survival during *P. aeruginosa* infection

FadE2 showed substrate preference for the metabolic intermediates of valine and leucine catabolism. We hypothesized that *P. aeruginosa* FadE2 represses the UPR^{mt}, host metabolism and host survival during infection by restricting the availability of valine and leucine catabolites. To test our hypothesis, we first asked whether we could counteract the repression of the UPR^{mt} during *P. aeruginosa* infection through simple supplementation of valine or leucine. Indeed, UPR^{mt} activity was maintained with valine or leucine supplementation, and to a lesser extent with

isoleucine (Fig 3.6A). In contrast, supplementation of *E. coli* OP50 with valine, leucine, or isoleucine did not activate the UPR^{mt} (S3.9 Fig).

We next tested the effect of supplementing BCAAs on host survival during infection with *P. aeruginosa*. Remarkably, valine supplementation enhanced host survival during infection with wild-type *P. aeruginosa* (Fig 3.6B; *p*-value <0.0001) whereas only a mild increase was observed with leucine supplementation (Fig 3.6C; *p*-value 0.031) and no difference was observed with isoleucine supplementation (Fig 3.6D; *p*-value 0.438). Valine or leucine supplementation also increased the lifespan of animals fed standard *E. coli* OP50 (S3.10 Fig; *p*-values 0.002 and 0.003, respectively), despite a lack of UPR^{mt} activation. However, this in line with the pro-longevity benefits of BCAAs that were previously reported [25].

In contrast, a relatively smaller increase in host survival was observed during infection with *fadE2*- when animals were supplemented with valine (Fig 3.6E; *p*-value 0.002), whereas no difference was observed with leucine supplementation (Fig 3.6F; *p*-value 0.519). As expected, isoleucine had no effect on host survival during infection with *fadE2*- (Fig 3.6G; *p*-value 0.2). Since the increase in host survival by valine or leucine supplementation was not additive to the increase in host survival observed with *fadE2*- suggest they both use a common mechanism of action. Therefore, valine or leucine catabolite availability determines UPR^{mt} activity and host survival rates during infection.

Since valine and leucine supplementation maintained the activity of the UPR^{mt} during infection with wild-type *P. aeruginosa*, we also examined whether this protective pathway was required for the associated extension in host survival. Indeed, loss of ATFS-1 function suppressed the increase in host survival observed with valine (Fig 3.6H; *p*-value <0.0001) or leucine supplementation (Fig 3.6I; *p*-value <0.0001), rendering animals hypersensitive to infection.

We then examined whether glycolysis and □-oxidation mediated the extension in host survival with valine or leucine supplementation since both metabolic pathways were required during infection with *fadE2*-. Reducing glycolysis using the *pfk-1.1(ola72)* mutant suppressed the increase in host survival with valine (S3.11A Fig; *p*-value 0.102) or leucine supplementation (S3.11B Fig; *p*-value 0.321). Similarly, impaired β-oxidation through treatment with etomoxir or the *cpt-5(gk5128)* mutant yielded similar outcomes (S3.11C-S3.11F Fig; *p*-value $\geq$0.075). Since both glycolysis and β-oxidation mediated the beneficial effects afforded by valine or leucine, we next explored whether the increase in host survival with valine or leucine supplementation was dependent on increased energy metabolism using *sucg-1(osa2)* animals. Similar to what was observed during infection with *fadE2*-, *sucg-1(osa2)* completely suppressed the extension in host survival conferred by valine (S3.11G Fig; *p*-value 0.808) and leucine (S3.11H Fig; *p*-value 0.461) during infection with wild-type *P. aeruginosa*. Therefore, valine and leucine promote host survival during *P. aeruginosa* infection via pathways related to host energy metabolism and UPR^{mt} activation.

DISCUSSION

We propose the following model explaining a mechanism used by *P. aeruginosa* to repress the UPR^{mt} during infection via the acyl-CoA dehydrogenase FadE2 (Fig 3.7). We show that FadE2 possesses substrate specificity for isobutyryl CoA and isovaleryl CoA, catabolites produced during the breakdown of the BCAAs valine and leucine, respectively. FadE2 activity during infection limits the availability of these catabolites for the *C. elegans* host which, through an as of yet unknown mechanism, hinders the activation of the UPR^{mt}. We also show that the actions of FadE2 impair host energy pathways such as glycolysis, □-oxidation, and amino acid metabolism, all of

which culminate with the TCA cycle. Consequently, loss of FadE2 results in a buildup of these catabolites in *P. aeruginosa*, resulting in a greater supply for the host which responds by restoring host energy metabolism and the ability to activate the UPR^{mt} through a mechanism that is currently not resolved. We favor a model in which loss of FadE2 allows the host to activate the UPR^{mt} in response to toxins produced by *P. aeruginosa* that target mitochondrial function (e.g. cyanide, pyocyanin etc.) in addition to the stress that is produced with increased mitochondrial respiration and the associated production of damaging ROS species. Together, both the increase in energy production and restored function of the UPR^{mt} promote host survival during infection.

The exact mechanism of how FadE2 affects UPR^{mt} activity during infection via changes in valine or leucine catabolite levels is presently not known. Recently, it was shown that the *C. elegans* bZIP transcription factor ZIP-3 is involved with the repression of the UPR^{mt} during infection with *P. aeruginosa* [15]. Here, *P. aeruginosa* exploits the repressive activities of this transcription factor on the UPR^{mt}. The mechanism of how *P. aeruginosa* manipulates this host transcription factor are unclear. One possibility is that ZIP-3 mediates the repressive activities exerted by FadE2 on the UPR^{mt}. Indeed, we have compared the genes negatively regulated by FadE2 and ZIP-3 and found modest overlap (S3.12 Fig), suggesting they may occur in the same pathway to some degree. Another possibility that might explain the repressive activities of FadE2 on the UPR^{mt} may relate to its ability to reduce host nutrient levels (e.g. amino acids, glucose) during *P. aeruginosa* infection. Accordingly, multiple host nutrient-sensing pathways [26] may be differentially regulated by FadE2 that may impact the activation of the UPR^{mt}. The molecular mechanism of UPR^{mt} repression by FadE2 during *P. aeruginosa* infection is discernibly an active area of investigation.

Our model posits that increased energy metabolism drives host survival during infection with *P. aeruginosa*. Consistent with our model, increased energy metabolism has also been connected with improved host survival during infection in zebrafish. Here, increased supply of TCA cycle metabolites increased zebrafish survival during infection with *Vibrio alginolyticus* [27, 28]. Similar benefits of increased metabolism have been observed in other experimental scenarios outside of infection. For example, enhanced oxidation of fuel sources via the TCA cycle was shown to be necessary for the extension in animal longevity that is observed upon caloric restriction [29]. Also, hepatocytes have been shown to increase TCA cycle flux to promote cell survival during ischemia [30]. In addition, we also show that the host responds metabolically to the presence or absence of *P. aeruginosa* FadE2 in part through transcriptional re-wiring. The ability of animals to adapt to different metabolic demands through a transcriptional regulatory mechanism has also been observed in other contexts. For example, a transcriptional rewiring program occurs in *C. elegans* to support the breakdown of propionate in lieu of low vitamin B12 levels that acts as an enzyme cofactor in the catabolism of this metabolite that can be toxic to the cell [31, 32]. Also, during mouse embryonic development, a transcriptional rewiring in glucose metabolism occurs to support chorioallantoic branching [33].

Our data supports a model in which intermediates of valine and leucine catabolism reinforce host survival during infection. As essential amino acids, BCAAs mediate numerous cellular functions including protein synthesis, as well as glucose and lipid metabolism [34]. In addition, valine supplementation was recently shown to increase macrophage phagocytosis of multiple bacterial pathogens including *P. aeruginosa* using mouse models of infection [35]. Valine supplementation is thought to increase macrophage phagocytosis through activation of PI3K/Akt1 and also through the production of nitric oxide [35]. What remains unclear are the

exclusive properties afforded by valine and leucine, but not isoleucine, that promote host survival during infection with *P. aeruginosa* in our *C. elegans* infection model. It is interesting that the CoA intermediates of valine and leucine are metabolized by FadE2, and that valine or leucine supplementation increased host survival. In contrast, FadE2 did not metabolize the CoA intermediate of isoleucine and consistently, isoleucine supplementation did not protect the host during infection. One possibility is that unique signaling pathways might be activated downstream of each of these essential amino acids. Indeed, leucine was shown to regulate the target of rapamycin complex 1 (TORC1), a pro-growth kinase, via acetylation of the TORC1 regulator Raptor using its final catabolic metabolite acetyl-CoA [36]. TORC1 was also shown to be activated via the cytoplasmic leucine sensor SESN2 [37, 38]. And, leucine has also been shown to increase insulin levels through allosteric activation of glutamate dehydrogenase [39]. With regard to metabolites related to valine catabolism, 3-HIB and beta-amino-isobutyric acid have been shown to induce their own signaling mechanisms [40]. Interestingly, 3-HIB is the only catabolite that lacks the CoA attachment, allowing the molecule to leave the mitochondrial matrix. Indeed, 3-HIB has been detected in plasma samples where it acts in paracrine signaling [40]. Based on the substrate preference of FadE2, it is likely that either isobutyryl-CoA and/or isovaleryl-CoA accumulation due to loss of FadE2 might stimulate the host to rewire its metabolism and allow activation of the UPR^{mt}. However, we cannot exclude the possibility that derivatives of these metabolites may instead play some role.

During the infection process, *P. aeruginosa* can also be viewed as a food source for *C. elegans* which it digests to extract important nutrients (although this is only a partial digestion since live *P. aeruginosa* is able to colonize the intestinal tract of *C. elegans*). As such, it is possible that the actions of FadE2 restricts the supply of valine and leucine catabolites, thus resulting in a

competition for nutrients between pathogen and host that dictates the potential for the UPR^{mt} to be activated. It is unknown whether a similar competition for nutrients would exist in the context of a *P. aeruginosa* infection in vertebrates. Nonetheless, it is tempting to speculate that *P. aeruginosa* FadE2 has a particular function during infection to restrict the supply of important metabolites. Indeed, *P. aeruginosa* FadE2 showed highest homology with acyl-CoA dehydrogenases from other pathogenic bacterial species and therefore may play an important role during infection of the host. Competition for nutrients critically determines the success of either the host or pathogen during infection since the site of infection can be a restrictive environment. For example, the host relies on certain amino acids during infection to mount an immune response [41]. From the perspective of the pathogen, specific amino acids have been linked with the expression of disease-promoting virulence factors. For example, L-glutamine levels dictate the expression of virulence factors in *Listeria monocytogenes* within macrophages [42]. Consequently, reducing L-glutamine availability restricts expression of *L. monocytogenes* virulence factors and increases health of the host.

Together, our study demonstrates that a *P. aeruginosa* metabolic pathway negatively impacts both host energy metabolism and the activation of the UPR^{mt}. This occurs presumably due to an ability of *P. aeruginosa* to successfully outcompete the host for specific nutrients related to the catabolism of valine or leucine. The molecular mechanisms linking these catabolites to host energy pathways and mitochondrial stress signaling are still unresolved and therefore will be an exciting area of future research.

MATERIAL AND METHODS

C. elegans strains

C. elegans was maintained on standard Nematode Growth Media (NGM) according to previously described methods [43]. *C. elegans* strains were provided by the Caenorhabditis Genetics Center: N2 Bristol; SJ4100 *zcIs13*[*hsp-6*::GFP], SJ4005 *zcIs4*[*hsp-4*::GFP], *pfk-1.1(ola72), cpt-5(gk5128* [loxP+P*myo-2*::GFP::*unc-54* 3'UTR + P*rps-27*::neoR::*unc-54* 3'UTR + loxP]) [44], AU133 *agIs17*[*irg-1*::GFP][22]. UTA37 *sucg-1(osa2)* was isolated in a forward genetics screen using ethyl methanesulfonate (Amin et al.; *in revision*). *atfs-1(cmh15)* was a gift from Dr. Cole M. Haynes (University of Massachusetts Medical School). All mutant animals were backcrossed to N2 at least four times prior to use.

Pathogen infection assays

P. aeruginosa plates were prepared using overnight cultures that were incubated for 18 hrs at 37°C before seeding 15 µL of bacterial culture onto NGM plates. The plates were incubated at room temperature for 24 hrs followed by transferring to 37°C for 24 hrs. The plates were then incubated at 25°C for 3 hrs before transferring the *C. elegans* animals for the infection assay. Wild-type animals were synchronized and grown at 16°C for 72 hrs until the fourth larval stage before transferring to *P. aeruginosa* plates. Survival assays was carried out at 25°C for the indicated time intervals. Statistical analysis was calculated using GraphPad Prism version 8 (GraphPad Software, San Diego, California, USA) where *p*-values were generated by the log-rank (Mantel-Cox) test. Statistical tests were performed for each strain/condition compared to the wild-type control. For all cases, *p*-values of <0.05 were considered significant. All statistical values are presented in Table S2.

Microscopy

Worms were imaged using a Zeiss AxioCam MRm mounted on a Zeiss Imager Z2 microscope. Same exposure time was used for each experiment. Total fluorescence was quantified using ImageJ and the relative intensity between worm strains were compared using a one-way ANOVA.

***C. elegans* pathogen avoidance**

The bacterial lawns were prepared as described earlier. Forty L4 worms for each condition were transferred outside the bacterial lawns, and the numbers of animals on and off the lawns were counted for each experiment after 18 hrs. Three 3.5-cm plates were used per trial in every experiment. The percent occupancy was calculated as (N_{on}/N_{total}) X 100. At least three independent experiments were performed.

P. aeruginosa fadE2* rescue in *P. aeruginosa* Δ*fadE2

The 1230 bp *fadE2* ORF along with 500 bp upstream sequence was amplified form *P. aeruginosa* wild-type genomic DNA using primers 5'-TTTGCTAGCCGCTTCGGTGAGGTCGGTCAT-3' and 5'-TTTAAGCTTTCAGCGGCTGCTGCGCAGCAT-3' and cloned into *NheI* and *HindIII* sites of the plasmid pUCP20T, thus replacing the original IPTG promoter of the plasmid with the upstream promoter region of *fadE2*. The resulting plasmid, pUCP20T::fadE2$_{pr}$::fadE2, was transformed into *P. aeruginosa fadE2*- using electroporation. The transformants were selected on plates containing gentamicin (50 µg/ml) and carbenicillin (300 µg/ml).

Oxygen consumption rate (OCR) assay

The OCR assay was performed according to [45]. The MitoXpress Xtra oxygen consumption assay kit (Agilent, USA) was used to calculate the OCR from 100 to 150 worms. Approximately 100-150 worms were recovered from NGM plates and washed three times in S-basal to remove excess bacteria. Worms were then transferred to wells of a 96-well plate in a final sample volume of 90 µl. The oxygen probe was then added to each sample at a volume of 10 µl. The 96-well plates were then sealed with two drops of mineral oil and sample wells were immediately read on Synergy Neo 2 plate reader using Gen5 software (BioTek, Wisnooski, VT, USA) in a time-resolved fluorescence mode with 380 nm excitation and 650 nm emission filters. Data were collected from 0 hr to 1 hr at 25°C. To eliminate background oxygen consumption, controls (in triplicates) with S-basal and S-basal plus oxygen probe, but no worms, were included in each respiration assay. The measured time profiles of fluorescence from each sample were normalized to the signal at time zero to obtain normalized intensity, and they were analyzed to determine the slope of each sample, the slopes, which reflect the oxygen consumption rates by nematodes, were determined by selecting the linear portion of the signal profile and applying the linear regression according to the probe's manufacturer's instructions. Calculated slopes were used to determine the respiration rates in each sample. The relative respiration rates of *C. elegans* was calculated as follows: R = (Ss – Sn)/Sp, where Ss, Sn and Sp is the slope of the sample, the negative control and the positive control. Each condition was analyzed in three replicates on the 96-well plates. The OCR experiment was repeated four times.

Measurement of ATP production

ATP was quantified using a bioluminescence ATP measurement kit (Thermo Fisher Scientific, Waltham, MA, USA). Worms were collected from NGM plates and washed three times in S-basal to remove bacteria and frozen into liquid nitrogen. Before starting the analysis, the samples were put into a heat block at 95°C for 15 min, then placed in ice for 5 min. Next, samples were spun down at 14,000 x *g* for 10 min at 4°C and the supernatant was used to measure ATP. 10 µl of each sample in duplicates were transferred into 96-well plates. The ATP assay solution was prepared according to the manufacturer's instructions. 90 µl of the assay solution was then added to each sample. Next, the sample wells were read on Synergy Neo 2 plate reader using Gen5 software (BioTek, Wisnooski, VT, USA) with a luminometer filter. An ATP standard curve was generated and the ATP concentration for each sample was calculated based on the standard curve.

Protein oxidation measurement by OxyBlot

The level of protein oxidation was measured with the OxyBlot protein oxidation detection kit (Millipore-Sigma, Burlington, MA, USA). Worms were collected from each condition, washed three times with S-basal and concentrated to 10 µl lysis buffer and frozen to -80 °C for storage. Worms were homogenized with a TissueLyser II (Qiagen, Germantown, MD, USA). The DNP reaction mixture was made by adding 15 µg protein for each sample adjusted in 7 µl, 3 µl of 15% SDS and 10 µl of DNP solution. The mixture was kept at room temperature for 15 min, after which 7.5 µl Neutralization buffer was added. Samples (27.5 µl) were run in 10% SDA-PAGE gels, transferred into nitrocellulose (Bio-Rad, Hercules, California, USA) and blocked with 5% non-fat milk for 1h. After washing, the membrane was incubated with the first antibody (1:150) overnight at 4 °C and then for 1h with the secondary antibody (1:300) at room temperature. Membranes were incubated with ECL plus detection reagent (Bio-Rad) and scanned using Chemiluminescent

scanner (Bio-Rad). Band densities were analyzed using ImageJ. Membranes were then incubated with 15% hydrogen peroxide for 30 min at room temperature and treated with actin antibody to derive a density value of actin for each lane, with which OxyBlot value was normalized.

Quantification of mitochondrial membrane potential

Young adult worms were infected with *P. aeruginosa* for 12, 24 or 48 hrs at 25 °C on NGM plates that were pre-treated with 500 nm tetramethylrhodamine ethyl ester perchlorate (TMRE). To remove excessive dye from gut, worms were transferred to NGM agar plates with appropriate *P. aeruginosa* backgrounds for an additional 1 hr. Photographs were taken immediately.

FadE2 protein sequence analysis

The FadE2 protein sequence was blasted against NCBI non-redundant protein database using BLASTP and the top ten hits were identified. Protein sequence of the top 10 hits were gathered from Uniprot and multiple sequence alignment of those protein sequences was performed through the ClustalW online alignment tool. The resulting alignment file was imported into Bio-Edit to construct the final alignment figure. For the generation of phylogenetic tree, the same alignment file was imported into MEGA 7.0 software and the tree generated using the Neighbor-joining method using 1000 bootstraps.

Bacterial growth on fatty acids and amino acids

Fatty acids (butyric acid, C4:0; N-caproic acid, C6:0; caprylic acid, C8:0; capric acid, C10:0; lauric acid, C12:0; myristic acid, C14:0; palmitic acid, C16:0 and oleic acid, C18:1) stock solutions at 3% (w/v) were made with equimolar KOH and 1% Brij-58 [poly(oxyethylene) cetyl ether]. Growth curves were performed in 1× M9 (containing 0.5 mM $MgCl_2$ and 0.02 mM $CaCl_2$)+1% Brij-58 supplemented with 20 mM glucose or 0.2% of different fatty acids as sole carbon source.

For BCAAs, 5% stock solution was made for valine and 2% for leucine and isoleucine. Growth curves were performed in 1x M9 (containing 0.5 mM $MgCl_2$ and 0.02 mM $CaCl_2$) with 0.2% amino acids as sole carbon source. Bacterial cultures were grown overnight in LB medium and then washed with PBS three times to get rid of media. Cultures of bacteria were diluted to an initial OD_{600} of 0.01 for fatty acid or amino acid media. Unless indicated otherwise, the cultures were grown at 37 °C with a shaking speed of 250 rpm.

To calculate the specific growth rate, we used OD_{600} values obtained 8–44h after inoculation. *p*-values were obtained from specific growth rates in three independent experiments using the Student's t-test.

Recombinant expression and purification of FadE2 protein in *E. coli*

For recombinant expression of FadE2 protein in *E. coli*, the 1230 bp coding sequence was amplified from *P. aeruginosa* wild-type genomic DNA using primers GCAGCCATATGATGGATTTCGCCTATTCCCCCAA and ATCATCTCGAGTTAGCGGCTGCTGCGCAGCATCT and ligated into *NdeI* and *XhoI* sites of the expression vector pET28a(+) to yield pET28a::fadE2. The recombinant strain, *E. coli fadE2*

was grown in LB medium supplemented with ampicillin (50 µg/ml). Cultures were grown at 37 °C with shaking at 280 rpm until optical density reached OD_{600} of 0.5, at which point cells were induced with 0.1mM IPTG at 25 °C for 6 hrs. After induction, cells were harvested and FadE2 purified using a His-Trap column procedure described previously [46]. Fractions were collected and analyzed with 10% SDS-PAGE under denaturing conditions.

Analysis of acyl-CoA dehydrogenase activity using purified FadE2 protein

The DCPIP method was used to determine the ACAD activity of FadE2 [47]. In brief, the 200 µl assay mixture contained 50 mM HEPES-KOH buffer (pH 8.0), 1mM KCN, 1mM salicylhdroxamic acid, 50 µM FAD, 100 µ/ml DCPIP, 100 µg/ml PMS 50 µM of each of the fatty-acyl CoA substrates, 50 µl of purified FadE2. The reaction was started by the addition of PMS and its progress was followed by measuring the decrease in absorbance at 600 nm at 25 °C. An absorption coefficient of DCPIP 13100 M^{-1} cm^{-1} was used to calculate rates. Reaction rates were calculated from the initial linear portions of the absorbance versus time plots.

***C. elegans* metabolic profiling**

Metabolic analyses were conducted in Metabolon as previously described [48]. Briefly, nematode pellet samples were homogenized and subjected to methanol extraction then split into aliquots by ultrahigh performance liquid chromatography/ mass spectrometry (UHPLC/MS) in the positive (two methods) and negative (two methods) mode. Metabolites were then identified by automated comparison of ion features to a reference library of chemical standards followed by visual inspection for quality control (as previously described, [49]). For statistical analyses and data

display, any missing values are assumed to be below the limits of detection; these values were imputed with the compound minimum (minimum value imputation). Bradford protein measurements were conducted in parallel to normalized data to amount extracted. For generation of graphs, p-value ≤ 0.05 is considered significant. An estimate of false discovery rate (Q-value) is also calculated to take into account the multiple comparisons that normally occurs in metabolomics-based studies, with $Q < 0.05$ used an indication of high confidence in result.

RNAseq, quality analysis, mapping, assembly and differential expression

The total RNA was extracted using Trizol reagent according to the manufacturer's instructions and purified using RNA purification kit. RNA purity was checked using the Nanodrop Spectrophotometer. The RNA integrity was assessed using the Bioanalyzer 2100 system.

Sequencing libraries were generated in Novogene Inc. (CA, USA) using the NEBNext Ultra RNA Library Kit from Illumina (NEB, Ipswich, MA, USA), following manufacturer's protocol. The prepared DNA library was sequenced on an Illumina Hiseq 4000 according to the manufacturer's instructions for paired-end 150-bp reads. Clean data were then obtained by removing reads containing the adapter, reads containing poly-N and low-quality reads (<Q30) from the raw data using the program Trimmomatic [50]. Cleans reads were aligned to the *C. elegans* reference genome using TopHat v.2.0.9 (Trapnell et al., 2012). The mapped reads from each sample was assembled using Cufflinks v.2.1.1 [51]. HTSeq v.0.6.1 [52] was used to count the number of reads mapped to each gene. In addition, the reads per kilobase million (RPKM) of each gene was calculated based on the length of the gene and the number of reads mapped to it. Pairwise differential expression analysis was performed using *DESeq*2 R package (v.1.10.1) [53]. Genes

with adjusted *p*-value ≤0.05 were considered to be differentially expressed. The raw sequencing data are available from the NCBI and are archived under the accession number (TBA). Heat maps were generated using R Studio.

P. aeruginosa **virulence assays**

Motility assay

Motility assay was performed to assess the ability of bacteria to swim. In this test, each strain is stabbed into motility agar (LB plates containing 0.3% agar) and the plates were incubated at 37 °C for 48 hrs. As nutrients deplete, cells swim outwards forming circles of cells, or 'swarms'. Cells defective in flagellar-mediated motility do not form swarms but remain clustered in the stabbing area.

Twitching motility assay

Twitching motility assay was performed to investigate the movement by some type IV pili which is independent of flagella. For this, the bacterial strains are stabbed into thin LB plates containing 1.5% agar with a toothpick and plates are incubated at 37 °C for 72 hrs. Strains proficient for type IV pili-mediated twitching motility form a hazy zone of growth at the interface between the agar and the petri plate.

Biofilm formation assay

A static biofilm assay was used with polypropylene tube. Bacterial strains were grown overnight at 37 °C under constant rotation. The resulting suspension was diluted with LB broth to give an optical density at 600 nm (OD_{600}) = 0.01. 1 ml of diluted culture was transferred into a polypropylene tube. The plate was incubated at 30 °C for 48h. Planktonic cells were carefully removed by washing tubes with sterile double distilled water three times, and the plate was air dried. A 2 ml volume of 0.1% crystal violet (w/v) in 20% (v/v) ethanol/water was added into each tube to stain biofilm cells and incubated at room temperature for 1 hr in dark. Unbound dye was removed by washing with water three times. The crystal violet bound to biofilm was dissolved in 1 ml of 100% ethanol. The crystal violet amount for biofilm cells was measured at 595 nm. The relative biofilm forming ability was calculated by dividing A_{595} nm by the total crystal violet by the A_{600} nm for the cell density.

Protease assay

Overnight grown bacterial culture was used to aseptically streak a single line onto freshly prepared Milk agar plates (10% skim milk, 2% agar, 0.5% peptone, pH 7.2). The plates were incubated overnight in an inverted position for 48 hrs at 37 °C. Milk agar plates were examined for the presence or absence of clear zone area or zone of proteolysis, surrounding the growth of each of the strains.

Elastase and Rhamnolipid assays

Elastase and Rhamnolipid assays were done following the protocol from [54]. In brief, bacterial strains were grown overnight at LB broth at 37 °C to reach stationary phase. The culture was then

diluted with LB broth to yield an initial OD_{600} of 0.01 and then grown under shaking conditions at 37 °C until they reach mid-log phase. Using an inoculation loop, bacterial culture was streaked as a single line on elastin or rhamnolipid plates and incubated for 48 hrs at 37 °C. Plates were examined for the appearance of clearings surrounding the culture.

Pyocyanin assay

Freshly grown bacterial colony was used to inoculate 5 ml LB with or without gentamicin for wild-type or *fadE2* mutants, respectively and grown at 37 °C for 40 hrs. the bacteria was pelleted by centrifugation and the amount of blue pigment pyocyanin was measure in supernatants at 690 nm. The relative pyocyanin excretion ability was calculated by dividing A_{960} nm by A_{600} nm for the cell density.

LPS determination

Determination of the Kdo sugars was used to estimate the LPS concentration in the sample using the TBA method as follows. Bacteria were grown on 35 mm NGM plates for 24 hrs at 37°C, collected from agar plates and resuspended in 1 ml of sterile water. 50 ul of sample (OD600=0.2) or standard (0 to 20 µg/ml) were mixed with 50 µl of 0.5 M H_2SO_4. Samples were boiled for 8 min to release the Kdo sugars and cooled at RT for 10 min. 50 µl of 0.1 M periodic acid was added, vortexed and incubated for 10 min. Next, 200 µl of 0.2 M sodium arsenite in 0.5 M HCl was added and vortexed, followed by the addition of 800 µl of freshly prepared 0.6% (w/v) thiobarbituric acid (TBA). After vortexing, samples and standards were boiled for 10 min, cooled at RT for 40 min and were split in two 575 µl portions. 750 µl of n-butanol equilibrated with 0.5 M HCl was added

to each tube, followed my vortexing and spinning at 12000 *x* g for 6 min. The organic phases were recovered and combined into a cuvette and the absorbance was immediately taken at 552- and 509 nm. The 509 nm readings were subtracted from 552 nm readings for the standards to get a linear standard curve that was used to generate the concentration of unknowns.

Cyanide quantification

Cyanide production was quantified as described previously [13]. Strains were grown on 35 mm NGM plates for 24 h at 37°C and then enclosed without lids in individual sealed chambers which also contained 1 ml reservoir of 4 M NaOH (in an inverted 35 mm plate lid). All chambers were incubated at 25°C for 4 hrs, the NaOH was collected and diluted to 0.09M NaOH to bring the concentration within the detectable range (0-10 µM). The cyanide in the sample was quantified by comparison with standards of KCN in 0.09M NaOH: 105 ul aliquots of samples or KCN standards were mixed with 350 µl aliquots of freshly prepared 1:1 mixture of 0.1M *o*-dinitrobenzene and 0.2 M *p*-nitrobenzaldehyde (both in ethylene-glycol monoethyl ether). After incubation of 30 min at 22 °C, OD578 was measured. Total protein was determined by collecting bacteria from agar plates and resuspending the cells in 1 ml of 0.85% NaCl. After centrifugation, the cells were lysed and protein precipitated in 5% trichloroacetic acid. Protein pellets were resuspended in 1 ml of 50 mM KH_2PO_4 and the total amount of protein was determined in Bio-rad protein measurement reagent.

ACKNOWLEDGMENTS

We would like to thank the *Caenorhabditis* Genetic Center and Shohei Mitani of the National BioResource Project for providing worm strains. *atfs-1(cmh15)* was a gift from Dr. Cole M. Haynes (University of Massachusetts Medical School). This work was supported in part by grants

from the National Institutes of Health (R35GM128885) and Cancer Prevention & Research Institute of Texas (RR160053) to M.W.P, a CPRIT Scholar in Cancer Research.

REFERENCES

1. Qureshi MA, Haynes CM, Pellegrino MW. The mitochondrial unfolded protein response: Signaling from the powerhouse. J Biol Chem. 2017;292(33):13500-6. Epub 2017/07/09. doi: 10.1074/jbc.R117.791061. PubMed PMID: 28687630; PubMed Central PMCID: PMCPMC5566509.

2. Shpilka T, Haynes CM. The mitochondrial UPR: mechanisms, physiological functions and implications in ageing. Nat Rev Mol Cell Biol. 2018;19(2):109-20. Epub 2017/11/23. doi: 10.1038/nrm.2017.110. PubMed PMID: 29165426.

3. Fiorese CJ, Haynes CM. Integrating the UPR(mt) into the mitochondrial maintenance network. Crit Rev Biochem Mol Biol. 2017;52(3):304-13. Epub 2017/03/10. doi: 10.1080/10409238.2017.1291577. PubMed PMID: 28276702; PubMed Central PMCID: PMCPMC5571472.

4. Haynes CM, Yang Y, Blais SP, Neubert TA, Ron D. The matrix peptide exporter HAF-1 signals a mitochondrial UPR by activating the transcription factor ZC376.7 in C. elegans. Mol Cell. 2010;37(4):529-40. Epub 2010/03/02. doi: 10.1016/j.molcel.2010.01.015. PubMed PMID: 20188671; PubMed Central PMCID: PMCPMC2846537.

5. Nargund AM, Pellegrino MW, Fiorese CJ, Baker BM, Haynes CM. Mitochondrial import efficiency of ATFS-1 regulates mitochondrial UPR activation. Science. 2012;337(6094):587-90. Epub 2012/06/16. doi: 10.1126/science.1223560. PubMed PMID: 22700657; PubMed Central PMCID: PMCPMC3518298.

6. Arnoult D, Soares F, Tattoli I, Girardin SE. Mitochondria in innate immunity. EMBO Rep. 2011;12(9):901-10. Epub 2011/07/30. doi: 10.1038/embor.2011.157. PubMed PMID: 21799518; PubMed Central PMCID: PMCPMC3166463.

7. Pellegrino MW, Nargund AM, Kirienko NV, Gillis R, Fiorese CJ, Haynes CM. Mitochondrial UPR-regulated innate immunity provides resistance to pathogen infection. Nature. 2014;516(7531):414-7. Epub 2014/10/03. doi: 10.1038/nature13818. PubMed PMID: 25274306; PubMed Central PMCID: PMCPMC4270954.

8. Liu Y, Samuel BS, Breen PC, Ruvkun G. Caenorhabditis elegans pathways that surveil and defend mitochondria. Nature. 2014;508(7496):406-10. Epub 2014/04/04. doi: 10.1038/nature13204. PubMed PMID: 24695221; PubMed Central PMCID: PMCPMC4102179.

9. Jeong DE, Lee D, Hwang SY, Lee Y, Lee JE, Seo M, et al. Mitochondrial chaperone HSP-60 regulates anti-bacterial immunity via p38 MAP kinase signaling. EMBO J. 2017;36(8):1046-65. Epub 2017/03/12. doi: 10.15252/embj.201694781. PubMed PMID: 28283579; PubMed Central PMCID: PMCPMC5391144.

10. Gao K, Li Y, Hu S, Liu Y. SUMO peptidase ULP-4 regulates mitochondrial UPR-mediated innate immunity and lifespan extension. Elife. 2019;8. Epub 2019/01/16. doi: 10.7554/eLife.41792. PubMed PMID: 30642431; PubMed Central PMCID: PMCPMC6355198.

11. Tan MW, Mahajan-Miklos S, Ausubel FM. Killing of Caenorhabditis elegans by Pseudomonas aeruginosa used to model mammalian bacterial pathogenesis. Proc Natl Acad Sci U S A. 1999;96(2):715-20. Epub 1999/01/20. PubMed PMID: 9892699; PubMed Central PMCID: PMCPMC15202.

12. Irazoqui JE, Troemel ER, Feinbaum RL, Luhachack LG, Cezairliyan BO, Ausubel FM. Distinct pathogenesis and host responses during infection of C. elegans by P. aeruginosa and S.

aureus. PLoS Pathog. 2010;6:e1000982. Epub 2010/07/10. doi: 10.1371/journal.ppat.1000982. PubMed PMID: 20617181; PubMed Central PMCID: PMCPMC2895663.

13. Gallagher LA, Manoil C. Pseudomonas aeruginosa PAO1 kills Caenorhabditis elegans by cyanide poisoning. J Bacteriol. 2001;183(21):6207-14. Epub 2001/10/10. doi: 10.1128/JB.183.21.6207-6214.2001. PubMed PMID: 11591663; PubMed Central PMCID: PMCPMC100099.

14. Kirienko NV, Kirienko DR, Larkins-Ford J, Wahlby C, Ruvkun G, Ausubel FM. Pseudomonas aeruginosa disrupts Caenorhabditis elegans iron homeostasis, causing a hypoxic response and death. Cell Host Microbe. 2013;13(4):406-16. Epub 2013/04/23. doi: 10.1016/j.chom.2013.03.003. PubMed PMID: 23601103; PubMed Central PMCID: PMCPMC3641844.

15. Deng P, Uma Naresh N, Du Y, Lamech LT, Yu J, Zhu LJ, et al. Mitochondrial UPR repression during Pseudomonas aeruginosa infection requires the bZIP protein ZIP-3. Proc Natl Acad Sci U S A. 2019. Epub 2019/03/10. doi: 10.1073/pnas.1817259116. PubMed PMID: 30850535.

16. Yoneda T, Benedetti C, Urano F, Clark SG, Harding HP, Ron D. Compartment-specific perturbation of protein handling activates genes encoding mitochondrial chaperones. J Cell Sci. 2004;117(Pt 18):4055-66. Epub 2004/07/29. doi: 10.1242/jcs.01275. PubMed PMID: 15280428.

17. Feinbaum RL, Urbach JM, Liberati NT, Djonovic S, Adonizio A, Carvunis AR, et al. Genome-wide identification of Pseudomonas aeruginosa virulence-related genes using a Caenorhabditis elegans infection model. PLoS Pathog. 2012;8(7):e1002813. Epub 2012/08/23. doi: 10.1371/journal.ppat.1002813. PubMed PMID: 22911607; PubMed Central PMCID: PMCPMC3406104.

18. Meisel JD, Kim DH. Behavioral avoidance of pathogenic bacteria by Caenorhabditis elegans. Trends Immunol. 2014;35(10):465-70. Epub 2014/09/23. doi: 10.1016/j.it.2014.08.008. PubMed PMID: 25240986.

19. Richardson CE, Kooistra T, Kim DH. An essential role for XBP-1 in host protection against immune activation in C. elegans. Nature. 2010;463(7284):1092-5. Epub 2010/02/26. doi: 10.1038/nature08762. PubMed PMID: 20182512; PubMed Central PMCID: PMCPMC2834299.

20. Dunbar TL, Yan Z, Balla KM, Smelkinson MG, Troemel ER. C. elegans detects pathogen-induced translational inhibition to activate immune signaling. Cell Host Microbe. 2012;11(4):375-86. Epub 2012/04/24. doi: 10.1016/j.chom.2012.02.008. PubMed PMID: 22520465; PubMed Central PMCID: PMCPMC3334869.

21. McEwan DL, Kirienko NV, Ausubel FM. Host translational inhibition by Pseudomonas aeruginosa Exotoxin A Triggers an immune response in Caenorhabditis elegans. Cell Host Microbe. 2012;11(4):364-74. Epub 2012/04/24. doi: 10.1016/j.chom.2012.02.007. PubMed PMID: 22520464; PubMed Central PMCID: PMCPMC3334877.

22. Estes KA, Dunbar TL, Powell JR, Ausubel FM, Troemel ER. bZIP transcription factor zip-2 mediates an early response to Pseudomonas aeruginosa infection in Caenorhabditis elegans. Proc Natl Acad Sci U S A. 2010;107(5):2153-8. Epub 2010/02/06. doi: 10.1073/pnas.0914643107. PubMed PMID: 20133860; PubMed Central PMCID: PMCPMC2836710.

23. Tang H, Pang S. Proline Catabolism Modulates Innate Immunity in Caenorhabditis elegans. Cell Rep. 2016;17(11):2837-44. Epub 2016/12/16. doi: 10.1016/j.celrep.2016.11.038. PubMed PMID: 27974198.

24. Griffith OW, Bridges RJ, Meister A. Transport of gamma-glutamyl amino acids: role of glutathione and gamma-glutamyl transpeptidase. Proc Natl Acad Sci U S A. 1979;76(12):6319-

22. Epub 1979/12/01. doi: 10.1073/pnas.76.12.6319. PubMed PMID: 42913; PubMed Central PMCID: PMCPMC411855.

25. Mansfeld J, Urban N, Priebe S, Groth M, Frahm C, Hartmann N, et al. Branched-chain amino acid catabolism is a conserved regulator of physiological ageing. Nat Commun. 2015;6:10043. Epub 2015/12/02. doi: 10.1038/ncomms10043. PubMed PMID: 26620638; PubMed Central PMCID: PMCPMC4686672.

26. Wang YP, Lei QY. Metabolite sensing and signaling in cell metabolism. Signal Transduct Target Ther. 2018;3:30. Epub 2018/11/13. doi: 10.1038/s41392-018-0024-7. PubMed PMID: 30416760; PubMed Central PMCID: PMCPMC6224561.

27. Yang MJ, Cheng ZX, Jiang M, Zeng ZH, Peng B, Peng XX, et al. Boosted TCA cycle enhances survival of zebrafish to Vibrio alginolyticus infection. Virulence. 2018;9(1):634-44. Epub 2018/01/18. doi: 10.1080/21505594.2017.1423188. PubMed PMID: 29338666; PubMed Central PMCID: PMCPMC5955478.

28. Yang MJ, Xu D, Yang DX, Li L, Peng XX, Chen ZG, et al. Malate enhances survival of zebrafish against Vibrio alginolyticus infection in the same manner as taurine. Virulence. 2020;11(1):349-64. Epub 2020/04/23. doi: 10.1080/21505594.2020.1750123. PubMed PMID: 32316833; PubMed Central PMCID: PMCPMC7199751.

29. Yuan Y, Kadiyala CS, Ching TT, Hakimi P, Saha S, Xu H, et al. Enhanced energy metabolism contributes to the extended life span of calorie-restricted Caenorhabditis elegans. J Biol Chem. 2012;287(37):31414-26. Epub 2012/07/20. doi: 10.1074/jbc.M112.377275. PubMed PMID: 22810224; PubMed Central PMCID: PMCPMC3438970.

30. Chan TS, Cassim S, Raymond VA, Gottschalk S, Merlen G, Zwingmann C, et al. Upregulation of Krebs cycle and anaerobic glycolysis activity early after onset of liver ischemia.

PLoS One. 2018;13(6):e0199177. Epub 2018/06/15. doi: 10.1371/journal.pone.0199177. PubMed PMID: 29902244; PubMed Central PMCID: PMCPMC6002017 Universite de Montreal is a philanthropic chair administered by Universite de Montreal that was initially founded through a joint initiative of the Canadian Liver Foundation and Novartis to help promote research in the field of liver disease. There are no patents, products in development or marketed products to declare. This does not alter our adherence to PLOS ONE policies on sharing data and materials.

31. Watson E, Olin-Sandoval V, Hoy MJ, Li CH, Louisse T, Yao V, et al. Metabolic network rewiring of propionate flux compensates vitamin B12 deficiency in C. elegans. Elife. 2016;5. Epub 2016/07/08. doi: 10.7554/eLife.17670. PubMed PMID: 27383050; PubMed Central PMCID: PMCPMC4951191.

32. Bulcha JT, Giese GE, Ali MZ, Lee YU, Walker MD, Holdorf AD, et al. A Persistence Detector for Metabolic Network Rewiring in an Animal. Cell Rep. 2019;26(2):460-8 e4. Epub 2019/01/10. doi: 10.1016/j.celrep.2018.12.064. PubMed PMID: 30625328; PubMed Central PMCID: PMCPMC6368391.

33. Miyazawa H, Yamaguchi Y, Sugiura Y, Honda K, Kondo K, Matsuda F, et al. Rewiring of embryonic glucose metabolism via suppression of PFK-1 and aldolase during mouse chorioallantoic branching. Development. 2017;144(1):63-73. Epub 2017/01/05. doi: 10.1242/dev.138545. PubMed PMID: 28049690; PubMed Central PMCID: PMCPMC5278628.

34. Neinast M, Murashige D, Arany Z. Branched Chain Amino Acids. Annu Rev Physiol. 2019;81:139-64. Epub 2018/11/30. doi: 10.1146/annurev-physiol-020518-114455. PubMed PMID: 30485760; PubMed Central PMCID: PMCPMC6536377.

35. Chen XH, Liu SR, Peng B, Li D, Cheng ZX, Zhu JX, et al. Exogenous l-Valine Promotes Phagocytosis to Kill Multidrug-Resistant Bacterial Pathogens. Front Immunol. 2017;8:207. Epub

2017/03/23. doi: 10.3389/fimmu.2017.00207. PubMed PMID: 28321214; PubMed Central PMCID: PMCPMC5337526.

36. Son SM, Park SJ, Lee H, Siddiqi F, Lee JE, Menzies FM, et al. Leucine Signals to mTORC1 via Its Metabolite Acetyl-Coenzyme A. Cell Metab. 2019;29(1):192-201 e7. Epub 2018/09/11. doi: 10.1016/j.cmet.2018.08.013. PubMed PMID: 30197302; PubMed Central PMCID: PMCPMC6331339.

37. Saxton RA, Knockenhauer KE, Wolfson RL, Chantranupong L, Pacold ME, Wang T, et al. Structural basis for leucine sensing by the Sestrin2-mTORC1 pathway. Science. 2016;351(6268):53-8. Epub 2015/11/21. doi: 10.1126/science.aad2087. PubMed PMID: 26586190; PubMed Central PMCID: PMCPMC4698039.

38. Wolfson RL, Chantranupong L, Saxton RA, Shen K, Scaria SM, Cantor JR, et al. Sestrin2 is a leucine sensor for the mTORC1 pathway. Science. 2016;351(6268):43-8. Epub 2015/10/10. doi: 10.1126/science.aab2674. PubMed PMID: 26449471; PubMed Central PMCID: PMCPMC4698017.

39. Sener A, Malaisse WJ. L-leucine and a nonmetabolized analogue activate pancreatic islet glutamate dehydrogenase. Nature. 1980;288(5787):187-9. Epub 1980/11/13. doi: 10.1038/288187a0. PubMed PMID: 7001252.

40. Jang C, Oh SF, Wada S, Rowe GC, Liu L, Chan MC, et al. A branched-chain amino acid metabolite drives vascular fatty acid transport and causes insulin resistance. Nat Med. 2016;22(4):421-6. Epub 2016/03/08. doi: 10.1038/nm.4057. PubMed PMID: 26950361; PubMed Central PMCID: PMCPMC4949205.

41. Li P, Yin YL, Li D, Kim SW, Wu G. Amino acids and immune function. Br J Nutr. 2007;98(2):237-52. Epub 2007/04/04. doi: 10.1017/S000711450769936X. PubMed PMID: 17403271.

42. Haber A, Friedman S, Lobel L, Burg-Golani T, Sigal N, Rose J, et al. L-glutamine Induces Expression of Listeria monocytogenes Virulence Genes. PLoS Pathog. 2017;13(1):e1006161. Epub 2017/01/24. doi: 10.1371/journal.ppat.1006161. PubMed PMID: 28114430; PubMed Central PMCID: PMCPMC5289647.

43. Brenner S. The genetics of Caenorhabditis elegans. Genetics. 1974;77(1):71-94. Epub 1974/05/01. PubMed PMID: 4366476; PubMed Central PMCID: PMCPMC1213120.

44. Au V, Li-Leger E, Raymant G, Flibotte S, Chen G, Martin K, et al. CRISPR/Cas9 Methodology for the Generation of Knockout Deletions in Caenorhabditis elegans. G3 (Bethesda). 2019;9(1):135-44. Epub 2018/11/14. doi: 10.1534/g3.118.200778. PubMed PMID: 30420468; PubMed Central PMCID: PMCPMC6325907.

45. Zuo YT, Hu Y, Lu WW, Cao JJ, Wang F, Han X, et al. Toxicity of 2,6-dichloro-1,4-benzoquinone and five regulated drinking water disinfection by-products for the Caenorhabditis elegans nematode. J Hazard Mater. 2017;321:456-63. Epub 2016/09/27. doi: 10.1016/j.jhazmat.2016.09.038. PubMed PMID: 27669387.

46. Hume AR, Nikodinovic-Runic J, O'Connor KE. FadD from Pseudomonas putida CA-3 is a true long-chain fatty acyl coenzyme A synthetase that activates phenylalkanoic and alkanoic acids. J Bacteriol. 2009;191(24):7554-65. Epub 2009/10/13. doi: 10.1128/JB.01016-09. PubMed PMID: 19820085; PubMed Central PMCID: PMCPMC2786608.

47. Bode K, Hooks MA, Couee II. Identification, separation, and characterization of acyl-coenzyme A dehydrogenases involved in mitochondrial beta-oxidation in higher plants. Plant

Physiol. 1999;119(4):1305-14. Epub 1999/04/10. doi: 10.1104/pp.119.4.1305. PubMed PMID: 10198089; PubMed Central PMCID: PMCPMC32015.

48. Long T, Hicks M, Yu HC, Biggs WH, Kirkness EF, Menni C, et al. Whole-genome sequencing identifies common-to-rare variants associated with human blood metabolites. Nat Genet. 2017;49(4):568-78. Epub 2017/03/07. doi: 10.1038/ng.3809. PubMed PMID: 28263315.

49. Dehaven CD, Evans AM, Dai H, Lawton KA. Organization of GC/MS and LC/MS metabolomics data into chemical libraries. J Cheminform. 2010;2(1):9. Epub 2010/10/20. doi: 10.1186/1758-2946-2-9. PubMed PMID: 20955607; PubMed Central PMCID: PMCPMC2984397.

50. Bolger AM, Lohse M, Usadel B. Trimmomatic: a flexible trimmer for Illumina sequence data. Bioinformatics. 2014;30(15):2114-20. Epub 2014/04/04. doi: 10.1093/bioinformatics/btu170. PubMed PMID: 24695404; PubMed Central PMCID: PMCPMC4103590.

51. Trapnell C, Roberts A, Goff L, Pertea G, Kim D, Kelley DR, et al. Differential gene and transcript expression analysis of RNA-seq experiments with TopHat and Cufflinks. Nat Protoc. 2012;7(3):562-78. Epub 2012/03/03. doi: 10.1038/nprot.2012.016. PubMed PMID: 22383036; PubMed Central PMCID: PMCPMC3334321.

52. Anders S, Pyl PT, Huber W. HTSeq--a Python framework to work with high-throughput sequencing data. Bioinformatics. 2015;31(2):166-9. Epub 2014/09/28. doi: 10.1093/bioinformatics/btu638. PubMed PMID: 25260700; PubMed Central PMCID: PMCPMC4287950.

53. Love MI, Huber W, Anders S. Moderated estimation of fold change and dispersion for RNA-seq data with DESeq2. Genome Biol. 2014;15(12):550. Epub 2014/12/18. doi:

10.1186/s13059-014-0550-8. PubMed PMID: 25516281; PubMed Central PMCID: PMCPMC4302049.

54. Rust L, Messing CR, Iglewski BH. Elastase assays. Methods Enzymol. 1994;235:554-62. Epub 1994/01/01. doi: 10.1016/0076-6879(94)35170-8. PubMed PMID: 8057926.

FIGURES

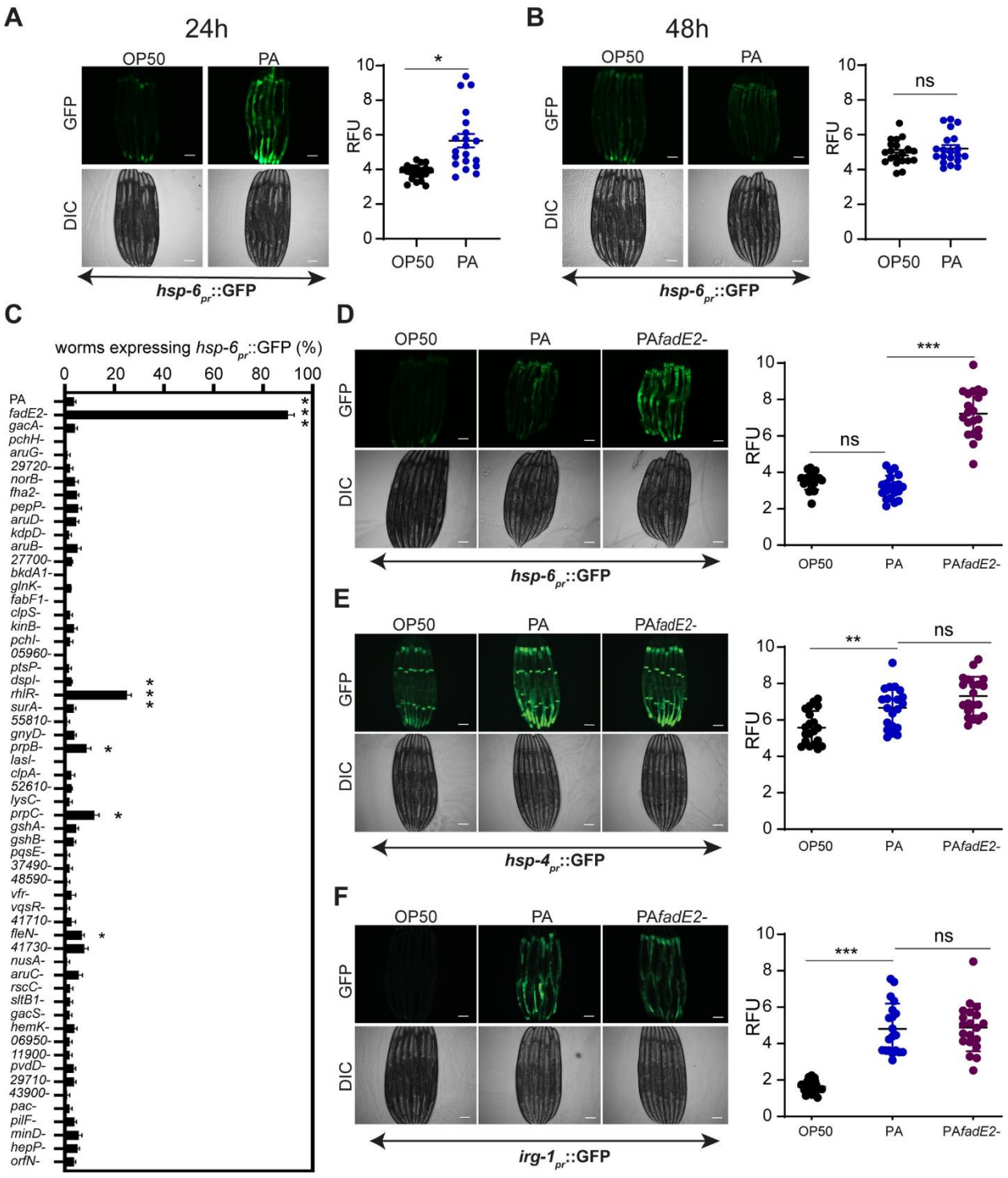

Figure 3.1 *P. aeruginosa* FadE2 mediates the repression of the UPRmt

(A, B) *hsp-6*$_{pr}$::GFP animals exposed to *E. coli* OP50 or wild-type *P. aeruginosa* (PA) for (A) 24 hrs or (B) 48 hrs with quantifications of fluorescence. RFU: Relative Fluorescence Units.

(C) Quantification of proportion of animals expressing *hsp-6*$_{pr}$::GFP animals exposed to various *P. aeruginosa* transposon insertion mutants following 48 hrs of infection.

(D-F) *hsp-6*$_{pr}$::GFP (D), *hsp-4*$_{pr}$::GFP (E), and *irg-1*$_{pr}$::GFP (F) animals grown in the presence of *E. coli* OP50, wild-type *P. aeruginosa* (PA), or *fadE2*- for 48 hrs with quantifications of fluorescence. RFU: Relative Fluorescence Units.

(A-F) Shown is the mean $\pm$ SEM ($n \geq 20$ worms). Scale bar is 100 μm for all images. *** denotes $p<0.001$, ** denotes $p<0.01$, *denotes $p<0.05$ using Student's *t*-test.

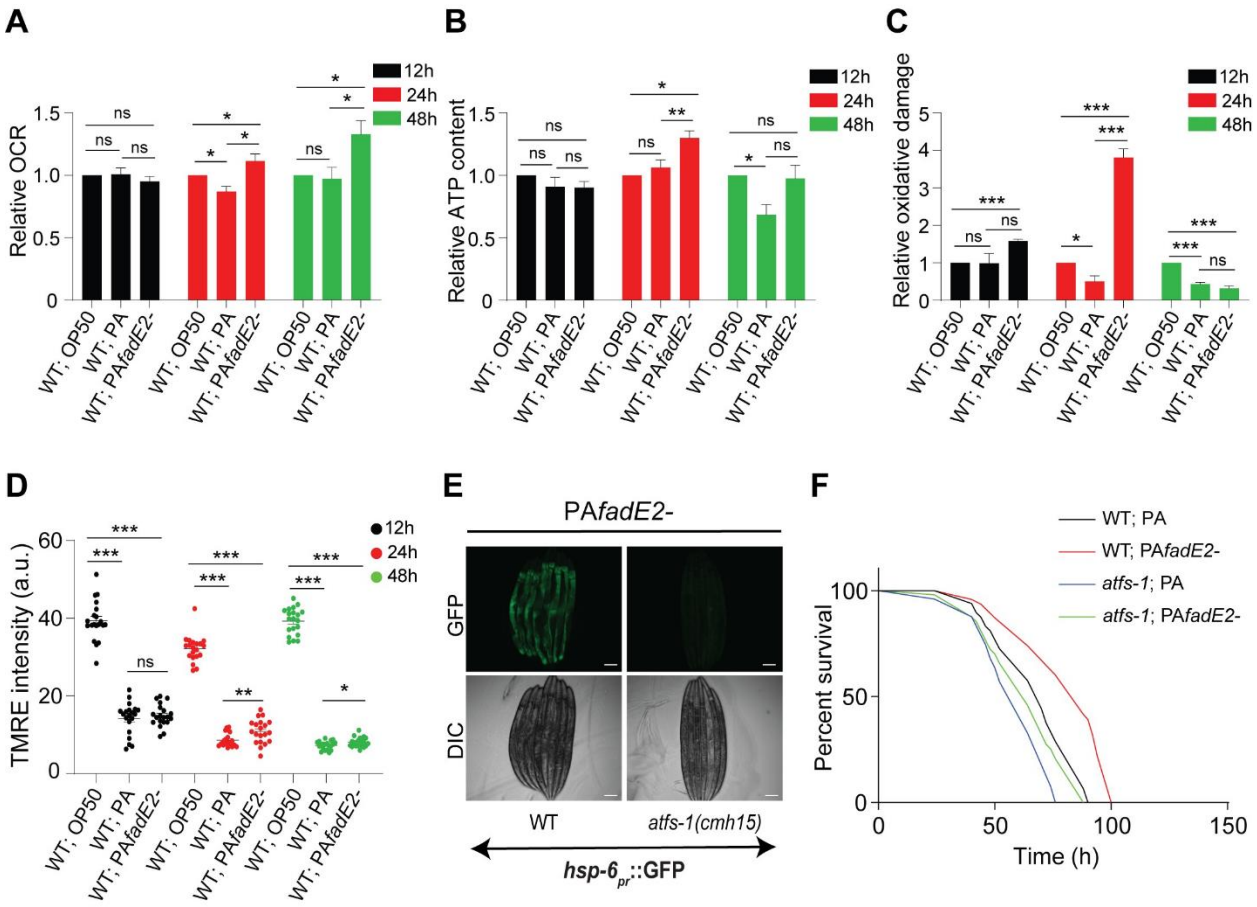

Figure 3.2 *P. aeruginosa* impairs host mitochondrial activity via FadE2

(A-C) Quantification of (A) oxygen consumption rate (OCR), (B) ATP production, (C) level of protein carbonylation for wild-type animals exposed to *E. coli* OP50, wild-type *P. aeruginosa* (PA) or *fadE2*- for the indicated amounts of time. Shown is the mean ± SEM normalized to total protein content (n=4 for A and B, n=3 for C).

(D) Quantification of mitochondrial membrane potential using TMRE for wild-type animals exposed to *E. coli* OP50, wild-type *P. aeruginosa* (PA) or *fadE2*- for the indicated amounts of time. A.U. arbitrary units. (n≥20).

(A-D) *** denotes p<0.001, ** denotes p<0.01, *denotes p<0.05 using Student's *t*-test.

(E) *hsp-6*$_{pr}$::GFP expression in wild-type and *atfs-1(cmh15)* animals infected with *fadE2*- for 48 hrs. Scale bar is 100 μm.

(F) Survival analysis of wild-type and *atfs-1(cmh15)* animals during infection with wild-type *P. aeruginosa* (PA) or *fadE2*-. See Table S2 for all survival data statistics.

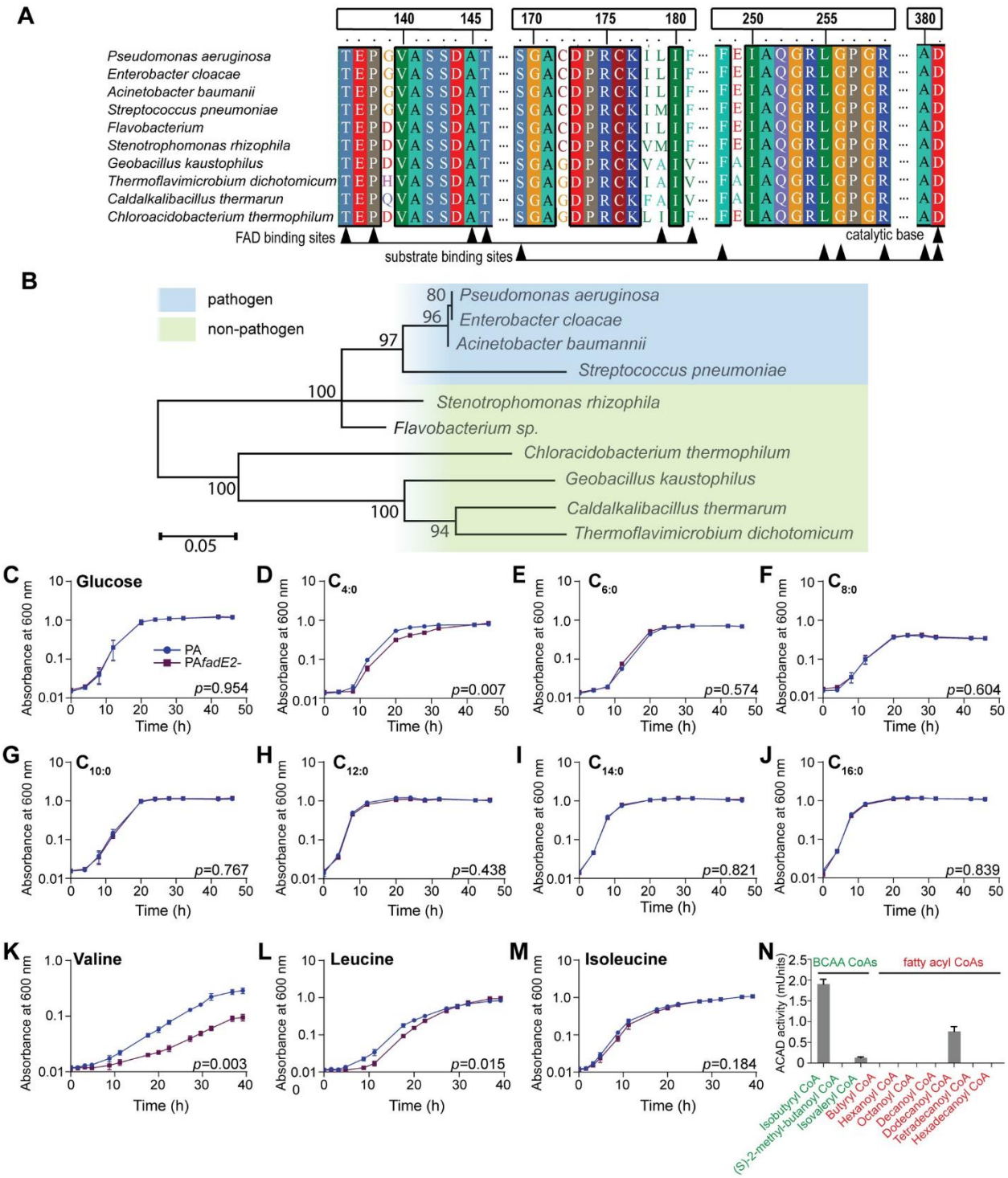

Figure 3.3 *P. aeruginosa* FadE2 is an acyl-CoA dehydrogenase involved in valine and leucine catabolism

(A) Protein alignment of FadE2 with other conserved acyl-CoA dehydrogenase homologs.

(B) Phylogenetic analysis of FadE2. Scale bars represents 0.05 substitutions per amino acid position.

(C-M) Bacterial growth analysis of wild-type *P. aeruginosa* (PA) and *fadE2*- using glucose or various fatty acids or BCAAs as the sole carbon source. Shown is the mean ± SEM (n=3). *p* values obtained using Student's *t*-test.

(N) Enzyme activity of FadE2 using the indicated CoA esters as substrates. FadE2 activity was measured as described in "Materials and Methods". Shown is the mean ± SEM of acyl-CoA dehydrogenase activity (n=3).

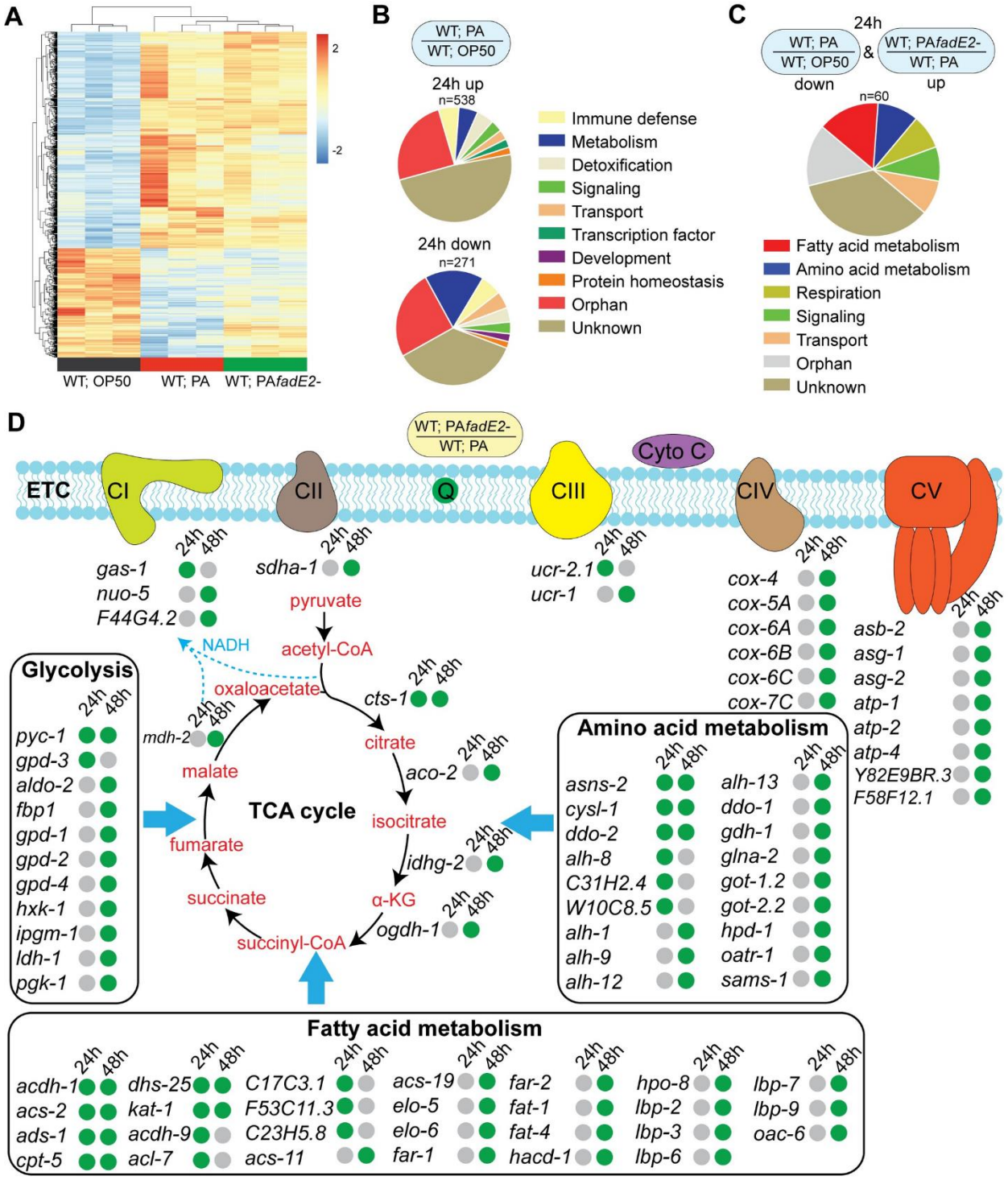

Figure 3.4 Host metabolic gene expression is repressed with *P. aeruginosa* in a FadE2 dependent manner

(A) Heat map representing the change in gene expression patterns of wild-type worms exposed to *E. coli* OP50, wild-type *P. aeruginosa* (PA) or *fadE2*- for 24 hrs (significantly different at P_{adj}<0.05).

(B) Pie chart analysis illustrating the gene categories upregulated and downregulated in wild-type animals infected with wild-type *P. aeruginosa* (PA) for 24 hrs relative to those exposed to *E. coli* OP50.

(C) Pie chart analysis illustrating the gene categories that were downregulated in animals exposed to wild-type *P. aeruginosa* (PA) relative to *E. coli* OP50 and were upregulated in animals exposed to *fadE2*-.

(D) Metabolic network of genes differentially expressed during infection with wild-type *P. aeruginosa* (PA) or *fadE2*- for 24 and 48 hrs (n=3). Green and grey dots represent increase or no change in gene expression, respectively.

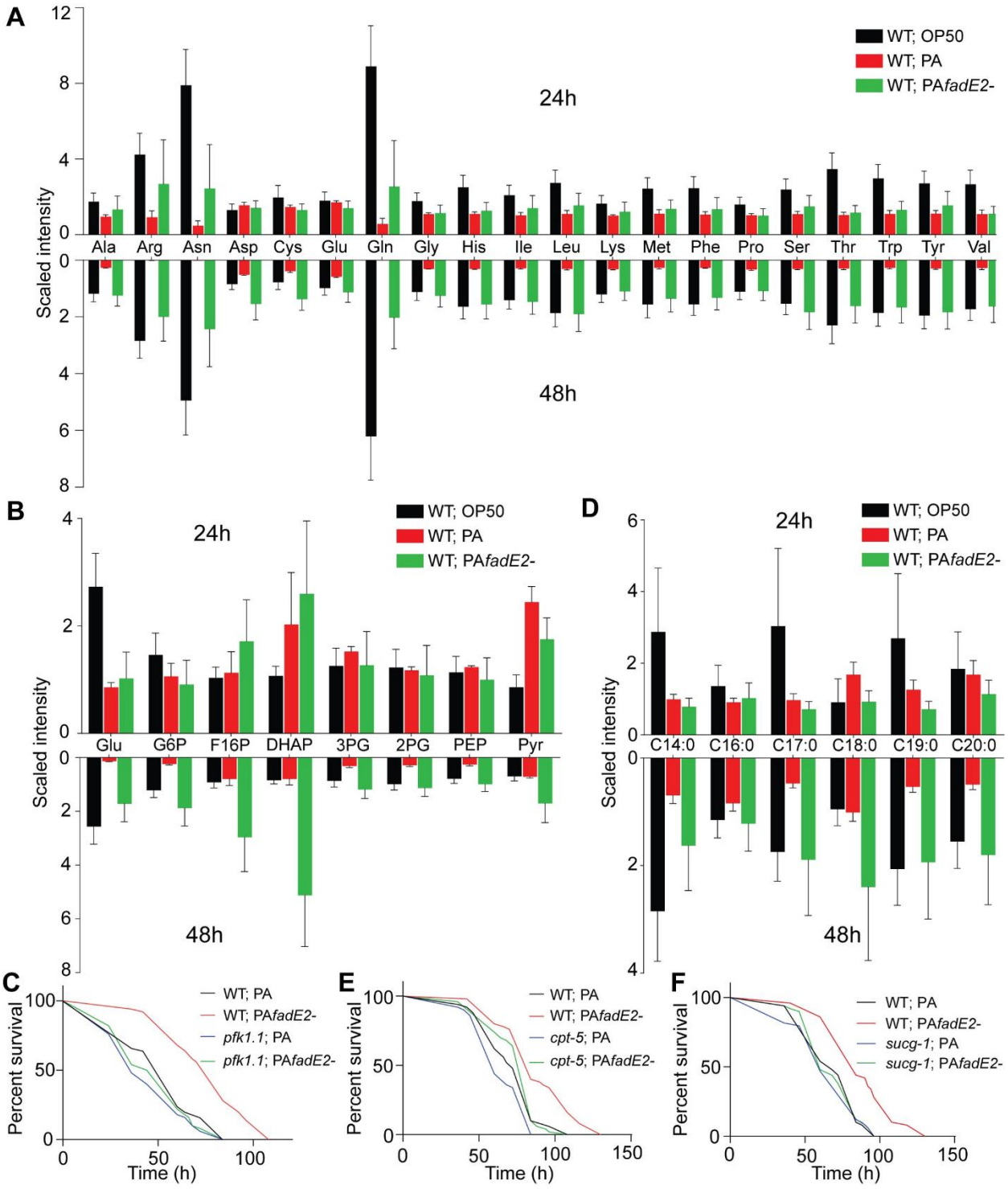

Figure 3.5 *P. aeruginosa* FadE2 mediates the suppression of host energy pathways during infection

(A, B) Quantification of (A) individual amino acids and (B) glycolysis/gluconeogenesis metabolites from wild-type animals exposed to *E. coli* OP50, wild-type *P. aeruginosa* (PA) or *fadE2*- following 24 and 48 hrs. ($n \geq 4$). See Table S1 for statistics.

(C) Survival of wild-type or *pfk-1.1(ola72)* animals infected with wild-type *P. aeruginosa* (PA) or *fadE2*-.

(D) Quantification of long-chain and very-long chain saturated fatty acids from wild-type animals exposed to *E. coli* OP50, wild-type *P. aeruginosa* (PA) or *fadE2*- following 24 and 48 hrs ($n \geq 4$). See Table S1 for statistics.

(E) Survival of *cpt-5(gk5128)* animals infected with wild-type *P. aeruginosa* (PA) or *fadE2*-.

(F) Survival of *sucg-1(osa2)* animals infected with wild-type *P. aeruginosa* (PA) or *fadE2*-.

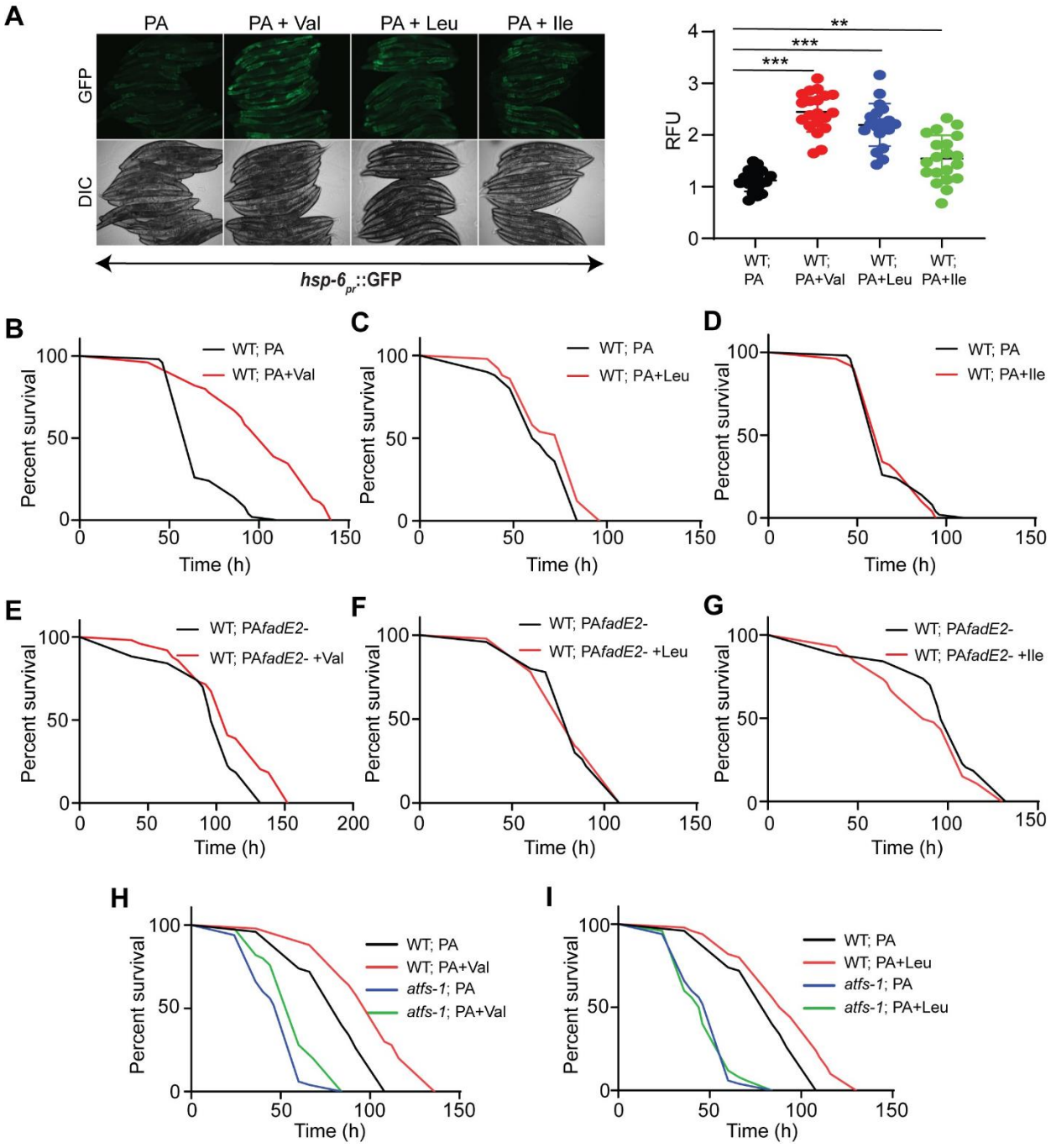

Figure 3.6 Valine or leucine supplementation is sufficient to restore the UPR^{mt} and protect the host during infection

(A) Expression of *hsp-6*$_{pr}$::GFP in animals exposed to wild-type *P. aeruginosa* (PA) in the presence or absence of 5mM valine (Val), leucine (Leu), or isoleucine (Ile) for 48 hrs with

quantifications of fluorescence. RFU: Relative Fluorescence Units. *** denotes $p<0.001$, ** denotes $p<0.01$, using Student's *t*-test.

(B-D) Survival of wild-type animals supplemented with 5 mM (B) valine, (C) leucine or (D) isoleucine infected with wild-type *P. aeruginosa*.

(E-G) Survival of wild-type animals supplemented with 5 mM (E) valine, (F) leucine or (G) isoleucine infected with *fadE2*-.

(H, I) Survival of wild-type or *atfs-1(cmh15)* animals supplemented with 5 mM (H) valine or (I) leucine infected with wild-type *P. aeruginosa*.

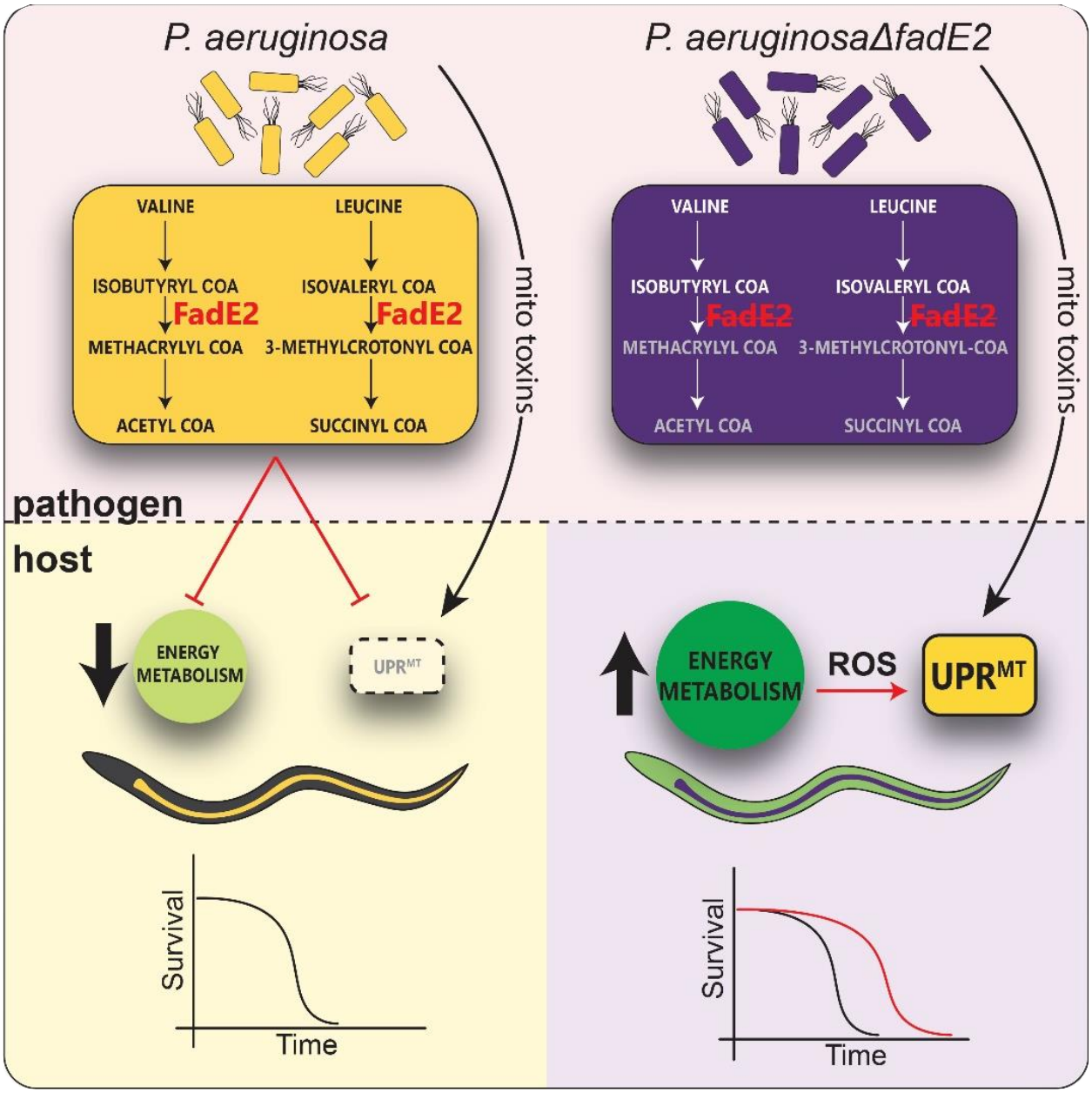

Figure 3.7 Model

During infection, *P. aeruginosa* FadE2 restricts valine and leucine catabolites which reduces host energy metabolic pathways and represses the UPR^{mt} through a presently undefined mechanism. However, loss of *P. aeruginosa* FadE2 results in accumulation of valine and leucine catabolites stimulating an increase in host energy metabolism and a restored ability to activate the UPR^{mt} that supports host survival. Consequently, the host relies on the activation of the UPR^{mt} to support

mitochondrial recovery resulting from the stress caused by enhanced energy metabolism and by toxins produced by *P. aeruginosa* that target mitochondrial function.

SUPPLEMENTARY FIGURE LEGENDS

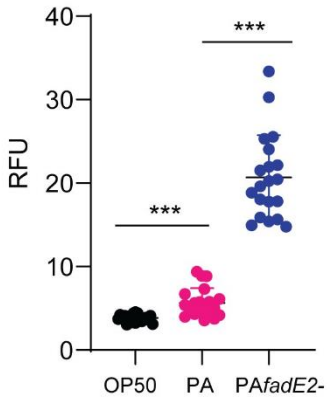

Supplementary Figure 3.1 Loss of P. aeruginosa FadE2 enhances UPRmt activity during infection.

Quantification of fluorescence from *hsp-6*$_{pr}$::GFP animals exposed to *E. coli* OP50, wild-type *P. aeruginosa* (PA) or *fadE2*- for 24 hrs. RFU: Relative Fluorescence Units. Shown is the mean $\pm$ SEM ($n \geq 20$ worms). *** denotes $p<0.001$ using Student's *t*-test.

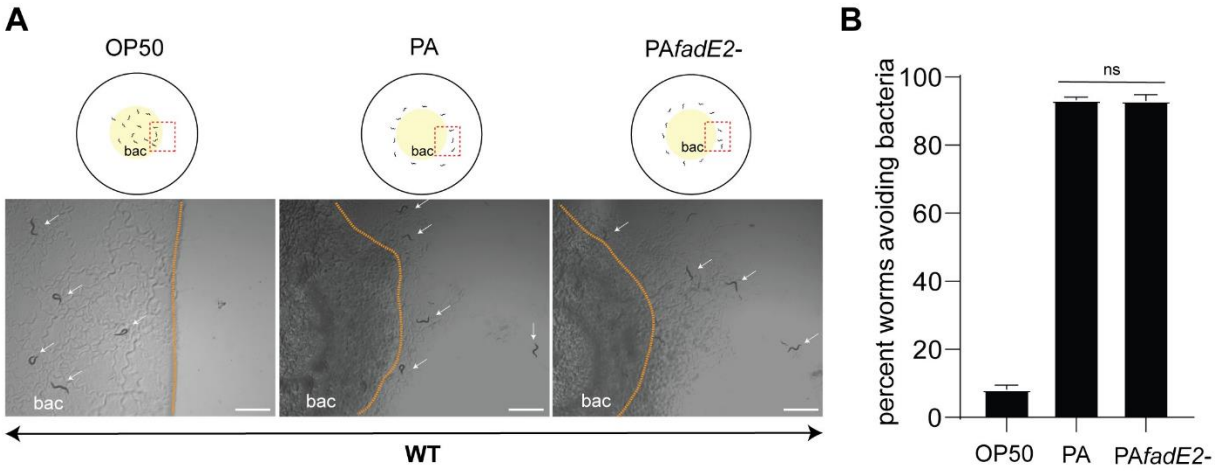

Supplementary Figure 3.2 fadE2- does not affect C. elegans avoidance behavior

(A) Photomicrographs of wild-type animals grown in the presence of *E. coli*, wild-type *P. aeruginosa* (PA), or *fadE2*-. Scale bar is 1 mm. bac = bacteria, arrows point to position of *C. elegans* relevant to bacterial lawn edge.

(B) Quantification of avoidance behavior of wild-type animals grown in the presence of *E. coli*, wild-type *P. aeruginosa* (PA), or *fadE2*-. Shown is the mean $\pm$ SEM ($n \geq 20$ worms). *ns* denotes no significance using Student's *t*-test.

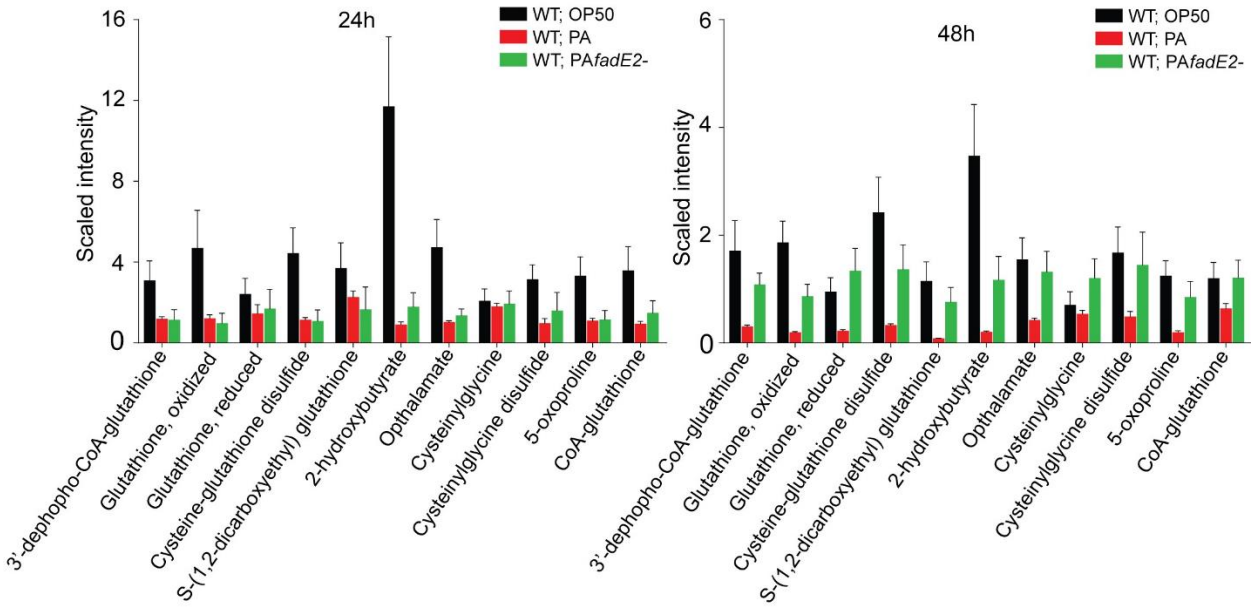

Supplementary Figure 3.3 Glutathione metabolism decreases during infection with P. aeruginosa in a FadE2-dependent manner

Quantification of metabolites related to glutathione biosynthesis metabolism by mass spectrometry using extracts of wild-type animals exposed to *E. coli* OP50, wild-type *P. aeruginosa* (PA) or *fadE2*- following 24 or 48 hrs. Shown is the mean $\pm$ SEM ($n \geq 4$). See Table S1 for statistics.

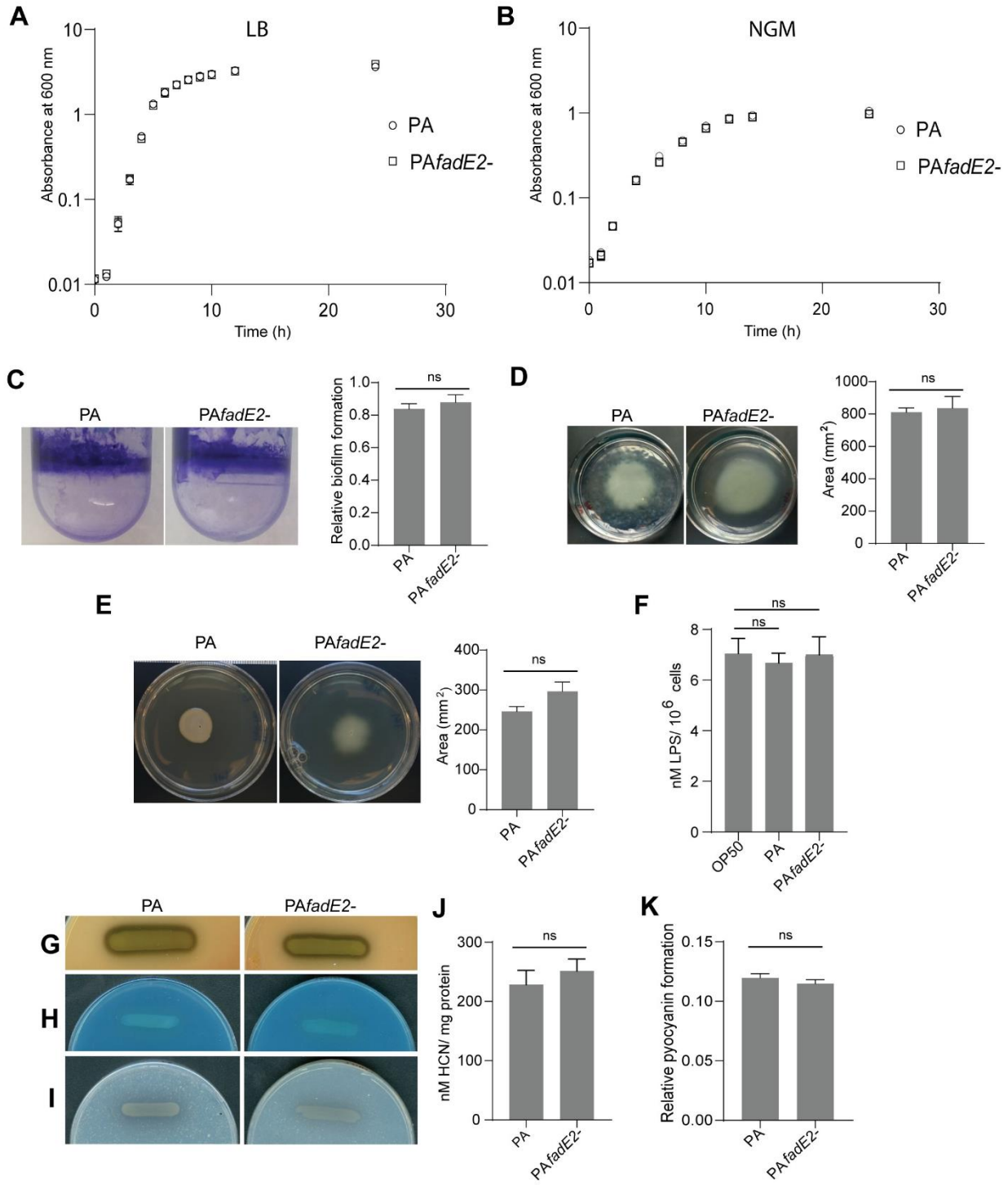

Supplementary Figure 3.4 P. aeruginosa fadE2- does not show evidence of impaired virulence

(A) Growth curves of wild-type *P. aeruginosa* (PA) or *fadE2*- in LB medium.

(B) Growth curves of wild-type *P. aeruginosa* (PA) or *fadE2*- in NGM.

(C) Photomicrographs and quantification of biofilm formation in wild-type *P. aeruginosa* (PA) or *fadE2*-. Shown is the mean ± SEM (n=3).

(D) Photomicrographs and quantification of motility in wild-type *P. aeruginosa* (PA) or *fadE2*-. Shown is the mean ± SEM (n=3).

(E) Photomicrographs and quantification of twitching motility in wild-type *P. aeruginosa* (PA) or *fadE2*-. Shown is the mean ± SEM (n=3).

(F) Quantification of LPS levels in wild-type *P. aeruginosa* (PA) or *fadE2*-. Shown is the mean ± SEM (n=3).

(G-I) Photomicrographs showing production of (G) proteases, (H) rhamnolipids, and (I) elastase in wild-type *P. aeruginosa* (PA) or *fadE2*-.

(J) Quantification of cyanide levels in wild-type *P. aeruginosa* (PA) or *fadE2*-. Shown is the mean ± SEM (n=3).

(K) Quantification of pyocyanin levels in wild-type *P. aeruginosa* (PA) or *fadE2*-. Shown is the mean ± SEM (n=3).

(C, D, E, F, J, K) *ns* denotes no significance using Student's *t*-test.

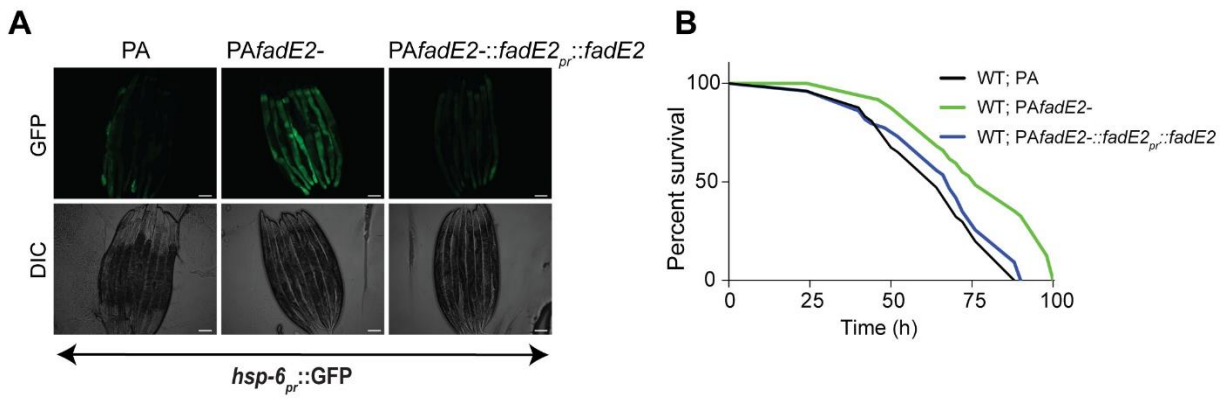

Supplementary Figure 3.5 Phenotypes associated with fadE2- can be rescued

(A) *hsp-6*$_{pr}$::GFP animals grown in the presence of wild-type *P. aeruginosa* (PA), *fadE2*-, or *fadE2*- expressing a FadE2 rescue plasmid for 48 hrs.

(B) Survival of wild-type animals during infection with wild-type *P. aeruginosa* (PA), *fadE2*-, or *fadE2*- expressing the FadE2 rescue plasmid. See Table S2 for survival assay statistics.

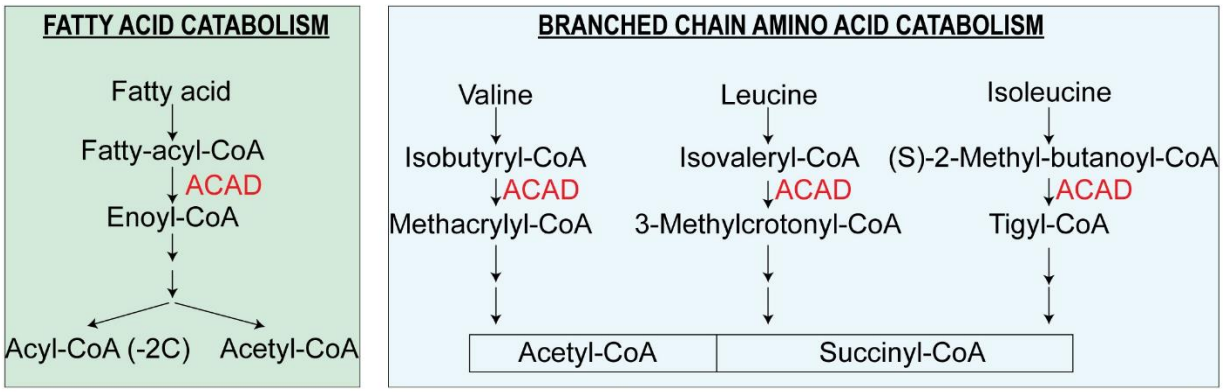

Supplementary Figure 3.6 Acyl-CoA dehydrogenases mediate fatty acid and BCAA catabolism

Schematic overview of the role of acyl-CoA dehydrogenases (ACAD) in fatty acid and BCAA catabolism.

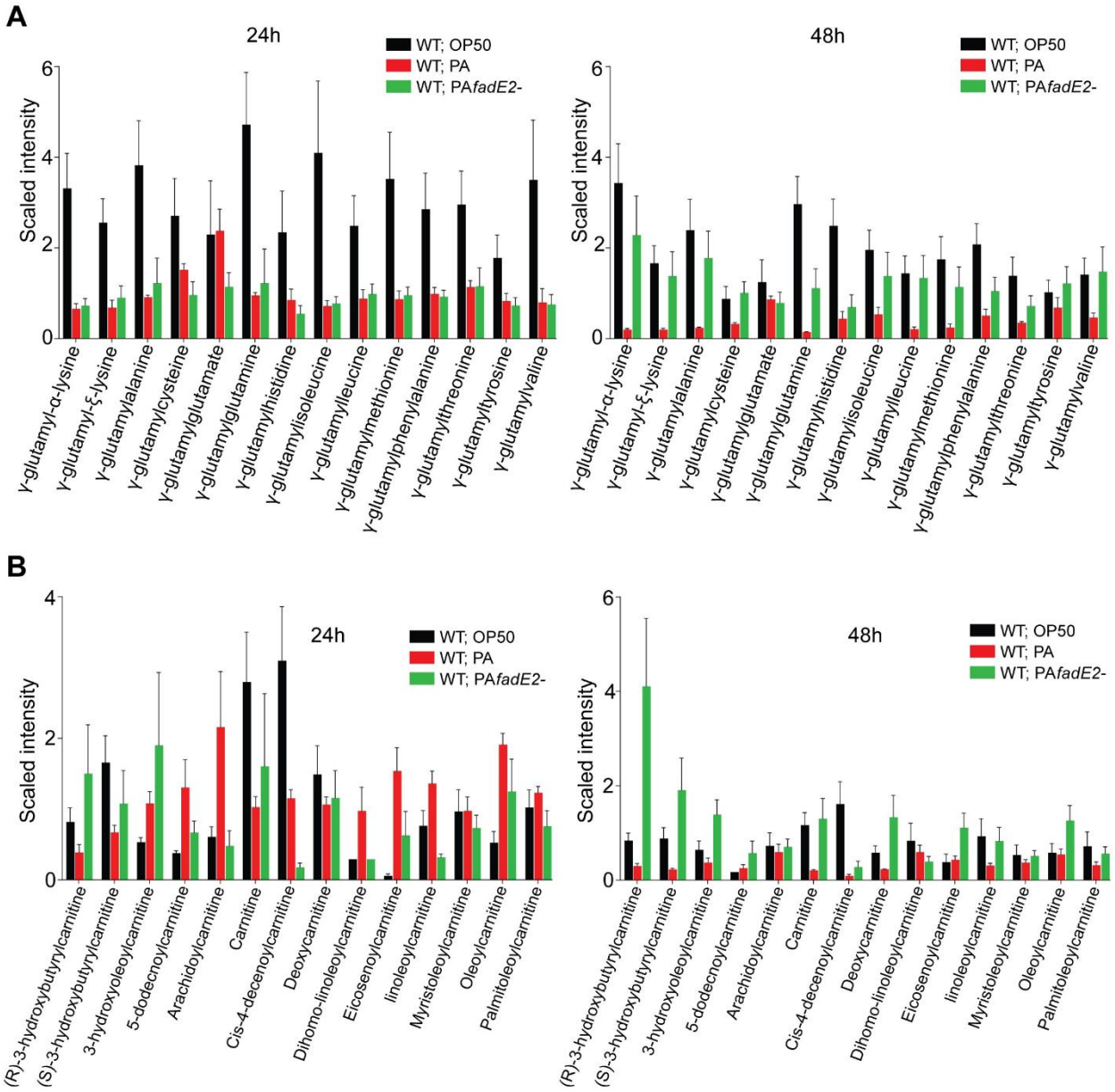

Supplementary Figure 3.7 Gamma-glutamyl amino acids and carnitine metabolism decrease during infection with P. aeruginosa in a FadE2-dependent manner

Quantification of metabolites related to (A) gamma-glutamyl amino acids, (B) carnitine metabolism by mass spectrometry using extracts of wild-type animals infected with wild-type *P. aeruginosa* (PA) or *fadE2*- following 24 or 48 hrs. Shown is the mean ± SEM (n≥4).

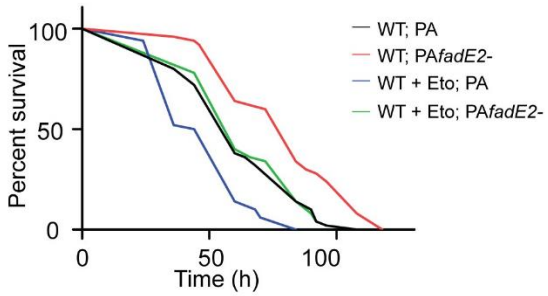

Supplementary Figure 3.8 Gamma-glutamyl amino acids and carnitine metabolism decrease during infection with P. aeruginosa in a FadE2-dependent manner

Survival of wild-type animals treated with 50 µM etomoxir (Eto) and infected with wild-type *P. aeruginosa* (PA) or *fadE2*-. See Table S2 for statistics.

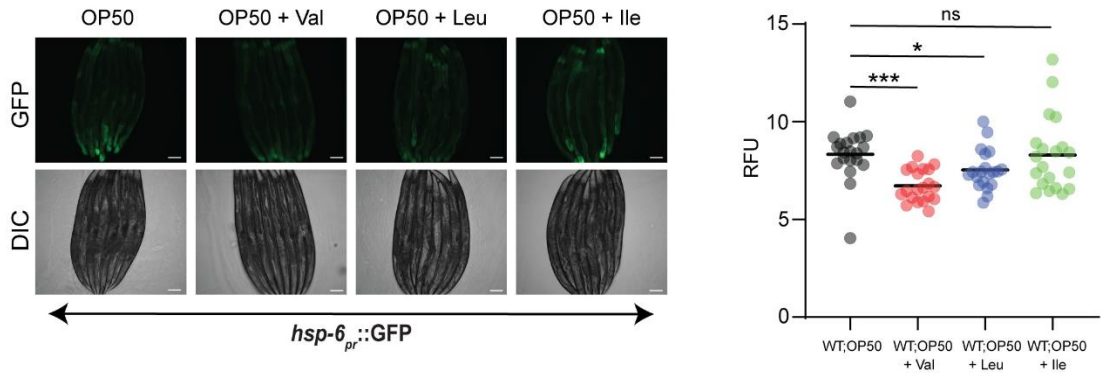

Supplementary Figure 3.9 Valine, leucine, or isoleucine supplementation does not activate the UPRmt upon exposure to E. coli OP50

Photomicrographs and quantifications of *hsp-6*$_{pr}$::GFP fluorescence for wild-type animals fed *E. coli* OP50 and supplemented with valine, leucine, or isoleucine. RFU: Relative Fluorescence Units. Shown is the mean ± SEM (n≥20 worms). Scale bar is 100 µm for all images. *ns* denotes no significance, *** denotes p<0.001, *denotes p<0.05 using Student's *t*-test.

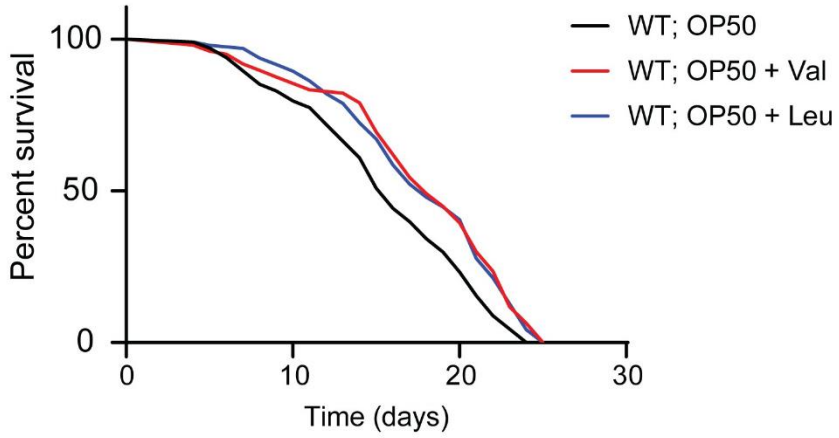

Supplementary Figure 3.10 Valine or leucine supplementation increases the lifespan of C. elegans fed E. coli OP50

(A, B) Lifespans of wild-type animals supplemented with 5 mM (A) valine or (B) leucine fed a diet of *E. coli* OP50.

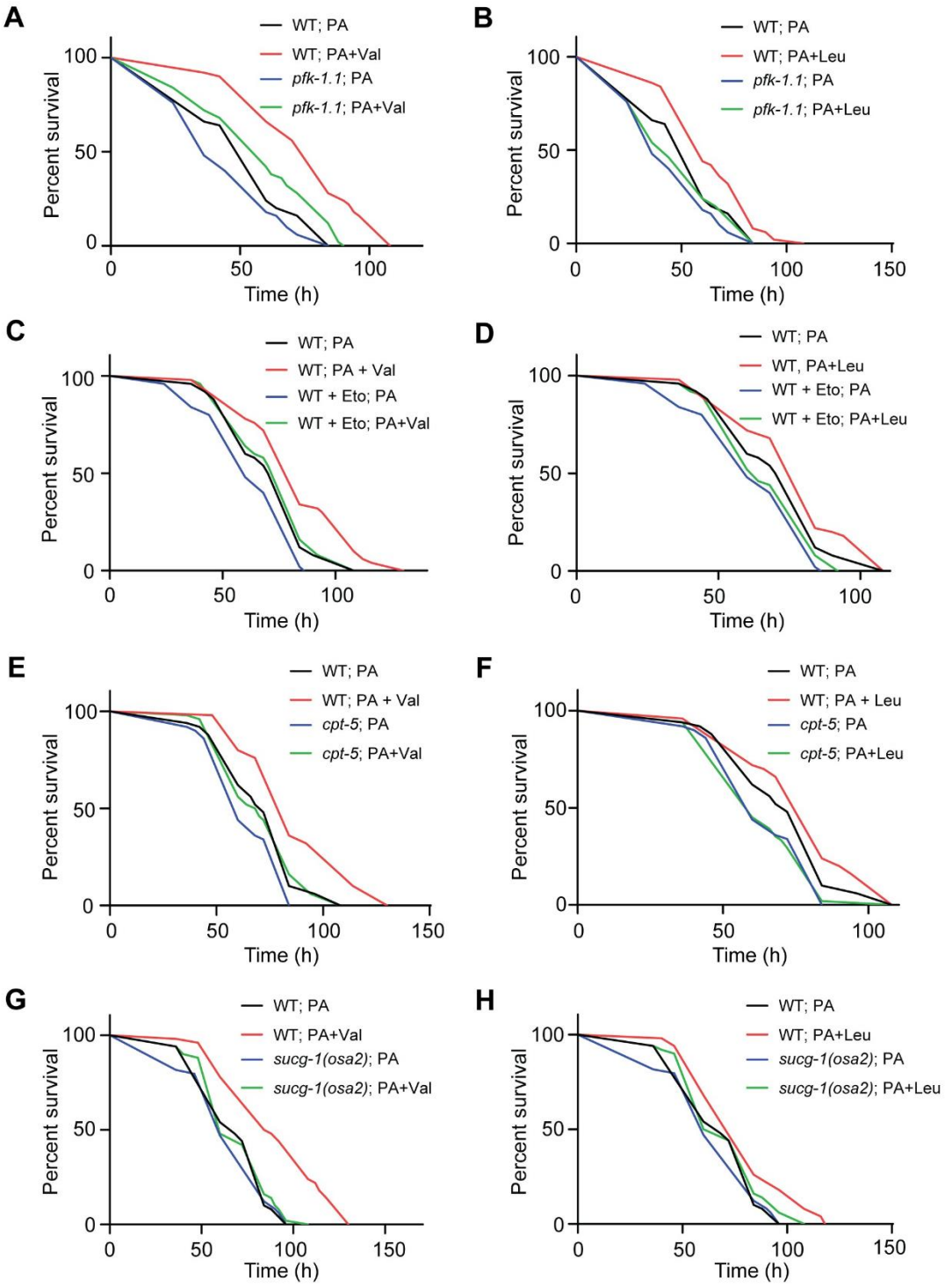

Supplementary Figure 3.11 Increased host survival during P. aeruginosa infection with valine and leucine supplementation depends on host energy metabolism pathways

(A, B) Survival of *pfk-1.1(ola72)* animals infected with wild-type *P. aeruginosa* (PA) and supplemented with 5 mM (A) valine or (B) leucine.

(C, D) Survival of wild-type animals treated with 50 µM etomoxir (Eto) and supplemented with 5 mM (C) valine or (D) leucine and infected with wild-type *P. aeruginosa* (PA).

(E, F) Survival of *cpt-5(gk5128)* animals infected with wild-type *P. aeruginosa* (PA) and supplemented with 5 mM (E) valine or (F) leucine.

(G, H) Survival of *sucg-1(osa2)* animals infected with wild-type *P. aeruginosa* (PA) and supplemented with 5 mM (G) valine or (H) leucine.

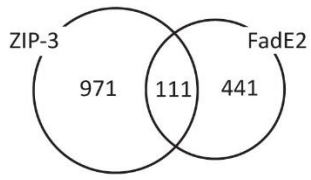

Supplementary Figure 3.12 Modest overlap in the number of genes negatively regulated by P. aeruginosa FadE2 and C. elegans ZIP-3

Venn diagram demonstrating the number of commons genes that are negatively regulated by *P. aeruginosa* FadE2 (see Table S3) and ZIP-3 (see reference [15]).

Supplementary Table 1. Metabolomic analysis of wild-type animals exposed to *E. coli* OP50, wild-type *P. aeruginosa* or *fadE2*- for the defined period.

Supplementary Table 2. Statistical analysis for all animal survival assays.

Supplementary Table 3. RNA sequencing analysis of wild-type animals exposed to *E. coli* OP50, wild-type *P. aeruginosa* or *fadE2*- for the defined period.

4. Elucidating valine's pro-survival role during infection via the mitochondrial UPR

M. Adnan Qureshi, Balan Ramesh and M.W. Pellegrino.

University of Texas at Arlington, Department of Biology, TX, USA.

ABSTRACT

The age-old battle between host and pathogen has driven numerous mechanisms used by each to outcompete the other. The mitochondrial unfolded protein response (UPR^{mt}) is one such pathway used by the host in the defense against infection. The UPR^{mt} not only helps in recovering damaged mitochondria during infection but also induces an immune response to thwart pathogen colonization. In the model organism *Caenorhabditis elegans*, pathogens such as *Pseudomonas aeruginosa* activate the UPR^{mt} through the production of damaging toxins but also can downregulate the UPR^{mt} during chronic infection. In our previous work, we uncovered that loss of the *P. aeruginosa* acyl-CoA dehydrogenase FadE2 impairs UPR^{mt} activity and host survival. FadE2 showed substrate preferences for the coenzyme A intermediates produced during the breakdown of the branched-chain amino acid valine and to a lesser extent, leucine. Our data suggests that during infection, FadE2 restricts the supply of valine to the host hindering host energy metabolism in addition to the UPR^{mt}. Consistently, valine supplementation re-established the UPR^{mt} and prolonged host survival during infection with *P. aeruginosa*. However, the mechanism by which valine promotes the UPR^{mt} during infection with *P. aeruginosa* is unclear. Using transcriptomic and genetic analysis, we uncovered a novel role for the conserved transcription factor MLS-2 in mediating the activation of the UPR^{mt} by valine during infection. We find that *mls-2* gene expression is downregulated during chronic infection of *P. aeruginosa*, which is

restored upon supplementation with valine. Loss of MLS-2 function was able to suppress the increase in host survival afforded by valine supplementation, while enhanced MLS-2 function was sufficient in prolonging host survival. Interestingly, MLS-2 acts cell non-autonomously in the regulation of the UPR^{mt} from either the nervous system or mesoderm. We are currently using a forward genetic approach to resolve the mechanism of MLS-2-mediated regulation of the UPR^{mt}.

INTRODUCTION

Mitochondria are double-membraned organelles responsible for energy production in eukaryotic cells. They consist of the outer mitochondrial membrane (OMM) and inner mitochondrial membrane (IMM) that encapsulates the intermembrane space (IMS). It also consists of its own mitochondrial DNA that precisely synchronizes with the nucleus to form functional proteins encoded by the two genomes. Primarily known as the powerhouse of the cell, they are responsible for almost 95% of energy production via OXPHOS and ATP production as well as nucleotide, amino acid, and lipid metabolism (Nunnari & Suomalainen 2012). Mitochondria are reservoirs of the proapoptotic and respiratory chain protein cytochrome c which is released during cellular damage leading to mitochondrial permeabilization. The release of cytochrome c further activates apoptotic proteins leading to cell death (Garrido et al. 2006).

Owing to their essential nature, mitochondria are often targeted by pathogen microbes during infection. Many pathogens have evolved mechanisms that specifically target mitochondrial function (reviewed in Mahmud et al. 2021a). As such, mitochondria have also evolved their own defense strategies in response to these infectious agents. For example, mitochondria are important mediators of critical immune responses such NF-kB signaling (Albensi 2019). Also, mitochondrial reactive oxygen species (ROS) that are produced as a natural by-product during OXPHOS, or when the organelle suffers damage, can be used as a signal to stimulate the immune response (Silwal et al. 2020) or can act directly as an antimicrobial agent (Shekhova 2020).

Cells support mitochondrial health by constant surveillance and repair mechanisms. One of the critical pathways in maintaining mitochondrial health is the mitochondrial unfolded protein response (UPR^{mt}). The UPR^{mt} supports mitochondrial function during stress through the regulation

of genes with mitoprotective roles, with such functions as proteostasis, free radical detoxification, mitochondrial dynamics regulation, and metabolic rewiring (Nargund et al. 2012);(Higuchi-Sanabria et al. 2018)(Pellegrino et al. 2013) (Muñoz-Carvajal & Sanhueza 2020). Previous studies in the model organism *Caenorhabditis elegans* have identified the bZIP transcription factor ATFS-1 as the central regulator of this stress response pathway. ATFS-1 harbors two signal sequences that target it to mitochondria or the nucleus in a stress-dependent manner (Nargund et al. 2012). ATFS-1 is preferentially localized to mitochondria under healthy conditions. However, during stress, import of proteins into mitochondria is impaired. This leads to the cytoplasmic accumulation of ATFS-1 and subsequent transit into the nucleus where it regulates gene expression relevant to mitochondrial recovery (Qureshi et al. 2017).

In addition to promoting mitochondrial recovery, the UPR^{mt} has also been associated with the induction of antimicrobial defenses during infection. This is consistent with mitochondria being targeted by various pathogens (E et al. 2015) (Spier et al. 2019) (Rudel et al. 2010). As such, the UPR^{mt} is both required and sufficient for host survival during infection (Pellegrino & Haynes 2015) .One such pathogen that activates the UPR^{mt} in *C. elegans* is the opportunistic bacterial pathogen *Pseudomonas aeruginosa* (Pellegrino et al. 2014). *P. aeruginosa* activates the UPR^{mt} due to toxins that damage mitochondria such as hydrogen cyanide and phenazines which impair OXPHOS efficiency (Pellegrino et al. 2014) (Deng et al. 2019). We recently discovered that the activation of the UPR^{mt} by *P. aeruginosa* is more complex than previously thought. The activation of the UPR^{mt} occurs transiently during *P. aeruginosa*. The momentary nature of the UPR^{mt} during *P. aeruginosa* infection is due to active suppression by the pathogen (Mahmud et al. 2020). Intriguingly, a *P. aeruginosa* metabolic enzyme, FadE2, was responsible for the repression of the UPR^{mt} (Mahmud et al. 2020). FadE2 is involved in catabolism of branched chain amino acids,

specifically valine and to a lesser extent leucine (Mahmud et al. 2020). The current model suggests that *P. aeruginosa* deprives the *C. elegans* host of valine (and to lesser extent, leucine) and the resulting scarcity of these nutrients is believed to be involved in the suppression of the UPR^{mt} during infection which subverts the survival of the host (Mahmud et al. 2020). Consistently, supplementation of *C. elegans* with exogenous valine or leucine restored the activity of the UPR^{mt} and prolonged host survival (Mahmud et al. 2020). The mechanism by which valine/leucine regulates the UPR^{mt} during infection with *P. aeruginosa* remains elusive.

The following chapter builds on this working model that explores the mechanism by which *P. aeruginosa* FadE2 suppresses the UPR^{mt} during infection by restricting valine/leucine from the host. This study specifically focuses on the mechanism by which valine restores the UPR^{mt} during chronic *P. aeruginosa* infection. We present our preliminary findings henceforth.

RESULTS

Transcriptomic analysis identifies the conserved transcription factor MLS-2 as a regulator of valine-mediated UPR^{mt} during *P. aeruginosa* infection

We sought to understand the mechanism by which valine restored UPR^{mt} activity during chronic *P. aeruginosa* infection. We hypothesized that valine supplementation during *P. aeruginos*a infection would exert changes in host transcription and that one or more of these differentially expressed genes may be involved maintaining UPR^{mt} activity. Our transcriptomic analysis identified 22 upregulated and 39 downregulated genes that were differentially expressed following

48 hrs of *P. aeruginosa* exposure. Functional categories of these differentially genes were enriched for genes in metabolism and immunity, as well as genes involved in cell signaling (Figure 4.1).

We next wished to identify which, if any, of these differentially genes were involved in maintaining the activity of the UPR^{mt} during chronic *P. aeruginosa* infection. If a differentially expressed gene were to be a positive mediator of valine-induced UPR^{mt} activity, then we predicted that disabling its function would fully or partially suppress the UPR^{mt} during *P. aeruginosa* infection in the presence of valine. We disabled gene function using either RNA interference knockdown and/or genetic mutants, if available. Using this approach, we discovered that a predicted null mutation (allele *cc615*) in the gene *mls-2* (mesodermal lineage specification) suppressed UPR^{mt} activation during chronic *P. aeruginosa* infection in the presence of valine (Figure 4.2A, B). *C. elegans mls-2* encodes an ortholog of human HMX1/3 (H6 family homeobox 1/3), a class of transcription factors that regulates cell differentiation in both species (Jiang et al. 2008). MLS-2 functions in the specification of the M lineage, a specialized subset of mesodermal cells including the vulval and uterine muscle, a fraction of body wall muscle, and the coelomocytes (Jiang et al. 2005b). MLS-2 also functions in tube morphogenesis of the excretory duct cell (I et al. 2012).In addition to the null mutation in *mls-2*, a gain of function allele, *tm252*, also exists in the form of an in-frame deletion that removes 61 amino acids (Jiang et al. 2005b). Interestingly, *mls-2(tm252gf)* animals activated the UPR^{mt} when animals were fed the standard *E. coli* OP50 diet (Figure 4.2B). Furthermore, *mls-2(tm252gf)* animals maintained UPR^{mt} activation during *P. aeruginosa* infection (Figure 4.2C). Supplementation of valine to *mls-2(tm252gf)* animals during *P. aeruginosa* infection further enhanced the activation of the UPR^{mt} (Figure 4.2C). Our data suggests that the conserved transcription factor MLS-2 plays an important role in maintaining the UPR^{mt} during infection with *P. aeruginosa* in the presence of valine.

We next used quantitative PCR to measure *mls-2* gene expression when animals were fed *E. coli* OP50 diet, as well as *P. aeruginosa* in the presence or absence of valine. We found that *mls-2* gene expression was reduced when wild-type animals were exposed to *P. aeruginosa* relative to those that were fed *E. coli* OP50 (Figure 4.3). However, *mls-2* gene expression was increased in animals infected with *P. aeruginosa* in the presence of valine (Figure 4.3). Therefore, *P. aeruginosa* infection appears to downregulate *mls-2* gene expression, presumably due to reduced availability of valine metabolites to the host.

Valine prolongs host survival during *P. aeruginosa* infection via MLS-2

We had previously found that supplementation with valine during infection with *P. aeruginosa* significantly extended host survival time (Mahmud et al. 2020a). Valine increased host survival during infection by maintaining the activity of the UPR^{mt} (Mahmud et al. 2020a). Our preliminary evidence suggests that MLS-2 is an important regulator that maintains UPR^{mt} activity in the presence of valine during *P. aeruginosa* infection. Thus, we predicted that loss of MLS-2 function should suppress the benefit of valine supplementation with respect to host survival. As expected, valine supplementation increased the survival of wild-type animals during *P. aeruginosa* infection (Mahmud et al., 2020, Figure 4.4A). Interestingly, we find that the *mls-2(cc615)* loss of function animals displayed reduced survival compared to wild-type animals during infection with *P. aeruginosa* (Figure 4.4B). Furthermore, and consistent with MLS-2 acting as a positive regulator of valine-induced UPR^{mt} activity, *mls-2(cc615)* loss of function animals displayed reduced

survival during *P. aeruginosa* infection compared to wild-type animals when each were supplemented with valine (Figure 4.4C).

We next examined the survival of *mls-2(tm252gf)* animals during infection with *P. aeruginosa* in the presence or absence of valine. We predicted that *mls-2(tm252gf)* animals would exhibit increased survival during infection owing to the activation of the UPR^{mt} it displayed when fed standard *E. coli* OP50 and also during chronic *P. aeruginosa* infection. Consistently, *mls-2(tm252gf)* animals survived longer during *P. aeruginosa* infection compared to wild-type animals (Figure 4.4D). Also, supplementation with valine resulted in a slight further increase in the survival of *mls-2(tm252gf)* animals (Figure 4.4E). Therefore, our results indicate MLS-2 promotes host survival during infection, likely by mediating the activation of the UPR^{mt}.

MLS-2 regulates the UPR^{mt} cell non-autonomously

During the early stages of M lineage development, *mls-2* expression appears to be regulated at both the transcriptional and post-transcriptional level (Jiang et al. 2005a). The expression of *mls-2* is restricted to a specific subset of cells during development. MLS-2 functions cell autonomously during the specification of the M lineage (Figure 4.4 and Jiang et al. 2005, 2008). Expression is also observed in a distinct number of head neurons including the AIM, ASH, and ASK neurons (Jiang et al. 2005, 2008).

Intriguingly, the regulation of the UPR^{mt} by MLS-2 appears to be limited to the intestine of the animal (Figure 4.2). Since MLS-2 is not expressed in the tissue displaying an active UPR^{mt}, we predicted that it regulated this stress response cell non-autonomously. To explore this further, we

expressed a *mls-2(tm252gf)* cDNA under the control of tissue-specific promoters including *vha-6* (intestine) (E et al. 2009), *ceh-51* (mesodermal cells)(Broitman-Maduro et al. 2009), *hlh-8* (M lineage-specific), and *rgef-1* (neurons) (Chen et al. 2011) (Figure 4.5A) and then examined which could activate the UPR^{mt} pathway. Amazingly, we observed that expression of *mls-2(tm252gf)* cDNA in either neurons or the *ceh-51*-expressing mesoderm activated the UPR^{mt} in the intestine (Figure 4.5B). While we are still in the process of creating the P$_{hlh-8}$::*mls-2(tm252gf)* cDNA construct and transgenic animal, our preliminary results thus far indicate that MLS-2 can act cell non-autonomously to regulate the UPR^{mt}.

A forward genetics approach identifies potential regulators of MLS-2-mediated UPR^{mt} activation

Our results strongly suggest that valine maintains the activity of the UPR^{mt} during *P. aeruginosa* infection by activating the transcription factor MLS-2. We also have found that overactivation of MLS-2 alone is sufficient to activate the UPR^{mt} in the absence of valine supplementation. We were interested in understanding the mechanistic basis of how MLS-2 regulates the UPR^{mt} using a genetic approach. We performed an F1 forward genetics screen for suppressors of the UPR^{mt} observed in *mls-2(tm252gf)* animals. Briefly, *mls-2(tm252gf); hsp-6pr*::GFP animals were mutagenized with ethylmethylsulfate (EMS), and animals in the following generation were selected based on the lack of UPR^{mt} activation (as observed using the *hsp-6pr*::GFP reporter as a readout) (Figure 4.6A). We were successful in identifying eight independent mutant animals for which the UPR^{mt} was suppressed in *mls-2(tm252gf)* animals (alleles *osa58-osa60* and *osa68-osa72*; Figure 4.6B). Because these identified mutants were selected in the F1 generation, the associated mutation is considered genetically dominant.

We were curious whether our identified suppressors represented core regulators of the UPR^{mt} or whether they specifically regulated the activation of the UPR^{mt} resulting from enhanced MLS-2 activity in the *mls-2(tm252gf)* background. To distinguish between these two possibilities, we exposed the *mls-2(tm252gf);hsp-6pr*::GFP suppressor animals to paraquat, a chemical reagent that inhibits complex I of the electron transport chain, resulting in increased mitochondrial reactive oxygen species and activation of the UPR^{mt} (Figure 4.6C; Runkel et al., 2013). Interestingly, suppressor mutants *osa58*, *osa59*, *osa70*, and *osa72* continued to activate the UPR^{mt} in the presence of paraquat (Figure 4.6C), suggesting that these represent mutations in genes that specifically modulate the UPR^{mt} downstream of MLS-2. In contrast, mutants *osa60*, *osa68*, *osa69*, and *osa71* also suppressed the activation of the UPR^{mt} in the presence of paraquat (Figure 4.6C), suggesting these represent mutations in genes that are likely core regulators of this stress response. Therefore, our forward genetics screen identified at least four regulators of MLS-2-mediated UPR^{mt} activation.

DISCUSSION

The UPR^{mt} in *C. elegans* is dynamically regulated during *P. aeruginosa* infection. While early infection with this pathogen results in an activation of the UPR^{mt}, persistent exposure dampens the response. One critical *P. aeruginosa* factor that mediates the repression of the UPR^{mt} with chronic infection is the acyl CoA dehydrogenase FadE2 that is involved in the catabolism of the branched chain amino acids valine and leucine (Mahmud et al. 2021b). The current working model suggests that *P. aeruginosa* limits nutrients related to valine and leucine catabolites that prevents the activation of the UPR^{mt}. Consistently, supplementation with valine or leucine restores the UPR^{mt}

with persistent *P. aeruginosa* infection. We sought to perform a preliminary investigation into how valine maintained the UPR^{mt} during chronic *P. aeruginosa* infection. Using transcriptomics and genetics, we identified the conserved transcription factor MLS-2 has an important mediator of valine-induced UPR^{mt} during *P. aeruginosa* infection. Our data suggests that *P. aeruginosa* infection results in a downregulation of *mls-2* gene expression which can be restored with supplementation of valine. Consistently, a gain-of-function mutant in *mls-2* which exhibits increased protein stability (Jiang et al. 2005b) can sustain the activity of the UPR^{mt} during chronic *P. aeruginosa* infection. Thus, MLS-2 levels appear to be a critical determinant of UPR^{mt} activity levels. MLS-2 was also found to be sufficient to activate the UPR^{mt} in the absence of *P. aeruginosa* infection, as observed using a gain-of-function *mls-2* mutant. Lastly, MLS-2 appears to regulate the UPR^{mt} in a cell non-autonomous manner, presumably from the post-embryonic mesoderm and/or nervous system based on our tissue-specific expression studies.

Our identification of MLS-2 as a regulator of the UPR^{mt} is intriguing considering that this transcription factor, to our knowledge, has not been associated with the regulation of a cellular stress response. Instead, MLS-2 and its mammalian ortholog have known roles in regulating cell fate specification and/or tissue morphogenesis (Jiang et al. 2008). The cell non-autonomous nature of MLS-2 in regulating the UPR^{mt} is also an exciting finding. The UPR^{mt} is known to be regulated cell non-autonomously from the nervous system through the employment of a rich set of secreted regulators. These include the neurotransmitter serotonin, neuropeptides, and Wnt (Shao et al. 2016). One possibility is that MLS-2 is involved in regulating the synthesis and/or release of these secreted signals. However, we suspect that the mechanism of this cell non-autonomous regulation may be more complex considering that our tissue-specific expression of *mls-2(tm252gf)* in the mesoderm was also able to activate the UPR^{mt}. To our knowledge, there are no known factors from

the mesoderm lineage that have been found to activate the UPR^{mt} cell non-autonomously. It will be interesting to identify what signal(s) MLS-2 may be controlling from this tissue type in the regulation of the UPR^{mt}.

The question still remains as to how MLS-2 modulates the UPR^{mt}. We are hopeful that the suppressor mutant animals identified in this preliminary study will shed light onto the mechanistic basis of MLS-2 regulation of the UPR^{mt}. It is curious, however, that some of the isolated suppressors did not seem to be involved in regulating the UPR^{mt} with mitochondrial stress conditions including increased oxidative stress. This suggests that MLS-2 may employ specific means to regulate the UPR^{mt}. Interestingly, a recent study has found that disruptions to mitochondrial dynamics (mitochondrial fusion or fission) activated the UPR^{mt} which could be suppressed by increasing autophagic flux (Haeussler et al. 2020). Mechanistically, it was proposed that increasing autophagic flux enhanced metabolic breakdown of triacylglycerols which are elevated in mitochondrial dynamics mutants (Haeussler et al. 2020). The increased metabolic activity was thought to restore mitochondrial membrane potential, hence reducing activity of the UPR^{mt} (Haeussler et al. 2020). However, increased autophagic flux was unable to suppress the UPR^{mt} for other mitochondrial stress conditions including increased mitochondrial proteotoxicity following loss of mitochondrial quality control protease SPG-7 (Haeussler et al. 2020).Our discovery that MLS-2 may also regulate the UPR^{mt} in a specific manner is therefore consistent with prior findings. The identification of the causative genes responsible for the regulation of the UPR^{mt} by MLS-2 in our suppressor animals will undoubtably shed light into the mechanistic basis this transcription factor plays in this stress response. We are currently mapping these suppressor mutants using a combination of polymorphism mapping and whole genome sequencing (HE et al. 2016).

MATERIALS AND METHODS

C. elegans strains and maintenance

C. elegans were grown using standard protocols of nematode growth medium (NGM) and *Escherichia coli* OP50 as a bacterial diet ((DL & S 1978). *C. elegans* strains were provided by the Caenorhabditis Genetics Center and include: N2 Bristol, SJ4100 zcIs[*hsp-6pr*::GFP], LW227 *mls-2(cc615)*, and LW425 *mls-2(tm252).*

RNA sequencing analysis and quantitative PCR

Trizol extraction method was used to recover total RNA from worms and RNA was purified using Direct-zol RNA Kit (Zymo Research, CA, USA). An Agilent 2100 Bioanalyzer was used to assess RNA integrity. Library construction and sequencing was done by Novogene Inc. (CA, USA). In short, mRNA was enriched using oligo(dT) beads and rRNA removed using the Ribo-Zero kit. mRNA was fragmented, followed by synthesis of first and second strand cDNA synthesis. Then sequencing adapters were ligated and the double-stranded cDNA library completed through size selection and PCR enrichment. The library was sequenced using an Illumina Hiseq 4000 following manufacturer's instructions for paired-end 150-bp reads. The raw data was cleaned by removing adapter sequences, reads containing poly-N and low-quality reads (Q<30) using Trimmomatic . Tophat v.2.0.9 was used to align clean reads to the *C. elegans* reference genome. The mapped reads from each sample was assembled using Cufflinks v.2.1.1 [41]. HTSeq v.0.6.1 was used to count the number of reads mapped to each gene. In addition, the reads per kilobase million

(RPKM) of each gene was calculated based on the length of the gene and the number of reads mapped to it. Differential expression analysis was performed using DESeq2 R package (v.1.10.1) [43]. Relative expression of genes with Benjamini-Hochberg corrected P-values (Padj)<0.05 were considered to be differentially expressed. Heatmaps were generated with pheatmap in R Studio.

Quantitative PCR was used to measure *mls-2* gene expression in the presence of *E. coli* OP50, *P. aeruginosa* PA14, or *P. aeruginosa* PA14 supplemented with 5 mM valine. We used *fer-1(hc1)* mutant animals to sterilize animals so as to prevent contamination from offspring. RNA was extracted as previously described. qPCR primers for *mls-2* were as follows GATCTCACCACTTACCATGTTCC and CATCGTCATCTTCTGCGTCA. The gene *act-3* was used as a standard control using primers ATCCGTAAGGACTTGTACGCCAAC and CGATGATCTTGATCTTCATGGTTC.

Microscopy

All fluorescent reporter expression assays were conducted using a Zeiss Observer Z1 upright microscope. Worms were anesthetized using 2.5 mM sodium azide in S-Basal and arranged on agarose pad-lined glass microscopy slides for visualization. ImageJ software was used for quantification of fluorescence intensity. Background fluorescence was subtracted from the intestinal fluorescence and divided by worm size to generate a fluorescence intensity value. All photomicrographs show a collection of representative animals. For quantification, at least 20 worms were scored blindly in three independent replicates.

***C. elegans* pathogen infection assays**

Worms were age-matched at the L4 stage by harvesting eggs using bleach/NaOH treatment of gravid hermaphrodites. Eggs were aliquoted on NGM plates containing *E. coli* OP50 and then 50 L4 worms were transferred to *P. aeruginosa* PA14 infection plates. To prepare infection plates, *P. aeruginosa* was inoculated from a fresh culture plate and grown overnight at 37˚C. The following day 15 µl of *P. aeruginosa* overnight culture was spotted onto NGM media plates. Plates were incubated overnight at room temperature and then transferred to 37˚C for an overnight incubation and used for the survival assay the following day. Animal deaths were recorded daily every 2 hrs for a 12 hr period each day. Statistical analysis was performed as described for the lifespan assays.

Plasmid construction and germline transformation

RNA was extracted from *mls-2(tm252gf)* animals (see protocol description in RNAseq) and the full-length *mls-2(tm252gf)* cDNA was isolated amplified by PCR using primers TTTGGATCCATGCCGACTTCAGTTATGAATC and AAACCCGGGTCACATGTTCTGCGCTTGAGC. The *mls-2(tm252gf)* cDNA was cloned into the BamHI and XmaI sites of pPD49.26. Tissue-specific promoters were then cloned immediately upstream of the *mls-2(tm252gf)* cDNA. We used germline transformation to express each tissue-specific construct of *mls-2(tm252gf)* cDNA using SJ 4100 *hsp-6pr*::GFP animals and standard techniques. Each plasmid was microinjected at 10 ng/µl along with P_{myo-2}::mCherry plasmid at 5 ng/µl as a co-injection marker. At least two independent transgenic lines were examined from each transformation.

EMS mutagenesis

Approximately 2000 *mls-2(tm252gf);hsp-6$_{pr}$*::GFP animals were harvested from NGM plates with S-basal, washed twice to remove bacteria and resuspended in 2 ml S-basal. 2 ml of 2X ethyl methyl sulfonate (EMS) solution (60 μM) was added to worm suspension and placed on a rocker for 4 hrs. After mutagenesis, worms were washed three times with S-basal, resuspended in 0.5 ml S-basal and plated onto seeded NGM plates. After overnight incubation, 50 adult worms were singled out into NGM plates and allowed to grow until F1 generation. F1 animals with reduced green fluorescence were selected for further study. Homozygous F2 mutants were selected from the F1 mutants for further study.

REFERENCES

Albensi BC (2019) What Is Nuclear Factor Kappa B (NF-κB) Doing in and to the Mitochondrion? *Front. Cell Dev. Biol.* 7. Available at: /pmc/articles/PMC6692429/ [Accessed October 2, 2021].

Broitman-Maduro G, Owraghi M, Hung WWK, Kuntz S, Sternberg PW & Maduro MF (2009) The NK-2 class homeodomain factor CEH-51 and the T-box factor TBX-35 have overlapping function in C. elegans mesoderm development. *Development* 136, 2735–2746.

Chen L, Fu Y, Ren M, Xiao B & Rubin CS (2011) A RasGRP, C. elegans RGEF-1b, Couples External Stimuli to Behavior by Activating LET-60 (Ras) in Sensory Neurons. *Neuron* 70, 51. Available at: /pmc/articles/PMC3081643/ [Accessed September 20, 2021].

Deng P, Uma Naresh N, Du Y, Lamech LT, Yu J, Zhu LJ, Pukkila-Worley R & Haynes CM (2019) Mitochondrial UPR repression during Pseudomonas aeruginosa infection requires the bZIP protein ZIP-3. *Proc. Natl. Acad. Sci. U. S. A.* Available at: http://feedproxy.google.com/~r/Pnas-RssFeedOfEarlyEditionArticles/~3/FWqdfc6LcJc/1817259116.short.

DL R & S B (1978) Indirect suppression in Caenorhabditis elegans. *Genetics* 89, 299–314. Available at: https://pubmed.ncbi.nlm.nih.gov/669254/ [Accessed September 27, 2021].

E A, D J & K N (2009) Loss of the apical V-ATPase a-subunit VHA-6 prevents acidification of the intestinal lumen during a rhythmic behavior in C. elegans. *Am. J. Physiol. Cell Physiol.* 297. Available at: https://pubmed.ncbi.nlm.nih.gov/19741196/ [Accessed September 20, 2021].

E L, JJ L & T A (2015) Mitochondria: a target for bacteria. *Biochem. Pharmacol.* 94, 173–185. Available at: https://pubmed.ncbi.nlm.nih.gov/25707982/ [Accessed October 2, 2021].

Garrido C, Galluzzi L, Brunet M, Puig PE, Didelot C & Kroemer G (2006) Mechanisms of

cytochrome c release from mitochondria. *Cell Death Differ. 2006 139* 13, 1423–1433. Available at: https://www.nature.com/articles/4401950 [Accessed September 27, 2021].

Haeussler S, Köhler F, Witting M, Premm MF, Rolland SG, Fischer C, Chauve L, Casanueva O & Conradt B (2020) *Autophagy compensates for defects in mitochondrial dynamics*,

HE S, AS F, A J-L & A G (2016) Mapping Challenging Mutations by Whole-Genome Sequencing. *G3 (Bethesda).* 6, 1297–1304. Available at: https://pubmed.ncbi.nlm.nih.gov/26945029/ [Accessed September 27, 2021].

Higuchi-Sanabria R, Frankino PA, Paul JW, Tronnes SU & Dillin A (2018) A Futile Battle? Protein Quality Control and the Stress of Aging. *Dev. Cell* 44, 139–163. Available at: http://linkinghub.elsevier.com/retrieve/pii/S1534580717310377.

I A-S, CE S, JI M & MV S (2012) The Nkx5/HMX homeodomain protein MLS-2 is required for proper tube cell shape in the C. elegans excretory system. *Dev. Biol.* 366, 298–307. Available at: https://pubmed.ncbi.nlm.nih.gov/22537498/ [Accessed September 27, 2021].

Jiang Y, Horner V & Liu J (2005a) The HMX homeodomain protein MLS-2 regulates cleavage orientation, cell proliferation and cell fate specification in the C. elegans postembryonic mesoderm. *Development* 132, 4119–30. Available at: https://www.ncbi.nlm.nih.gov/pmc/articles/PMC3624763/pdf/nihms412728.pdf.

Jiang Y, Horner V & Liu J (2005b) The HMX homeodomain protein MLS-2 regulates cleavage orientation, cell proliferation and cell proliferation and cell fate specification in the C. elegans postembryonic mesoderm. *Development* 132, 4119–4130.

Jiang Y, Shi H, Amin NM, Sultan I & Liu J (2008) Mesodermal expression of the C. elegans HMX homolog mls-2 requires the PBC homolog CEH-20. *Mech. Dev.* 125, 451–461.

Mahmud SA, Qureshi MA & Pellegrino MW (2021a) On the offense and defense: mitochondrial recovery programs amidst targeted pathogenic assault. *FEBS J.*, 1–24.

Mahmud SA, Qureshi MA & Pellegrino MW (2021b) On the offense and defense: mitochondrial recovery programs amidst targeted pathogenic assault. *FEBS J.*, 1–24.

Mahmud SA, Qureshi MA, Sapkota M & Pellegrino MW (2020a) A pathogen branched-chain amino acid catabolic pathway subverts host survival by impairing energy metabolism and the mitochondrial upr. *PLoS Pathog.* 16, 1–27. Available at: http://dx.doi.org/10.1371/journal.ppat.1008918.

Mahmud SA, Qureshi MA, Sapkota M & Pellegrino MW (2020b) A pathogen branched-chain amino acid catabolic pathway subverts host survival by impairing energy metabolism and the mitochondrial UPR. *PLOS Pathog.* 16, e1008918. Available at: http://dx.doi.org/10.1371/journal.ppat.1008918.

Mark W. Pellegrino, Amrita M. Nargund, Natalia V. Kirienko, Reba Gillis, Christopher J. Fiorese and CMH (2015) Mitochondrial UPR-regulated innate immunity provides resistance to pathogen infection. 516, 414–417.

Mark W. Pellegrino, Amrita M. Nargund and CMH (2013) Signaling the Mitochondrial Unfolded Protein Response. 31, 1713–1723.

Mohammed A. Qureshi, Cole M. Haynes MWP (2017) The mitochondrial unfolded protein response: signaling from the powerhouse. *J. Biol. Chem.*

Muñoz-Carvajal F & Sanhueza M (2020) The Mitochondrial Unfolded Protein Response: A Hinge Between Healthy and Pathological Aging. *Front. Aging Neurosci.* 0, 300.

Nargund AM, Pellegrino MW, Fiorese CJ, Baker BM & Haynes CM (2012) Mitochondrial import efficiency of ATFS-1 regulates mitochondrial UPR activation. *Science (80-.).* 337, 587–590.

Nunnari J & Suomalainen A (2012) Mitochondria: In Sickness and in Health. *Cell* 148, 1145–1159. Available at: http://www.cell.com/article/S0092867412002358/fulltext [Accessed September 27, 2021].

Pellegrino MW & Haynes CM (2015) Mitophagy and the mitochondrial unfolded protein response in neurodegeneration and bacterial infection. *BMC Biol.* 13, 1–9.

Rudel T, Kepp O & Kozjak-Pavlovic V (2010) Interactions between bacterial pathogens and mitochondrial cell death pathways. *Nat. Rev. Microbiol. 2010 810* 8, 693–705. Available at: https://www.nature.com/articles/nrmicro2421 [Accessed October 2, 2021].

Shao L-W, Niu R & Liu Y (2016) Neuropeptide signals cell non-autonomous mitochondrial unfolded protein response. *Cell Res. 2016 2611* 26, 1182–1196. Available at: https://www.nature.com/articles/cr2016118 [Accessed September 27, 2021].

Shekhova E (2020) Mitochondrial reactive oxygen species as major effectors of antimicrobial immunity. *PLOS Pathog.* 16, e1008470. Available at: https://journals.plos.org/plospathogens/article?id=10.1371/journal.ppat.1008470 [Accessed October 2, 2021].

Silwal P, Kim JK, Kim YJ & Jo E-K (2020) Mitochondrial Reactive Oxygen Species: Double-Edged Weapon in Host Defense and Pathological Inflammation During Infection. *Front. Immunol.* 0, 1649.

Spier A, Stavru F & Cossart P (2019) Interaction between Intracellular Bacterial Pathogens and Host Cell Mitochondria. *Microbiol. Spectr.* 7. Available at: https://journals.asm.org/journal/spectrum [Accessed October 2, 2021].

Runkel ED, Liu S, Baumeister R, Schulze E. Surveillance-Activated Defenses Block the ROS-Induced Mitochondrial Unfolded Protein Response. *PLoS Genet*. 2013;9(3). doi:10.1371/journal.pgen.1003346

FIGURES

A

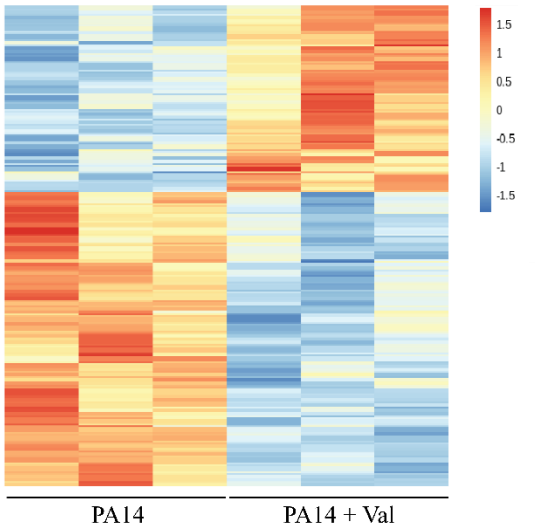

B

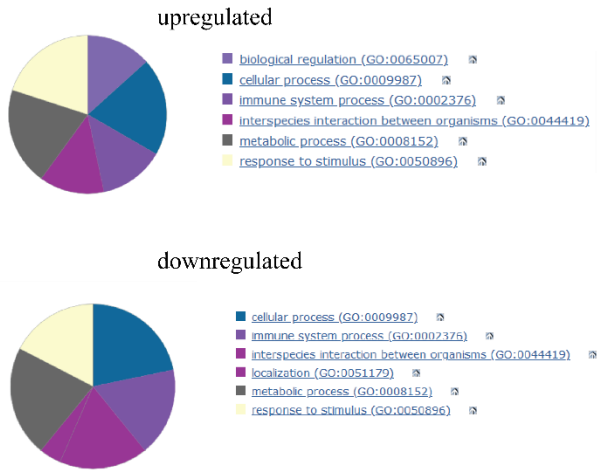

C

downregulated

#	Gene	Foldchange	GO Term
1	T22F3.11	4.231494	membrane;transmembrane transport
2	F42A10.7	4.018306	
3	F09C8.1	2.316575	phospholipid metabolic process; acting on ester bonds
4	Y53G8AM.5	2.292726	
5	F35E12.2	2.280263	membrane; transmembrane transport; innate immune response
6	pud-3	2.227302	
7	lipl-1	2.171896	hydrolase activity; lipid catabolic process; lipase activity; acting on ester bonds; lysosome
8	H39E23.3	2.079571	microtubule binding
9	clec-60	2.020488	carbohydrate binding
10	C30G12.2	2.012371	
11	pcp-1	2.000203	serine-type peptidase activity; dipeptidyl-peptidase activity
12	asm-3	1.903026	lysosome; metabolic process; hydrolase activity; acting on glycosyl bonds; metal ion binding; extracellular region; ceramide biosynthetic process
13	ora-1	1.890469	
14	pud-2.2	1.808439	
15	F07B7.8	1.801646	
16	asah-1	1.801258	lipid metabolic process; lysosome; ceramidase activity; hydrolase activity, acting on carbon-nitrogen bonds
17	F45D11.14	1.800876	
18	ugt-66	1.746747	membrane; transferase activity; UDP-glycosyltransferase activity
19	R193.2	1.737567	membrane; integral component of membrane;
20	pud-1.2	1.701934	
21	pud-4	1.685059	
22	asm-2	1.666593	lysosome; metabolic process; hydrolase activity; metal ion binding
23	best-1	1.646814	membrane; chloride channel activity; integral component of membrane
24	Y65B4BR.1	1.626618	phospholipid metabolic process; phospholipase activity; hydrolase activity, acting on ester bonds
25	T23E7.2	1.614503	
26	C25E10.5	1.575195	membrane; integral component of membrane
27	clec-74	1.572884	carbohydrate binding
28	F28H7.3	1.570114	hydrolase activity; lipid metabolic process
29	sodh-1	1.552228	cytoplasm; metal ion binding; zinc ion binding; oxidoreductase activity; alcohol dehydrogenase (NAD) activity
30	F41E6.5	1.536513	catalytic activity; oxidoreductase activity; oxidation-reduction process; FMN binding
31	cdf-2	1.509274	membrane; integral component of membrane; zinc ion transmembrane transporter activity; gut granule membrane
32	C50B6.7	1.503198	catalytic activity; carbohydrate metabolic process; cation binding; alpha-amylase activity
33	dhs-26	1.497812	membrane; integral component of membrane; oxidoreductase activity; oxidation-reduction process
34	cah-4	1.460196	zinc ion binding; carbonate dehydratase activity; small molecule metabolic process
35	nep-17	1.446213	membrane; metalloendopeptidase activity; metallopeptidase activity; membrane raft
36	cat-4	1.44104	cytoplasm; metabolic process; nucleotide binding; GTP binding; zinc ion binding; dopamine biosynthetic process
37	ZK1193.2	1.433348	
38	irg-4	1.42979	innate immune response
39	ZK596.1	1.428868	

upregulated

#	Gene	Foldchange	GO Term
1	madd-2	4.054017	metal ion binding; zinc ion binding; protein binding; neuronal cell body; signaling receptor binding; dorsal/ventral axon guidance
2	ins-19	3.00529	extracellular region; hormone activity; signal transduction
3	mls-2	2.508195	DNA binding; nucleus; regulation of transcription, DNA-templated; sequence-specific DNA binding; nematode larval development
4	fbxb-18	2.392807	
5	cyp-35D1	2.200855	cytoplasm; metal ion binding; intracellular membrane-bounded organelle; oxidoreductase activity; oxidation-reduction process
6	clec-196	2.142484	carbohydrate binding
7	rig-5	2.054787	
8	Y82E9BR.17	2.01032	
9	cutl-20	1.811823	
10	unc-39	1.804622	nucleus; DNA binding; regulation of transcription, DNA-templated; sequence-specific DNA binding; transcription regulatory region sequence-specific DNA binding; multicellular organism development
11	irg-5	1.764097	innate immune response; defense response to Gram-positive bacterium
12	cutl-16	1.639448	membrane; integral component of membrane
13	clec-266	1.634844	carbohydrate binding; membrane; integral component of membrane
14	clec-174	1.619891	carbohydrate binding
15	C08F1.10	1.565339	membrane; integral component of membrane
16	linc-11	1.553887	
17	fbxb-66	1.504828	protein binding
18	Y9D1A.1	1.499467	
19	fbxb-88	1.491977	protein binding
20	Y46H3C.7	1.488422	
21	K10D3.4	1.427899	serine-type endopeptidase inhibitor activity; negative regulation of endopeptidase activity
22	Y6E2A.4	1.417402	

Figure 4.1 Valine supplementation results in changes to gene expression in wild-type animals during chronic *P. aeruginosa* infection.

(A) Heat map of transcriptomic analysis of wild-type *C. elegans* exposed to wild-type *P. aeruginosa* PA14 in the presence or absence of 5mM valine following 48 hrs.

(B) Pie chart of functional categories of genes up-regulated or down-regulated in *C. elegans* during infection of *P. aeruginosa* PA14 in the presence or absence of 5 mM valine following 48 hrs.

(C) List of genes up-regulated or down-regulated in *C. elegans* during infection of *P. aeruginosa* PA14 in the presence or absence of 5 mM valine following 48 hrs.

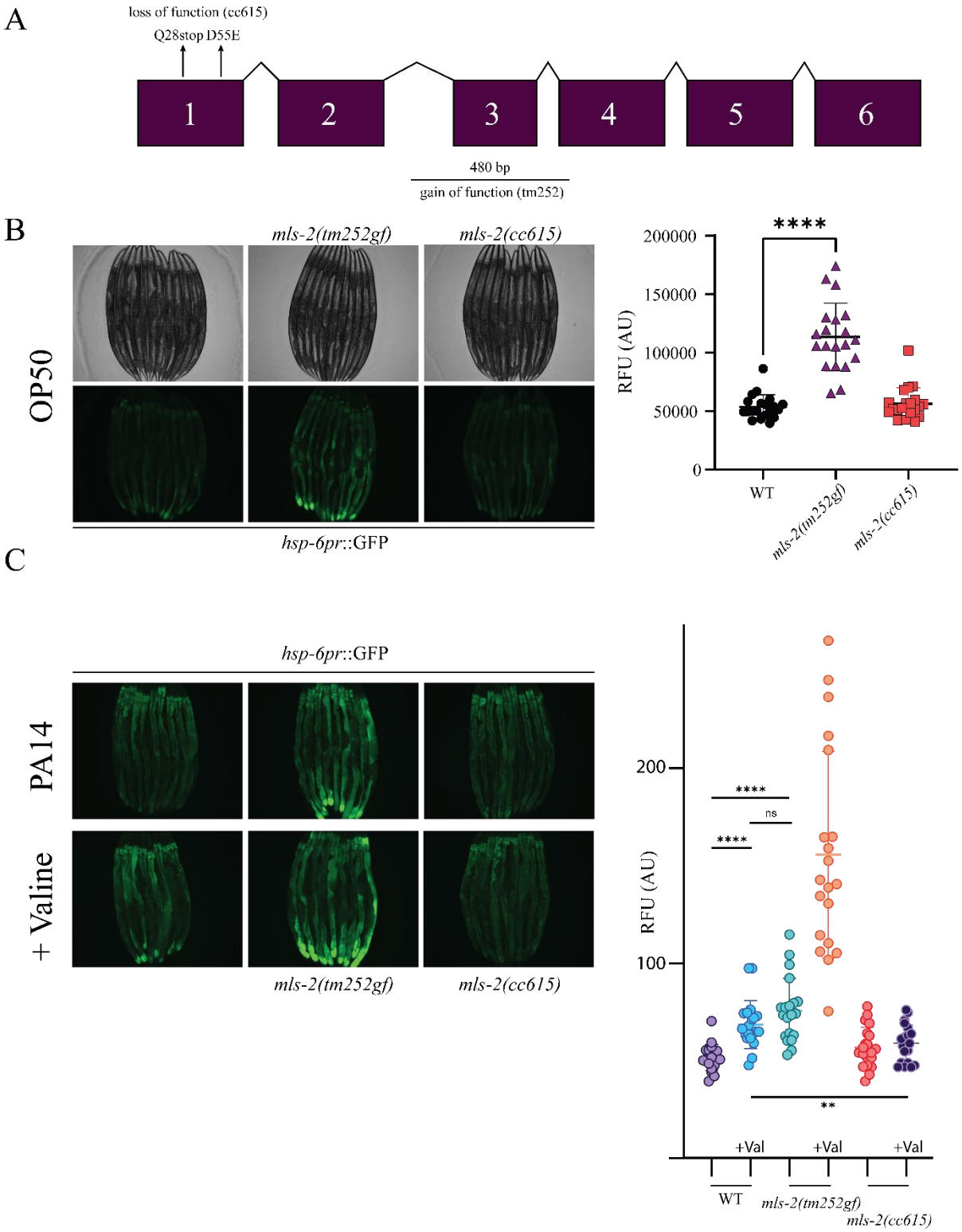

Figure 4.2 The transcription factor MLS-2 is a positive mediator of valine-induced UPR^{mt} activity during chronic *P. aeruginosa* infection.

(A) Gene structure of *mls-2* including locations of *cc615* and *tm252* mutation alleles.

(B) Photomicrographs and quantification of *hsp-6*$_{pr}$::GFP expression wild-type, *mls-2(cc615), or mls-2(tm252gf)* animals exposed to *E. coli* OP50. RFU; Relative Fluorescence Units. **** denotes $p<0.05$ using Student's *t*-test; (n=20).

(C) Photomicrographs and quantification of *hsp-6*$_{pr}$::GFP expression wild-type, *mls-2(cc615), or mls-2(tm252gf)* animals exposed to *P. aeruginosa* PA14, in the presence or absence of 5 mM valine. RFU; Relative Fluorescence Units. **** denotes $p<0.005$ using Student's *t*-test; (n=20).

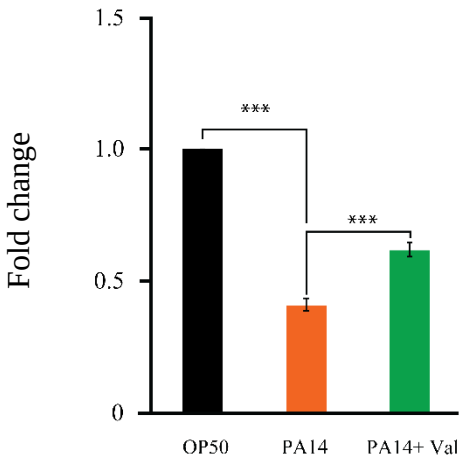

Figure 4.3 *P. aeruginosa* infection downregulates *mls-2* gene expression due to a lack of valine availability.

Representative quantitative PCR analysis of *mls-2* transcript levels for *fer-1(hc1)* animals exposed to *E. coli* OP50, *P. aeruginosa* PA14, or *P. aeruginosa* PA14 supplemented with 5 mM valine following 48 hrs infection.

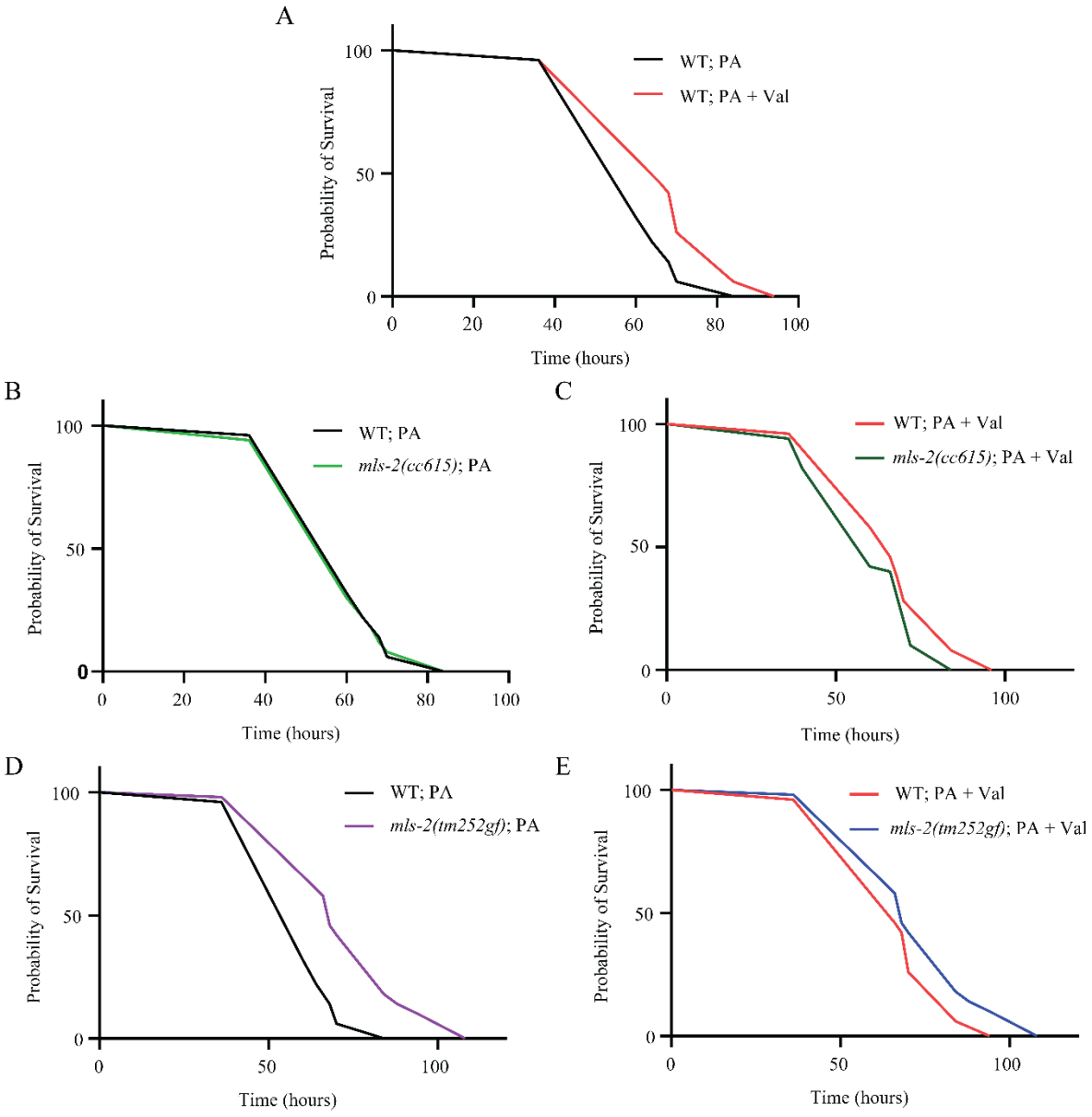

Figure 4.4 Valine promotes host survival during infection via MLS-2.

(A) Survival of wild-type animals infected with *P. aeruginosa* PA14 in the presence or absence of 5 mM valine.

(B) Survival of wild-type or *mls-2(cc615)* animals infected with *P. aeruginos*a PA14.

(C) Survival of wild-type or *mls-2(cc615)* animals infected with *P. aeruginosa* PA14 supplemented with 5 mM valine.

(D) Survival of wild-type or *mls-2(tm252gf)* animals infected with *P. aeruginosa* PA14.

(E) Survival of wild-type or *mls-2(tm252gf)* animals infected with *P. aeruginosa* PA14 supplemented with 5 mM valine. See Table 3 for all statistics related to survival analysis.

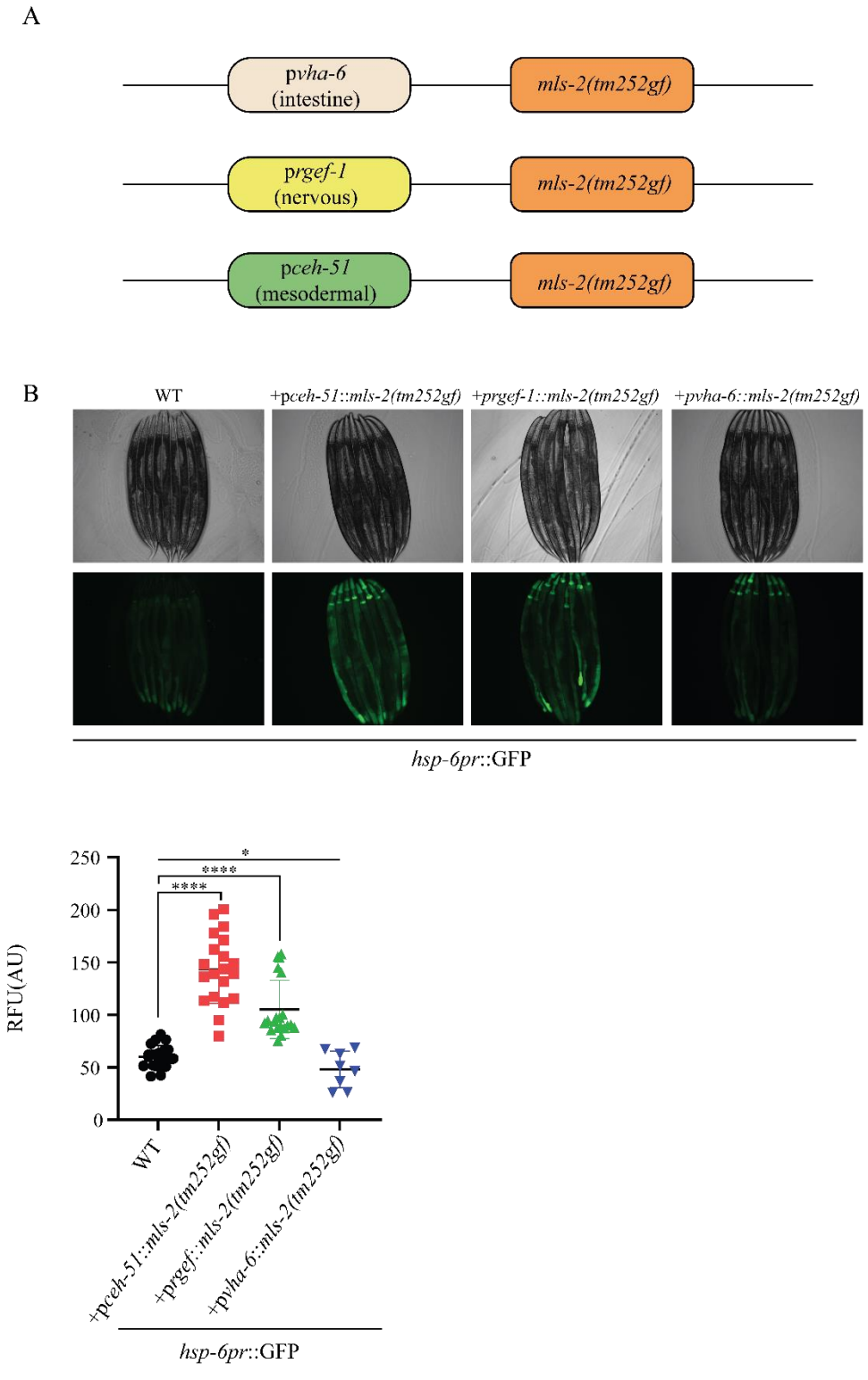

Figure 4.5 MLS-2 acts cell non-autonomously in the regulation of the UPR^{mt}

(A) Schematic representations of tissue specific constructs driving the expression of the *mls-2(tm252gf)* cDNA.

(B) Photomicrographs and quantification of *hsp-6*$_{pr}$::GFP expression for wild-type animals or transgenic wild-type animals expressing P$_{vha-6}$::*mls-2(tm252gf)*, P$_{rgef-1}$::*mls-2(tm252gf)*, or P$_{ceh-51}$::*mls-2(tm252gf)*. **** denotes $p<0.005$ using Student's *t*-test; (n=8-20).

Figure 4.6

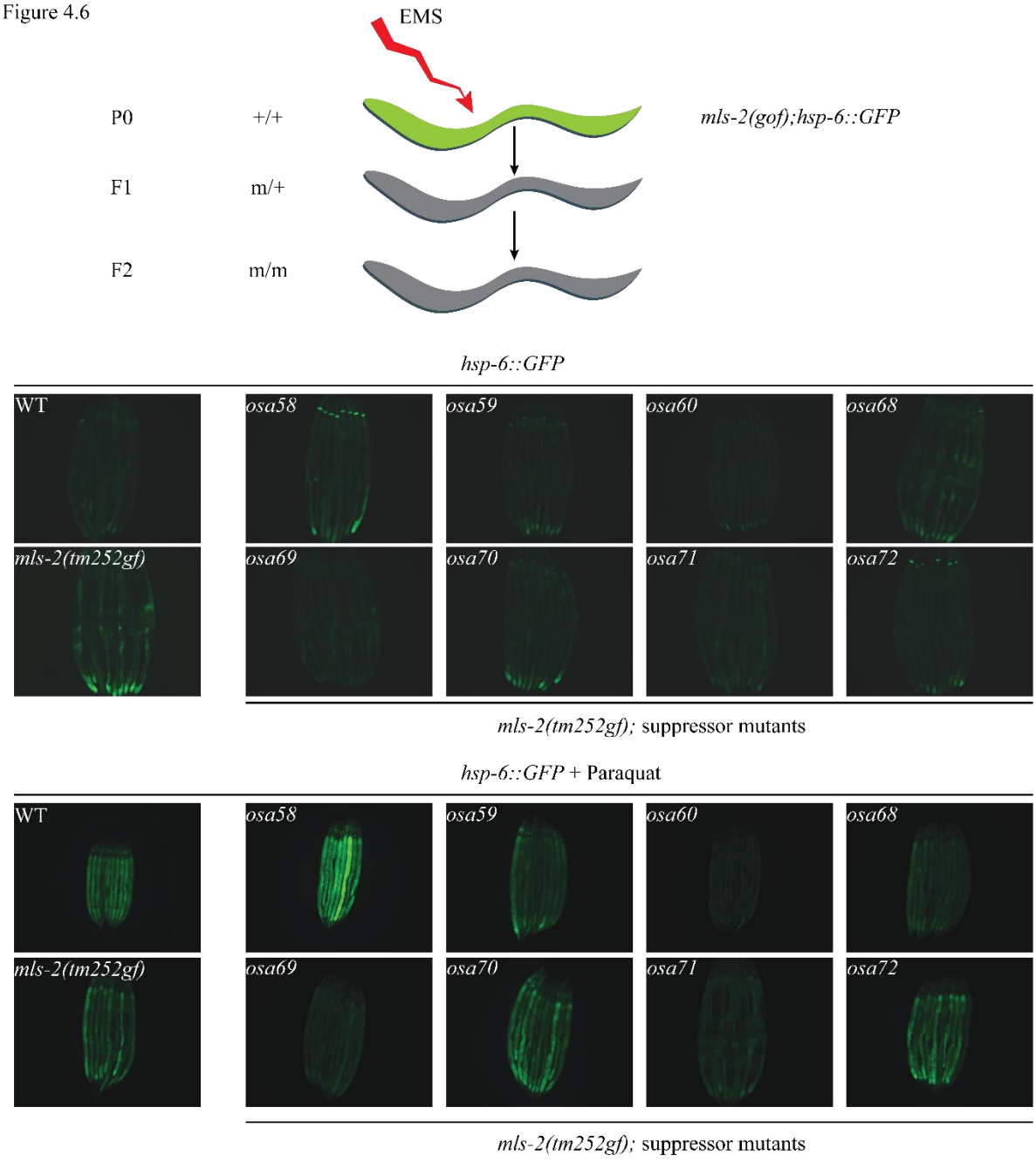

Figure 4.6 Forward genetic screen for suppressors of *mls-2(tm252gf)* activation of the UPR^{mt}.

(A) Schematic outlining the forward genetic suppressor strategy.

(B) Photomicrographs and quantification of *hsp-6*$_{pr}$::GFP expression for wild-type, *mls-2(tm252gf)*, or *mls-2(tm252gf)* suppressor animals fed *E. coli* OP50. **** denotes $p<0.005$ using Student's *t*-test; (n=20).

(C) Photomicrographs and quantification of *hsp-6*$_{pr}$::GFP expression for wild-type, *mls-2(tm252gf)*, or *mls-2(tm252gf)* suppressor animals fed *E. coli* OP50 in the presence of 5mM paraquat. **** denotes $p<0.005$ using Student's *t*-test; (n=20).

Table 4.1 Survival statistics

Figure	Strain 1	Mean Survival 1	Strain 2	Mean Survival 2	Percentage change	p-value	p-value summary
4.4 A	WT; PA	62.32	WT; PA+Val	68.40	9.76	<0.0001	significant
4.4 B	WT; PA	63.32	*mls-2(cc615)*; PA	62.08	-1.96	0.9911	ns
4.4 C	WT; PA + Val	68.40	*mls-2(cc615)*; PA + Val	63.20	-7.60	0.0493	significant
4.4 D	WT; PA	65.32	*mls-2(tm252gf)*; PA	74.40	13.90	<0.0001	significant
4.4 E	WT; PA + Val	68.40	*mls-2(tm252gf)*; PA + Val	83.68	22.34	<0.0005	significant